THE DEVELOPMENT OF COLLISION DYNAMICS MODELS TO ESTIMATE THE RESULTS OF FULL-SCALE RAIL VEHICLE IMPACT TESTS

A thesis
submitted by

Kristine J. Severson

In partial fulfillment of the requirements
for the degree of

Master of Sciences
in
Mechanical Engineering

TUFTS UNIVERSITY

November 2000

Advisor: Professor A. Benjamin Perlman

ABSTRACT

In an effort to study occupant survivability in train collisions, analyses and tests were conducted to understand and improve the crashworthiness of rail vehicles. A collision dynamics model was developed in order to estimate the rigid body motion of rail cars in a collision, which could be used to estimate the likelihood and severity of injuries experienced by occupants in collisions. The collision dynamics model, with input from finite element models, was used to generate accurate results in much less time than the finite element model.

The objective of this thesis was to develop a model of a conventional passenger rail car to analyze the crush response and rigid body motion experienced by the car during a collision. The model was used as an analysis tool in coordination with full-scale testing of rail cars to assist in the development of the test requirements, and to estimate the results of the impact tests. The model developed and validated as part of this thesis was based on an existing rail car design. The model will be used in planned follow-on work (out of the scope of this thesis), to evaluate the collision performance of rail cars that will be modified to incorporate crashworthiness features.

The model consists of a series of lumped masses connected by non-linear springs. The force-deflection characteristics for the springs were estimated from a detailed finite element model of a rail car similar to the cars that were tested. Estimates for some of the spring characteristics were initially based on component or sub-assembly impact testing. These spring characteristics were incorporated into the model and modified as necessary to reach better agreement with full-scale test results.

The model was exercised to evaluate the crush response and rigid body motion of the vehicles under full-scale, single-car and two-car impact test conditions. The results developed with the single-car and two-car collision dynamics models were compared with the data from the respective tests. Both models were shown to represent the test data reasonably well in terms of longitudinal acceleration-time history, force/crush behavior and relative impact velocity. The model was described in detail. The methods of filtering and interpreting the test data were also included. A parametric study was conducted to evaluate the influence of different variables on the results.

ACKNOWLEDGEMENTS

First and foremost, I have to thank my thesis advisor, Professor Benjamin Perlman, for his boundless enthusiasm and encouragement during the course of this project. Without his consistent, positive support, I do not know how I would have finished this thesis.

Thank you also to David Tyrell and Professor Robert Greif for serving on my thesis committee. David in particular has provided a wealth of advise, knowledgeable insight and general support throughout this project. Without the benefit of his knowledge and experience, the quality of this thesis would be significantly diminished.

A big thank-you goes to the Volpe National Transportation Systems Center and the Fellows Program that provided the funding for my Master's Degree. I am grateful for being part of a workplace that places such value on higher education. Without financial backing and a culture that encourages continuous learning, I doubt I would have considered pursuing a Master's Degree.

Thank you to John Zolock for developing the filtering algorithm and for processing the test data once, twice, three times, and never complaining! Thank you to Ann Walker for generously offering to edit this thesis and for pointing out the inconsistencies in the text.

Finally, I would like to thank my family, especially my husband, Allan. While they did not do much to directly affect this thesis, their constant love and support have put me in a position to tackle such an endeavor!

TABLE OF CONTENTS

LIST OF FIGURES

LIST OF TABLES

Table **Page**

The Development of Collision Dynamics Models to Estimate the Results of Full-Scale Rail Vehicle Impact Tests

1. INTRODUCTION

The objective of this thesis was to develop collision dynamics models of conventional U.S. passenger rail cars under collision conditions. Simulations of both a single car and two coupled cars impacting a rigid wall at moderate speed were investigated. The models were used in conjunction with full-scale passenger car collision tests sponsored by the Federal Railroad Administration (FRA) of the U.S. Department of Transportation (USDOT). The models were used to develop the test requirements, including instrumentation specifications, collision speed and placement of high-speed cameras. The models also were used to estimate the results of the tests. In the future, they will be used to evaluate collisions over a range of closing speeds and collisions involving multiple-car trains.

The crashworthiness of rail vehicles has attracted the attention of the news media, the riding public, and the rail industry. Whenever there is a train crash, particularly a fatal one, the media tends to raise questions about the safety of rail travel. While rail travel is one of the safest modes of transportation, when several people are seriously injured or die in one catastrophic event, it can alter the public's perception of rail safety. The rail industry, including equipment manufacturers, suppliers and rail service operators, along with the FRA, all have a common interest in providing the safest rail transportation possible.

Other factors which have increased the attention on rail vehicle crashworthiness are 1) the introduction of high-speed rail service in the United States, 2) expanding passenger rail service, and 3) new equipment purchases by several commuter rail authorities.

In an effort to further improve the level of rail transportation safety, Congress passed the Federal Rail Safety Authorization Act in 1994 [1]. The Act legislated that the FRA and rail industry work collaboratively to develop regulations aimed at improving the safety of U.S.

passenger rail cars. One aspect of this comprehensive rulemaking was vehicle crashworthiness. As a result of the partnership between the Government and the rail industry, the Passenger Equipment Safety Standards; Final Rule, was published in May 1999 [2].

The Volpe National Transportation Systems Center, which is part of the USDOT, has been supporting the rulemaking activity by conducting research into rail equipment crashworthiness [3,4,5,6] which includes developing and applying computer simulations to provide a technical basis for the rules. Specifically, the models were used to estimate the behavior of both conventional and modified rail vehicles, and to estimate the forces and accelerations experienced by occupants, in a range of collision scenarios. Accident data and component and sub-scale test data were relied upon to develop the models, providing a level of assurance in the analysis results. Full-scale testing was required to establish the collision performance of existing equipment, and to evaluate and improve the fidelity of the models. Once the current vehicle performance is assessed, structural modifications will be incorporated and tested. The performance of modified vehicles can then be compared to the current vehicles, in order to measure the improvement in crashworthiness.

Conventional passenger rail equipment is generally built to a “strength-design.” That is, vehicles are built with essentially uniform longitudinal strength, designed to resist large forces. The effect in a collision is that the vehicles tend to crush from front to rear, crushing occupied and unoccupied areas indiscriminately.

Modifications to equipment design can be incorporated to improve a vehicle's crashworthiness. Unoccupied areas can be designed to crush at a relatively low force, thus absorbing collision energy while preserving occupied areas built to withstand larger forces. This concept is known as crash energy management, and can be used to pass crush back to

unoccupied parts of adjacent cars in a train, rather than imparting all or most of the damage to the lead car.

Before appropriate modifications can be designed and incorporated in conventional equipment, it is necessary to have a better understanding of how the conventional equipment performs in a collision. A series of three moderate speed, in-line collision tests have been planned to characterize the collision behavior of conventional equipment: 1) single car impacting a rigid wall, 2) two coupled cars impacting a rigid wall, and 3) a cab-car-led train colliding with a locomotive-led train.

The objectives of the single-car test conducted on November 16, 1999, [7,8,9] were to:

1) Measure the rigid body motion of the car.

2) Measure the force/crush behavior.

3) Observe the failure modes of major structural elements.

4) Evaluate the effectiveness of several occupant protection strategies.

The objectives for the two-car test conducted on April 4, 2000, [10,11,12] were the same as for the single-car test, with the added objective of learning more about coupled car-to-car interaction. The objectives for the train-to-train test (planned for November 2000) include all of the above, as well as observing the interaction between the colliding cars.

Head-on collisions were chosen in part to increase the repeatability, and thus, predictability of the tests. Being head-on collisions, the lateral and vertical motions were likely to be small, compared with the longitudinal motion. The results of oblique, or offset collisions would be susceptible to small changes in initial conditions and geometry features, reducing the repeatability and predictability of the tests, making model validation more difficult.

Moderate speed collisions were chosen to induce permanent deformation of at least 3 feet at the impacting end of the vehicle, enough to validate models with relatively large amounts of crush. Also, moderate speed collisions were sufficient to crush occupied areas of a passenger car and induce potentially severe or fatal secondary impacts for passengers. Tests of conventional equipment must be reasonably severe to potentially demonstrate an improvement in occupant safety when similar planned tests are conducted with modified, "crashworthy" equipment.

1.1. BACKGROUND

The idea of designing rail vehicles to better withstand collisions is not a new one. While trains have traditionally been built with functionality as the principal design objective, the need for crashworthy structures has been realized for many years. In a pamphlet published in the United Kingdom circa 1850, M.A. Garvey proposed "The Patent Spondyloid Life Train," which had the objective, "To secure perfect safety to passengers by railway on case of collision, by entirely dissipating the shock before it can reach the passengers…. by rendering it impossible for the carriages to mount over one another, to be thrown off the rails, or to be crushed together." A schematic of this train is found in Reference 13.

It was known that to improve the crashworthiness of rail vehicles, the absorption of kinetic energy must be controlled. In order to control energy absorption, the motion of the rail cars under impact conditions must be understood. Several studies have been performed in search of this understanding. A review of selected research endeavors will highlight noteworthy achievements toward the understanding of collision behavior. After reviewing what has been accomplished, it will become more apparent what next steps are necessary to further advance rail vehicle crashworthiness.

The mechanics of train collisions were studied by Pin Tong [14] in the 1970's. In the analysis, collisions were numerically simulated, and then compared to full-scale test data. The simulations consisted of a simple, lumped-parameter model, and a more detailed model using the finite element method. In the simple model, each car was modeled as one mass. The longitudinal stiffness between each car was represented by an elastic spring with constant value. The value for the spring was based on the cross-sectional properties of the center sill, which was the main structural member, running longitudinally down the center of the underframe. Because of the assumption of a constant stiffness, longitudinal force was proportional to the impacting velocity. The model compared favorably to a full-scale collision with an 18-mph impact speed.

The more detailed model was used to predict the results of a 30-mph full-scale collision. In this model, each car was represented by deformable beams, with mass and rotational inertia distributed at six nodes. With the higher impact speed, more collision energy caused more structural deformation and the simple model did not sufficiently represent the structure. This model compared favorably with the test data for an initial period of about 20 milliseconds, after which the data collection system failed.

This approach to crashworthiness analysis was applied by several groups in the 1970's [15,16,17]. Similar approaches are still followed today. However, advances in technology make it feasible to increase model complexity and fidelity tremendously. Theoretically, this should result in more sophisticated finite element and collision dynamics analyses, resulting in more accurate model results.

In 1980, a study was performed to increase the crashworthiness of rail transit vehicles [18]. An approach similar to Tong's was taken, in that a simple one degree-of-freedom model was developed, as well as a more detailed model. The detailed model was used to perform a

parametric study to determine which parameters were critical in accurately determining structural crush, override, and crush with subsequent override. An objective of the study was to improve impact control devices for transit cars.

In the detailed model, each car was represented by 6 masses with linear and rotational inertias. The masses were rigidly connected to elastic-plastic beams, which transferred shear loads between the underframe and the superstructure. This was a clever way to account for the strength and energy absorption capability of the less-strong side panels.

The force-deflection characteristics of every vehicle are unique, but there are industry standards and/or government regulations that specify minimum loading requirements. The loads are generally expressed as proof loads; i.e., loads incurred by the structure without permanent deformation. The loading requirements serve two purposes: to enable the structure to withstand service loads, and to protect crew and passengers in the event of an accident. Historically, the approach to accident survivability has been to simply make the structure very strong. However, this is not always the best way to make the vehicles crashworthy.

In a 1987 paper [19], A. Scholes of British Railways described the conflict between defining proof loads and improving vehicle crashworthiness. He proposed alternative methods to meet the basic goals of crashworthiness, one being to achieve a graduated, controlled response of the vehicle to increasing energy levels in collisions. He proposed that a distinction be made for each loading requirement purpose. Proof loads should be defined to meet service requirements, and energy absorption requirements should be defined to resist the effects of accidents.

Both the British and the French have studied and developed controlled energy absorption methods in train collisions, and have performed dynamic tests to validate the designs [20,21,22]. British Rail's approach was to specify acceptable consequences for collisions at increasing speeds. Acceptable consequences were defined as a given level of energy absorption for given collision conditions. Energy dissipation of 1 MJ (7.37E+05 ft-lb) and a permanent deformation of 1 m (3.281 ft), at each vehicle interface, were considered to be economic limits. The dynamic tests demonstrated that energy absorption can be distributed along a train, rather than being concentrated at the point of impact. Controlled energy absorption is now a requirement on all new vehicles built for use on the British railway system.

The FRA has sponsored a significant volume of work in vehicle crashworthiness over the last 10 years. The FRA's strategy has been to survey relevant accidents, propose methods for improving occupant survivability, and to apply analytic tools and testing techniques to evaluate the potential improvements. The categories of collisions addressed include in-line, oblique, and offset collisions, collisions involving locomotives and cab cars, grade crossing collisions, and collisions involving coupled car and colliding car override.

A 1995 FRA-sponsored study of in-line passenger train collisions proposed developing crush zone force/crush characteristics and occupant volume strength based on maximum acceptable deceleration levels in the occupied areas of the car [23]. Idealized characteristics were first developed, then applicable constraints on crush zone length and maximum occupant volume strength were applied. The FRA used results from this study as a technical basis to require specific levels of collision energy absorption in the high-speed trains currently being built for Amtrak's high-speed rail service on the Northeast Corridor, from Boston, Massachusetts to Washington, D.C.

A number of other studies also have been sponsored by the FRA [24,25,26,27,28]. These studies have covered a range of accident scenarios, from in-line and oblique collisions, as well as grade crossing collisions and train rollover incidents. Tests conducted have been component tests [29,30,31], sub-scale assembly tests [32], and full-scale car tests [7,8,9, 10,11,12]. The results are being applied to improve safety standards for the design of rail vehicles, which ultimately will result in safer trains and a reduction in occupant injury and fatality.

While a lot of testing and analysis has been performed in the last 20-30 years, incorporating the results into more crashworthy rail vehicles is a slow process. Rail vehicles typically have a life of 40 years or longer. With an average of roughly 100 new passenger rail cars purchased each year in the United States (as opposed to millions of new automobiles), new crashworthy features are not incorporated as easily or as quickly when compared to the automotive industry. The cost of a new rail car is approximately 50 times more than the cost of a new automobile. This cost ratio makes crash testing on the scale of the automotive industry out of the question. In terms of vehicle crashworthiness, the rail industry is currently where the automotive industry was about 20 years ago. However, the testing and analysis initiated by the U.S. Government and supported by the rail industry as part of the rulemaking effort, are resulting in significant crashworthy improvements in U.S. passenger rail cars.

2. MODELING APPROACH

During a multi-million dollar full-scale testing program, it would be foolish not to perform analytic modeling to guide the test implementation and to estimate the test results. When developing the test requirements for the aforementioned single- and two-car tests, several models were used collectively to gather information about the likely test outcome. The test parameters were then determined based on the desired test results. This Chapter describes the three-step modeling approach.

As an example, one objective of the test was to crush the impacting end of the car by approximately 3-5 feet, in order to validate models with large amounts of crush. Without performing any computational analysis, it would be difficult to determine an appropriate impact velocity that would result in 3-5 feet of crush. Another objective was to evaluate several occupant protection strategies. In order to evaluate the effectiveness of compartmentalization and lap and shoulder belts, it was desired to have a moderately severe secondary collision environment in which the strategies had a chance of being successful. Without pre-test analysis, it would be difficult to determine the impact velocity that would result in a secondary collision environment that is neither too benign nor too catastrophic.

The testing and the modeling were mutually dependent upon one another. The modeling was required to help determine the test parameters, and the testing was required to calibrate and validate the modeling. Test parameters to be determined included the impact velocity, the placement of accelerometers and strain gages, and the appropriate range of accelerometers to be used. The modeling enabled the observation of sensitivities to friction on the impact wall, slight perturbations in the direction of the impact force, the effect of having a coupler (or not) on the impacting car end, and the influence of the vertical car motion on the occupant trajectories.

The flow chart in Figure 2-1 illustrates the approach used by the Volpe Center to study rail vehicle crashworthiness. A finite element model of a single-car impact was used to provide initial estimates for the force/crush behavior of discrete nonlinear springs in the lumped-parameter, or collision dynamics model. A collision dynamics model of a single-car impact was then used to estimate the rigid body motion of the car, the force/crush behavior at the impacting end of the car, as well as the acceleration environment for interior occupant analysis. The 3-dimensional acceleration-time history calculated in the collision dynamics model was then used as input to the interior occupant analysis to measure the forces and accelerations experienced by occupants during such a collision.

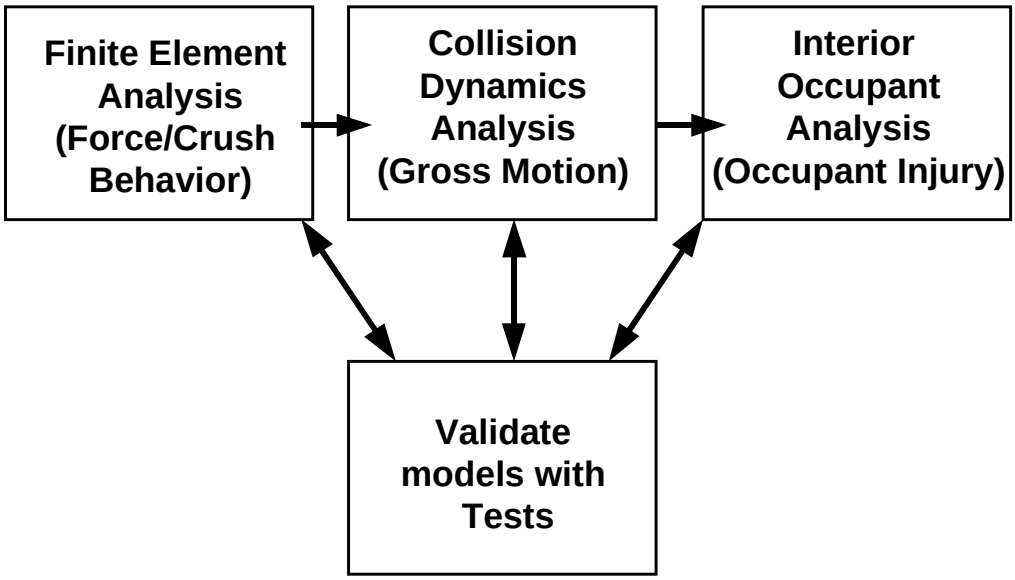

Figure 2-1. Modeling Approach

Being an iterative process, full-scale test measurements from the single-car test were used to modify parameters in the collision dynamics model to increase the fidelity of estimated behavior. A second car was added to the collision dynamics model to analyze the two-car test. Once data were available from the two-car test, the parameters of the impacting car were modified such that both models estimated the results of the respective

tests with reasonable accuracy. The validated models then could be employed to estimate crashworthiness behavior under collision conditions for which test data are not available.

There were advantages and disadvantages to both finite element and collision dynamics models. A detailed finite element model was necessary to estimate the force/crush behavior of a structure, but it was very costly to run in terms of model development and computational time. For example, the single-car finite element model used in this work took approximately 24 hours to analyze the first 0.5 seconds of the collision. Collision dynamics models are much more computationally efficient, but they rely on input from finite element models to define the force/crush behavior of the springs. The single-car collision dynamics model developed for this thesis took approximately 1 minute of computer time to analyze the first 0.5 seconds of the collision. The short run-time makes the collision dynamics model very useful for running a variety of cases, to analyze the influence of a variety of input parameters.

Before the full-scale tests were conducted, a previously developed detailed finite element model [27] was the best source of information available about the force-crush behavior of the vehicle end structure. The model represents an Amfleet car (see Figure 2-2), which is structurally very similar to the Pioneer cars tested. Both cars were designed and built by the Budd Company [33]. The geometry and materials of the primary longitudinal structural members, i.e. draft sill, center sill, side sills and roof sills are very similar in both the Amfleet and Pioneer cars. The finite element model did not account for the vertical suspension characteristics between the trucks and the car body, nor did it adequately account for the lateral forces between the wheels and the track. Lacking these details, the model was not capable of providing a reasonable estimate of the rigid body motion of the vehicle.

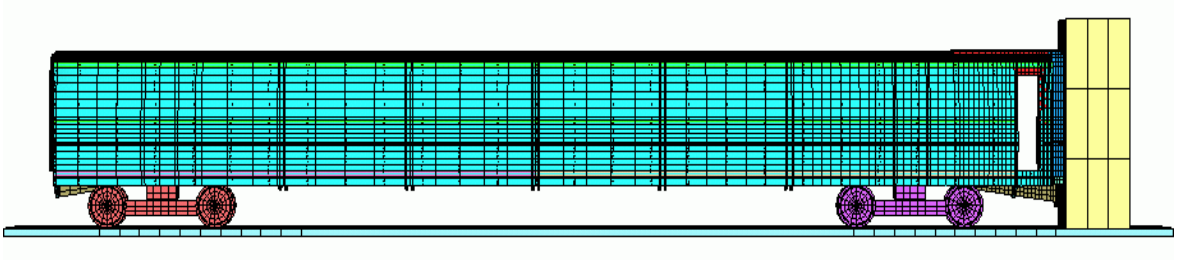

Figure 2-2. Finite Element Model

Figure 2-3 and Figure 2-4 schematically illustrate the primary longitudinal structural members of the car body. The draft and center sills provide the majority of the longitudinal strength. The side and roof sills and the body panels provide additional strength. The body bolsters are lateral members that reinforce the car body where the trucks are attached.

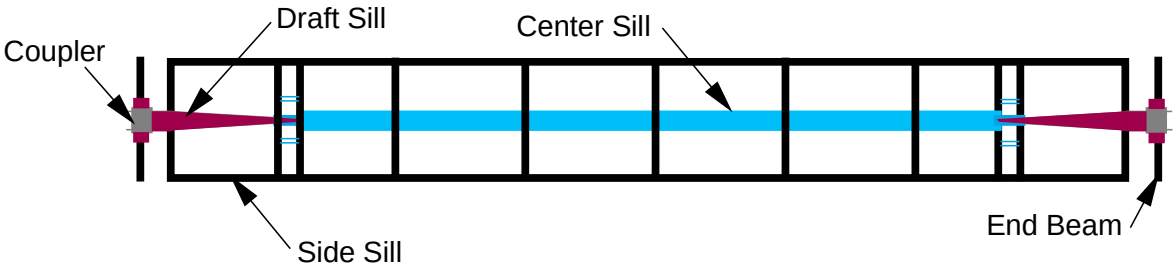

Figure 2-3. Plan View of Structural Underframe Members

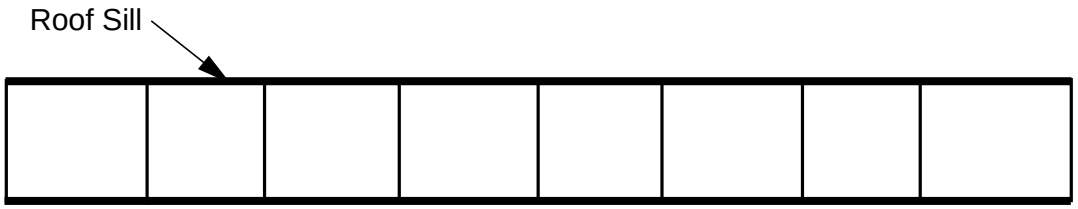

Figure 2-4. Plan View of Structural Roof Members

To perform the collision dynamics analysis, a number of tools could have been chosen. Equations of motion for a relatively complex system (four masses times six degrees of freedom, less a few constraints) could have been written and solved with a Fortran program or with a software program like Mathcad of Matlab. Ultimately, ADAMS was chosen. ADAMS is a software program from Mechanical Dynamics, Inc. [34] that enables a user to build a model and simulate the motions of a mechanical system. ADAMS was the

advantageous choice for the following reasons: 1) The equations of motion did not have to be written manually, 2) ADAMS models have been previously developed [25,26], which contain useful features like wheel/rail interaction forces and car body/truck suspension elements, that could be directly incorporated into a new model, 3) ADAMS can be linked with user-written subroutines to calculate forces, and 4) ADAMS has an IMPACT function that can be used to separate the initial rate-dependent impact force from the "steady state" crushing force.

The collision dynamics models developed in ADAMS are central to this thesis. The schematics in Figure 2-5a and Figure 2-5b represent the single-car and two-car models, respectively. The models were used to estimate the rigid body motion of the cars and the collapse of the vehicle structure during an impact with a rigid wall. The collision dynamics models use a series of discrete masses connected by non-linear springs and dampers. They run much more quickly than the finite element model and the force/crush behavior is more readily modified to better estimate the rigid body motion of the car during the impact tests.

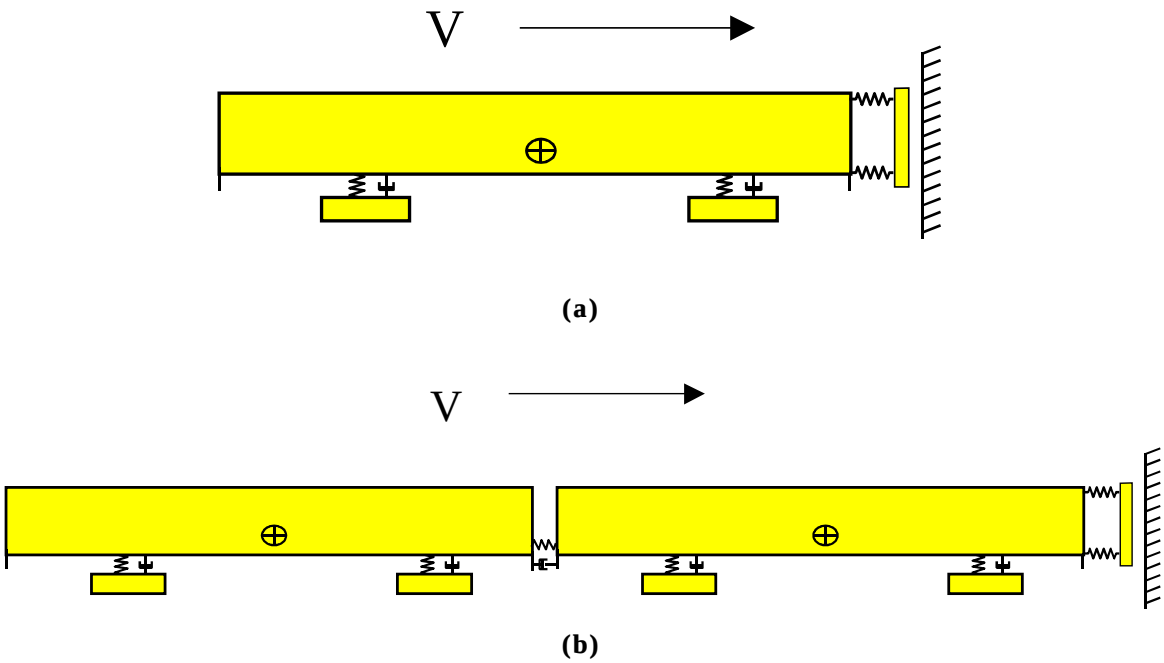

Figure 2-5. Schematic of Collision Dynamics Model

The impacting cars in both models were identical, and consisted principally of four rigid masses that represented the front portion of the vehicle, the trucks and the main car body. The trailing car in the two-car model did not have a separate mass representing the leading end of the vehicle, because little crush was expected between the two cars. The models were capable of 3-dimensional motion since each mass was allowed three translational and three rotational degrees of freedom. However, for this study the masses representing the front end and the main car body were constrained to translate longitudinally with respect to one another. For the in-line collisions analyzed with these models, the only significant relative motion anticipated between the front end and the main body was translational. The two masses were constrained to translate together in order to simplify the model. Non-linear springs and dampers that represent the crushable end structure, the truck/car body suspension, and the coupler, were used to connect the masses. For more information on the parameters used in the model, see Chapter 3 and Appendix F.

The car body accelerations calculated with the collision dynamics model were used as input to an interior seat/occupant model (Figure 2-6). This model also used as input the force-deflection behavior of passenger seats that had been previously calculated during static tests [30,31]. Using the interior dynamics model, the forces and accelerations experienced by occupants in a collision can be estimated. Using these forces and accelerations, injury criteria for the head, neck, chest and femur can be calculated. The injury criteria can be used to evaluate and compare the level of protection provided to occupants under different collision conditions.

A three-step approach used to analyze rail vehicle crashworthiness has been described. The material in this thesis focuses primarily on the middle step, the collision dynamics

modeling. The details and the results of the finite element and the interior seat/occupant models are not included in this work.

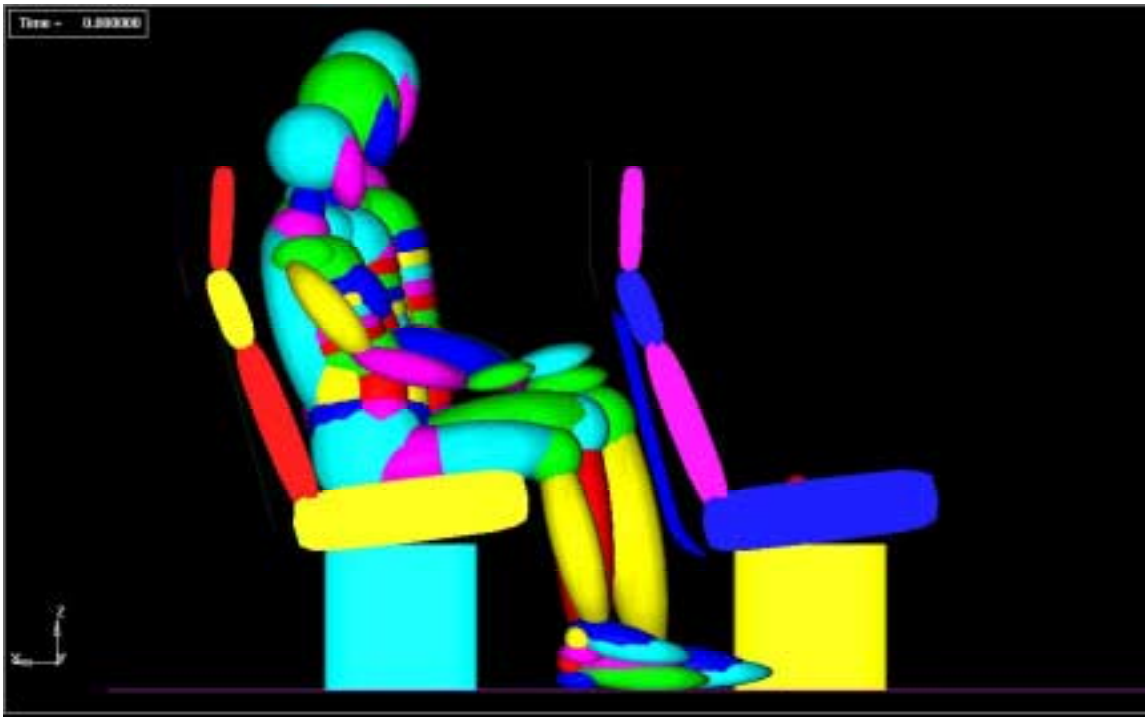

Figure 2-6. Interior Seat/Occupant Model

3. MODEL DESCRIPTION

3.1. MODELING ISSUES

The collision dynamics models were designed for a specific set of collision conditions. The applicable scenarios include in-line, frontal collisions with a rigid wall, at speeds up to approximately 50 mph. In these collision scenarios, the damage is expected to be limited to the 12-foot car length between the front of the car and the body bolster. The model does not realistically account for structural crushing beyond the front body bolster, but could be modified to do so without much difficulty.

Clearly, in-line collisions are less complicated than offset or oblique collisions. That is precisely why the first series of tests are restricted to in-line collisions – to minimize the uncertainty in the outcome of the collision. Another series of full-scale tests are tentatively planned to investigate the behavior of a passenger car when the primary structural members, i.e., the draft sill/center sill are not loaded directly. These models were developed such that they could be readily adapted to simulate oblique collisions in the future. For example, five collision springs were defined to represent the two side sills, two roof sills and the draft sill, even though the masses were constrained such that all five springs had the same deflection. One spring could have been used to represent the collection, but having the corners and center sills defined separately will makes the model more easily modified to analyze impacts at the corners.

While there was expected to be some vertical and lateral motion in the in-line collisions, the dominant force was expected to be longitudinal. The model can be used to estimate the vertical and lateral motion resulting from in-line, frontal collisions, but it was not meant to be applied in collisions where the principal forces are in the lateral or vertical direction. The model is designed to handle collision forces at the front end of the car, but not from the side

or the top. To model side impacts, the model would need to be modified to incorporate impact elements and springs based on the force/crush behavior at the point of impact. Also, the lateral and vertical connection between the trucks and the car body would need to be modified to handle the potentially extreme forces between the two masses.

During in-line collisions, vertical motion develops when the longitudinal collision forces are offset vertically from the center of gravity (CG) and consequently the car body bounces and pitches on its secondary suspension. Due to the long, slender geometry of a rail car, small angles of rotation can lead to significant vertical and lateral forces. Once vertical motion is initiated, it can lead to car-to-car override, especially between colliding cars. The models can be used to estimate the vertical motion during an in-line collision.

Similarly, small car body yaw angles can lead to lateral buckling of the cars within a train. In the model, small perturbations in the direction of the longitudinal force are used to develop car body yaw, and hence lateral forces. By modestly varying the direction of the collision force, the model can be used to bound the range of anticipated lateral motion.

3.2. MODELING FEATURES

Two models were developed as part of this thesis – a single-car model and a two-car model. The single-car model was developed from scratch, its principal features being the crushable end structure and the method of impact with the wall. In order to extend the model to analyze the two-car test, a second car was added. The second car was taken directly from a lateral buckling train model previously developed by Robert Rancatore of Arthur D. Little, Inc. (ADL), in support of the Volpe Center [25]. This car did not have a crushable end structure, but it did have a coupler element to transfer collision forces from the leading car to the trailing car, and lateral and vertical force elements representing the wheel/rail contact.

There were minor parameter differences between the first and second cars, such as masses and inertias, CG locations, truck/car body suspension, etc. The car body mass was set equal to the mass of the car tested. The inertias from the second car body were scaled accordingly and applied to both cars. The wheel/rail contact forces from the second car were also applied to the first car. The suspension definition of the second car was modified slightly and applied to the first car. The modified parameters of the lead car in the two-car model were also applied to the single-car model, such that the impacting cars in both models were identical.

The impacting car in the single- and two-car models consists of six masses, representing the main car body, two trucks, front end plate, and front and rear coupler masses that transfer impact forces from the coupler to the main car body (see schematic in Figure 2-5). Each mass has six degrees of freedom, with the exception that the end plate is constrained to translate longitudinally with respect to the main car body, forcing the displacement, or crush, in each of the springs to be identical. The constraint simplifies the model, which is appropriate when modeling in-line collisions. There is expected to be little if any angular motion between the front plate and the main car body. The front and rear coupler masses were originally used in the ADL model to distribute a portion of the main car body mass to approximate the mass of material crushed in a collision, and have been retained in the current model. The trailing car in the two-car model has only five masses – it does not have the front end plate.

The secondary suspension characterization between the trucks and car bodies has been taken from the ADL model. The stiffness and damping values were modified in accordance with suspension data provided on the type of trucks used in the test [35]. The secondary suspension in the model is a combination of spring and damper elements that are linear for small displacements and represent compression and extension stops for large displacements.

These elements transmit forces between the car bodies and trucks in the lateral, longitudinal and vertical directions. Each truck has elements to transmit vertical and lateral forces to the rails, one for each rail. These elements have been taken directly from the ADL model.

In order to model the single-car and two-car impact tests, the following items had to be represented:

- Car-to-Wall Interaction,
- Force/Crush Behavior,
- 3-Dimensional Rigid Body Motion, and
- Car-to-Car Interaction.

3.2.1. Car-to-Wall Interaction

In both models, the collision forces between the car and the wall were characterized using a sphere-to-sphere IMPACT function. The IMPACT function defines the magnitude of the force, based on sphere penetration. The sphere-to-sphere contact defines the direction of the force; i.e., the force acts along the line that connects the centers of the spheres. In ADAMS, the IMPACT function generates an elastic restoring force based on Hertz contact when the colliding spheres try to penetrate one another. The IMPACT force has both stiffness and damping components associated with it. The stiffness coefficient, k, is a function of the penetration between the two spheres. The damping coefficient, c, is a function of the speed of the penetration. This feature allows some degree of separation of the velocity-dependent “transient” forces and the “steady-state” collision forces calculated with the subroutine.

The impact wall is represented by a rigidly-fixed sphere that has a radius of 100 feet, such that the impact surface approaches a flat plane, as in the tests. The coupler at the impacting end of the car is represented by a sphere that has a radius of 0.5 feet. The coupler

sphere is rigidly attached to the front end plate, representing the front face of the car body. The IMPACT force acts along a line that connects the centers of the spheres. The motion of the coupler sphere relative to the wall sphere determines the direction of the IMPACT force acting on the car body.

3.2.2. Force/Crush Behavior

The impact forces are transferred from the coupler/front plate to the main car body via five non-linear, longitudinal springs in parallel. These springs represent the force/crush behavior of the draft sill, two side sills and two roof sills. A user-defined subroutine has been written to determine the spring forces at each time step (see Appendix E for a listing of the subroutine). The subroutine keeps track of the current and maximum spring displacement. When unloading, the force in the springs follows the initial slope downward. If the springs are subsequently reloaded, the force will follow the initial slope back up, then continue where it left off along the prescribed force-crush curve.

Figure 3-1 is a schematic of the assumed force/crush behavior of the main longitudinal structural members. The force/crush values at each break point for each spring, which are defined in the user-defined subroutine, are listed in Table 3-1. A large initial force is required to initiate buckling/crushing of the draft sill, after which the force to continue crushing the structure drops off substantially. After about 1 foot of crush of the coupler/draft sill, the car body makes contact with the wall. An increase in the collision force is required to initiate crushing of the side sills, roof sills and body panels. Once buckling is initiated, the force drops off again. The majority of the strength of the end structure comes from the draft sill. The side sills and roof sills carry a smaller portion of the load.

The percentage of the load carried by the draft sill was originally estimated using the single-car finite element model. Two models were exercised: one of the entire car body, and one of just the draft sill. The force vs. crush behavior resulting from an impact with a rigid wall was calculated and compared (see Figure 3-2). Roughly 80% of the energy dissipated by the entire vehicle during the first foot of crush was dissipated by the draft sill alone. The coupler, which transmits the impact force to the draft sill, extends about a foot beyond the end of the car body, thus it initially carries most of the load. After the first foot of crush, the sills and body panels began to carry a percentage of the total load.

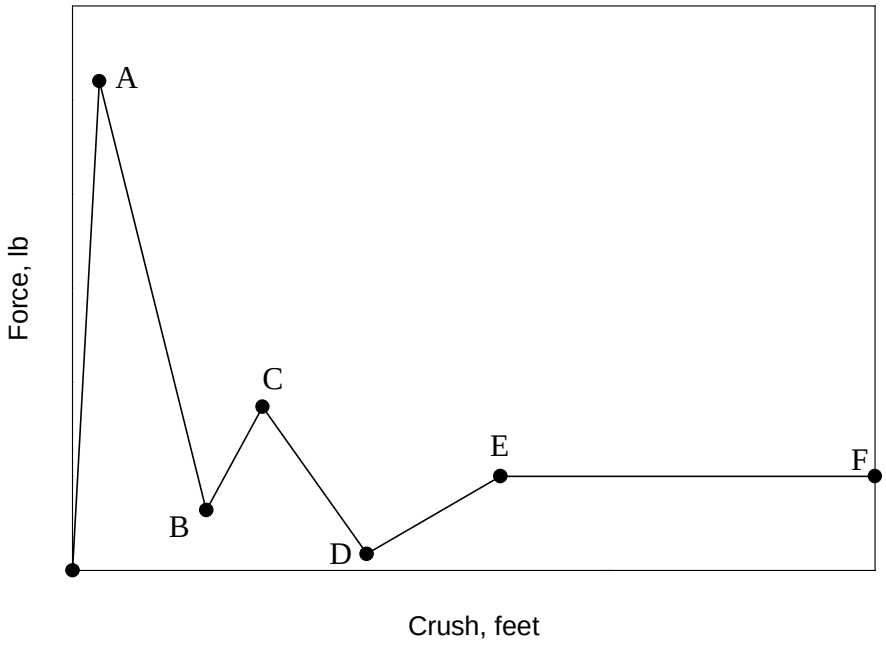

Figure 3-1. Schematic of Longitudinal Force/Crush Behavior of Collision Springs

Table 3-1. Force/Crush Values for Collision Springs

Point in Figure 3-1	Crush, feet	Force, lb		
		Draft Sill	Side Sill	Roof Sill
A	0.1	2.6E+06	0	0
B	0.5	3.2E+05	0	0
C	0.71	6.7E+05	6.667E+04	3.33e+04
D	1.1	5.8E+04	1.0E+04	5.0+03
E	1.6	3.5E+05	5.0E+04	2.5+04
F	10	3.5E+05	5.0E+04	2.5+04

The magnitude of the force for each of the five springs was determined such that the results of the collision dynamics model approximated the test results in terms of force versus crush. Since no direct measurement was made of the force on the wall, the force between the car and the wall was estimated as the product of the total mass of the car and the acceleration of the CG. The crush was estimated as the displacement of the CG of the car. See Appendix A for more detail.

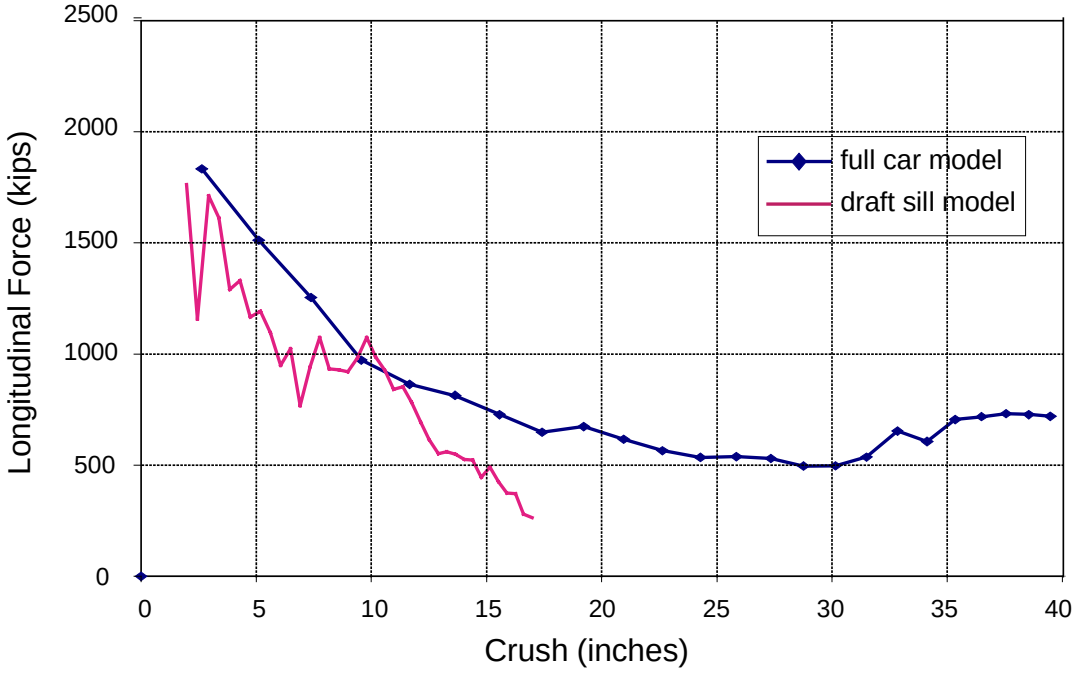

Figure 3-2. Force/Crush Behavior for Full Car and Draft Sill Only

3.2.3. Three-Dimensional Rigid Body Motion

The longitudinal motion was governed by the IMPACT function, the collision springs, and the coupler (in the two-car model only). To account for the vertical motion, a flexible truck/car body suspension was defined which allowed the car body to bounce and pitch. Also, depending upon the height of the coupler sphere relative to the car body CG, a moment due to the impact force could potentially contribute to the vertical motion. The lateral motion in the two-car test was captured by defining a small lateral perturbation in the direction of the

impact force, which was resisted to some extent by the lateral wheel/rail forces. There was not significant lateral motion in the single-car test.

3.2.4. Car-to-Car Interaction

The car-to-car interaction in the two-car test was captured in the definition of the coupler. The coupler was effectively a rigid pin that was attached to each car by a spherical joint. The ends of the pin could also translate longitudinally with respect to the cars. Longitudinal, lateral and vertical forces were transferred from the lead car to the rear car via the coupler.

Table 3-2 is a list of the centroidal mass and principle mass moments of inertia that were prescribed to represent the bodies of the leading passenger car in the two-car model. These values were adapted from the ADL model. Prior to the single-car test, a series of "shake-and-bake" tests were conducted with the test vehicle to estimate the CG height of the vehicle and the roll, pitch and yaw inertias [7]. The CG height of the car body was estimated to be between 69.7 and 76.7 inches from the top of the rail. The CG height of the car body in the model was 69.36 inches. The roll, pitch and yaw inertias were considerably larger (~50%) than the values used in the ADL model, which compare reasonably well with $\frac{1}{12} \cdot m \cdot l^2$ for the pitch and yaw inertias, assuming the car body is similar to a long slender rod. Because of the uncertainty in the test data, the inertia values from the ADL model were not modified based on the test data.

Table 3-2. Vehicle Parameters

Component	Mass, lb	I_{xx}, lb-ft^2	I_{yy}, lb-ft^2	I_{zz}, lb-ft^2
Main Car Body[1]	3.5579E+04	9.67E+05	2.22E+07	2.245E+07
Trucks	1.37E+04	3.55E+04	1.08E+05	9.28E+04
Front End Plate	2.252E+03	9.62E+04	4.75E+04	4.89E+04
Front Coupler/Draft Sill Mass	3.748E+03	10	10E+03	10E+03
Rear Coupler/Draft Sill Mass	6.0E+03	10	10E+03	10E+03

3.3. SUMMARY

The features and parameters of the models have been described in this section. (For additional information on model details, see Appendix F for a selected listing of the command file for the single-car model.) The models are capable of estimating force/crush results and rigid body motion during in-line frontal impacts of passenger rail vehicles. Before the model results are compared with the test results, a parametric analysis of critical modeling parameters examines the sensitivities of the models to variations in these characteristics.

[1] The main car body mass and inertias were scaled down such that the total vehicle mass was approximately equal to the mass of the vehicle tested in the single-car test. Originally the test vehicle weighed about 100,000 lb. However, the total weight was reduced when the interior seats and some auxiliary equipment were removed. To partially compensate, about 10,000 lb of concrete was poured under the floor, resulting in a total car weight of 74,289 lb.

4. PARAMETRIC ANALYSIS WITH SINGLE CAR

A significant number of physical car body parameters needed to be defined for the collision dynamics model to properly estimate the rigid body motion during impact. These parameters included geometry (length, height, width, CG height), masses and inertias (for the car body, trucks, front end, coupler), and vertical location of the impact sphere. The spring and damper characteristics for the truck suspension, coupler, and crushable end structure of the car also had to be estimated. The total vehicle mass and some geometry components were the only parameters that could be measured easily and with certainty. Consequently, assumptions were required to assign reasonable values to the other parameters.

Parametric studies were performed with the simpler single-car model to evaluate the sensitivity of the results to changes in various input parameters, which provided a level of assurance in the quality of the values chosen. The values used in the single-car model that best approximated the test results were considered the “baseline” values. Varying one parameter at a time provided a snapshot of the sensitivity to variations in each parameter. It was not practical to modify every possible parameter. The following parameters were modified and evaluated:

- IMPACT function parameters k, c, and m,
- Vertical location of impact sphere,
- Force/crush characteristic of collision springs, and
- Impact velocity.

The IMPACT function parameters were selected because they have a significant influence on the calculated force on the wall, plus there was little information on which to base the initial estimates. The vertical location of the impact sphere was chosen because a

significant amount of vertical motion was observed during the tests, and the average vertical location of the impact force may have had a large influence on the vertical motion of the car body. The collision springs were chosen because the values used to approximate the test data were quite different from values used in previous collision models. Finally, impact velocity was chosen to determine if the model could be expected to provide reasonable results for a wider range of impact speeds.

4.1. IMPACT FUNCTION

The IMPACT function had several parameters associated with it, but the values for k, c, and m were estimated to be the most critical and least certain. Initially, the IMPACT function stiffness and damping coefficients, k and c, developed in the ADL model were used to govern the car body impact with the wall. These values were then modified in order to get better model agreement with the full-scale test data. Subsequently, a parametric analysis was performed to evaluate the sensitivity of the model results to variations in k, c, and m, the mass of the impact sphere, and to establish criteria to determine appropriate k, c, and m values in lieu of test data.

In addition to the stiffness and damping coefficients, the mass of the coupler sphere/front plate also had an effect on the force acting between the impact spheres. The mass of the coupler sphere was chosen rather arbitrarily to be 70 slugs, or 2,252 lb. The sensitivity of the sphere-to-sphere force to variations in the coupler sphere mass was also investigated.

In the parametric analysis, the values for k, c, and m for the sphere-to-sphere impact function were modified one at a time as outlined in Table 4-1. The highlighted values were used as the baseline values when another parameter was being modified. The results used to compare the effect of the IMPACT parameter variations were 1) the force acting between the

spheres, and 2) the force acting on the entire vehicle, estimated by the total vehicle mass multiplied by the longitudinal acceleration at the center of gravity of the main car body.

Both forces were plotted as a function of spring crush at the lead end of the car. These two curves were then integrated to calculate the energy dissipated, which was then compared with the total kinetic energy, i.e. $\frac{1}{2}mv^2$. These energies are presented in a bar graph/table format, as it is only a single value that is of interest. The force/crush curves, however, illustrate that there is more than a single value to match than just energy, i.e., the force peaks, the crush associated with those peaks, the high-frequency oscillation, etc.

Table 4-1. Impact Parameter Variation

Parameter	Case 1	Case 2	Case 3	Case 4
K, lb/ft	6.0E+05	6.0e+06	6.0e+07	6.0e+08
C, lb-s/ft	2.0E+03	2.0E+04	2.0E+05	2.0E+06
M, lb	1.0E+03	2.252E+03	3.0E+03	4.0E+03

The bar graphs in Figure 4-1 through Figure 4-3 illustrate the influence of the respective parameters on the energy dissipated during the collision. The coupler mass, m, and the damping coefficient, c, did not have a significant effect on the energy dissipation based on the force calculated with either method. However, the stiffness coefficient, k, did have a large effect on the energy dissipated by the non-linear collision springs. A relatively small stiffness coefficient (Case 1) allowed the collision spheres to penetrate one another by over 2 feet. Energy was absorbed elastically by the spheres, which prevented the transfer of collision energy to the collision springs. As the value of k was increased, the collision spheres were effectively more rigid, allowing minimal penetration and transferring more energy to the collision springs. If k was too large, the spheres became too rigid, which created a chattering effect.

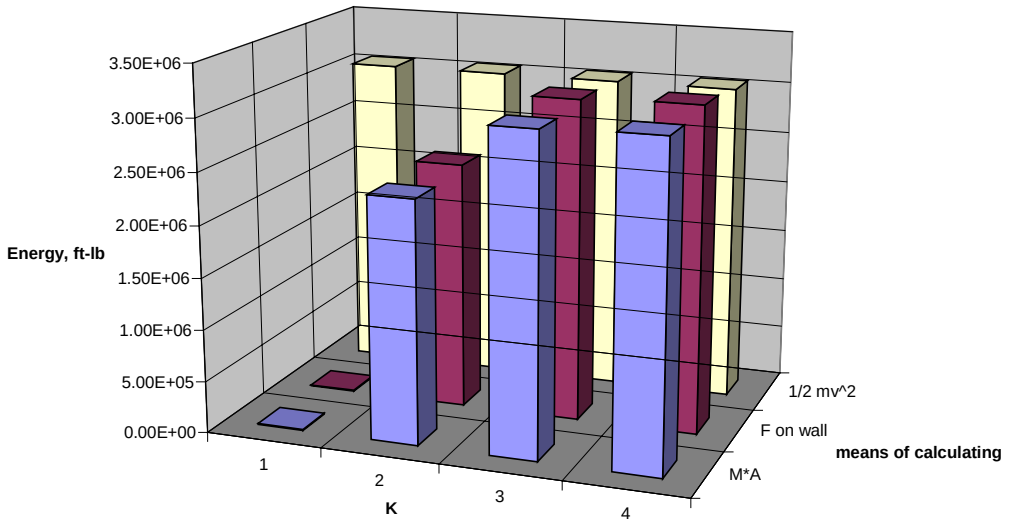

	1	2	3	4
M*A	9.96E+03	2.34E+06	3.06E+06	3.09E+06
F on wall	8.83E+03	2.39E+06	3.10E+06	3.13E+06
1/2 mv^2	3.06E+06	3.06E+06	3.06E+06	3.06E+06

M*A F on wall 1/2 mv^2

Figure 4-1. Influence of K on Energy Absorbed

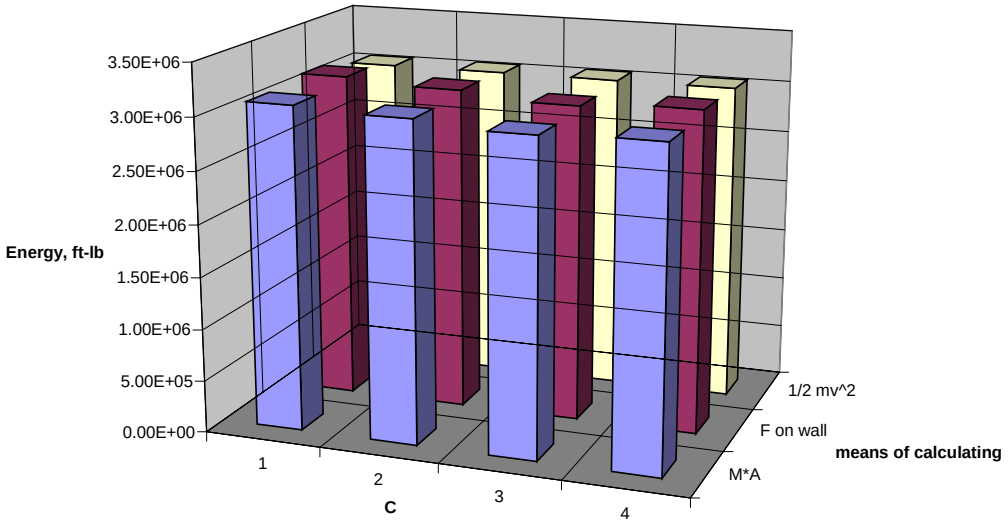

	1	2	3	4
M*A	3.10E+06	3.06E+06	3.00E+06	3.03E+06
F on wall	3.15E+06	3.10E+06	3.03E+06	3.08E+06
1/2 mv^2	3.06E+06	3.06E+06	3.06E+06	3.06E+06

M*A F on wall 1/2 mv^2

Figure 4-2. Influence of C on Energy Absorbed

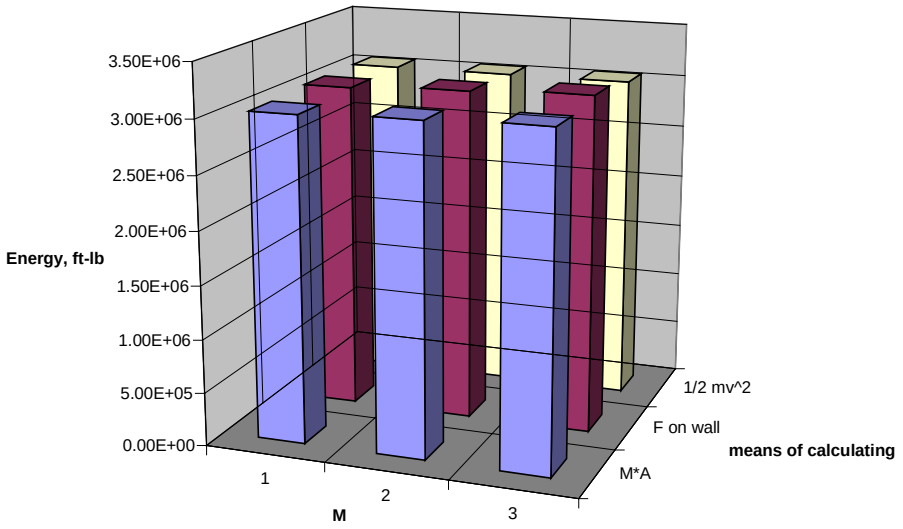

	1	2	3
M*A	3.03E+06	3.06E+06	3.09E+06
F on wall	3.06E+06	3.10E+06	3.14E+06
1/2 mv^2	3.06E+06	3.06E+06	3.06E+06

Figure 4-3. Influence of M on Energy Absorbed

Varying either the damping or the mass, as indicated in Table 4-1, had a modest effect on the amount of crush at the end of the car (less than 7% variation for the cases considered). Varying the stiffness had a large influence on the amount of car crush (nearly 100% variation for the cases considered), because the impact force did not get transferred properly to the collision springs when the stiffness coefficient was too small (i.e., below ~ 1.0E+07).

The influence of the variation of the mass or the damping on the equivalent force (see Appendix A for a description of equivalent force) was not very significant (see Figure 4-4 and Figure 4-6). However, the force in the IMPACT element was quite sensitive to the variation in c and m (see Figure 4-5 and Figure 4-7), even though the integral of the IMPACT force vs. the spring crush did not change significantly. The IMPACT force oscillated significantly when the damping coefficient was too low, i.e., less than 2.0E+04 lb-s/ft, or if the mass was too small, i.e., less than 1.5E+03 lb.

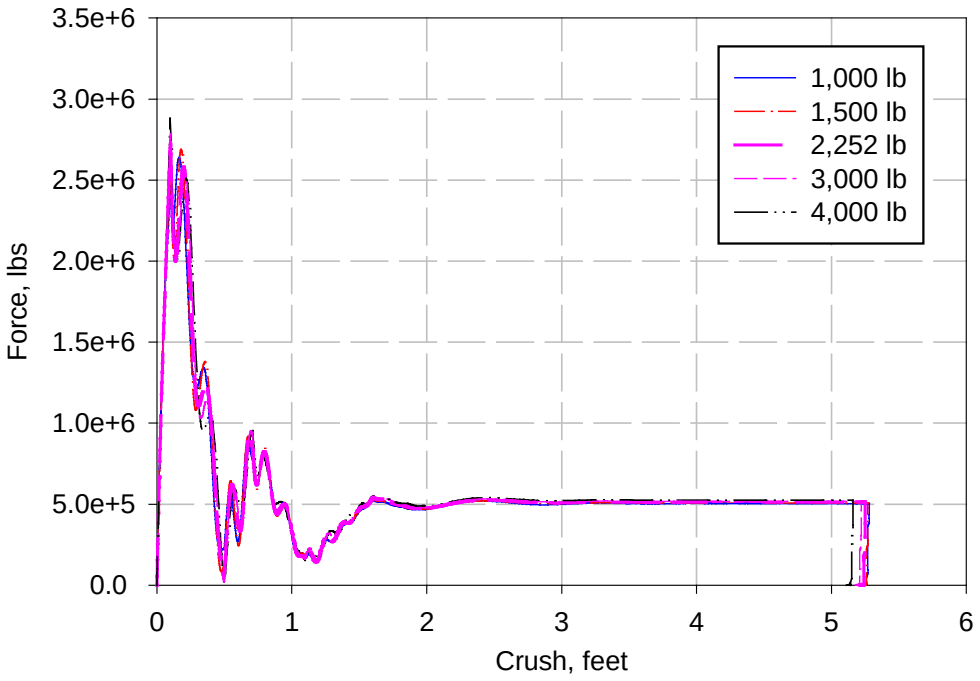

Figure 4-4. Influence of Variation of M on F=M*A vs. Crush

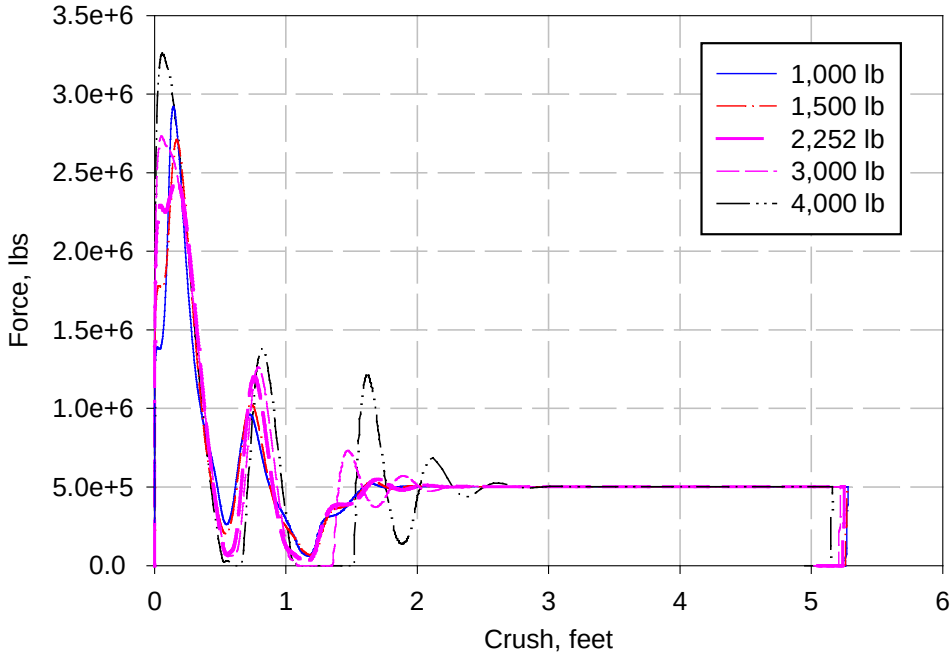

Figure 4-5. Influence of Variation of M on Force in Impact Element vs. Crush

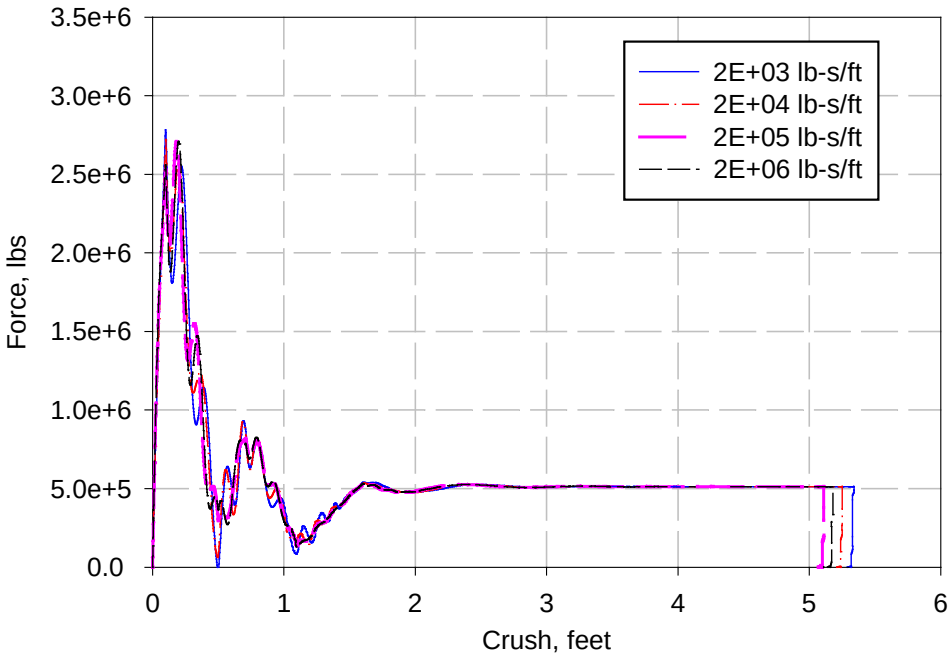

Figure 4-6. Influence of Variation of C on F=M*A vs. Crush

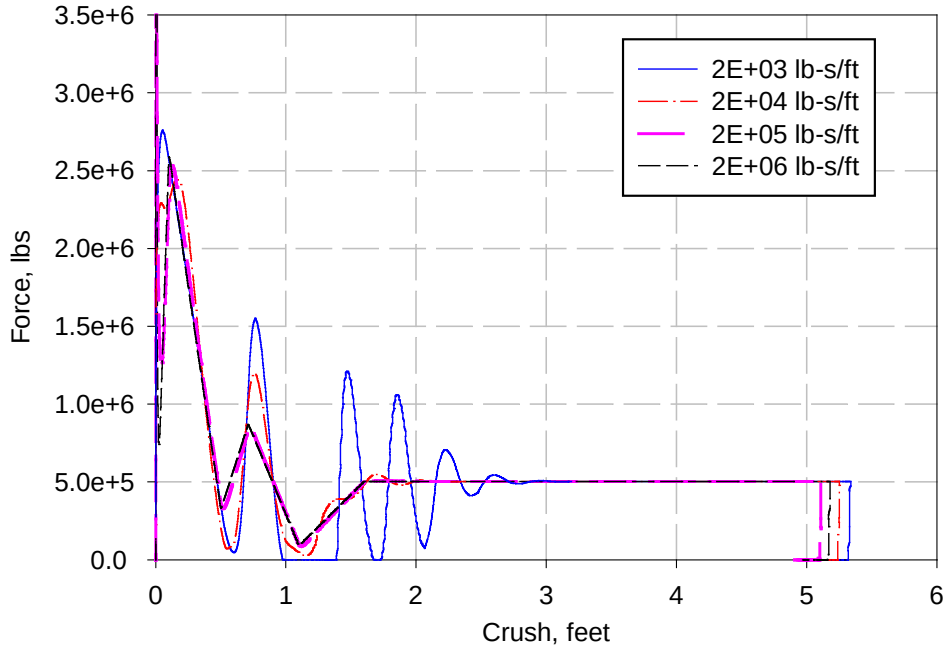

Figure 4-7. Influence of Variation of C on Force in Impact Element vs. Crush

The variation of the stiffness coefficient had a small influence on the equivalent force (see Figure 4-8). However, the force in the IMPACT element was fairly sensitive to variations in

k (Figure 4-9), even though the integral of the IMPACT force vs. the spring crush did not change significantly. The IMPACT force oscillated significantly when the stiffness coefficient was high, i.e., greater than 6E+07 lb/ft.

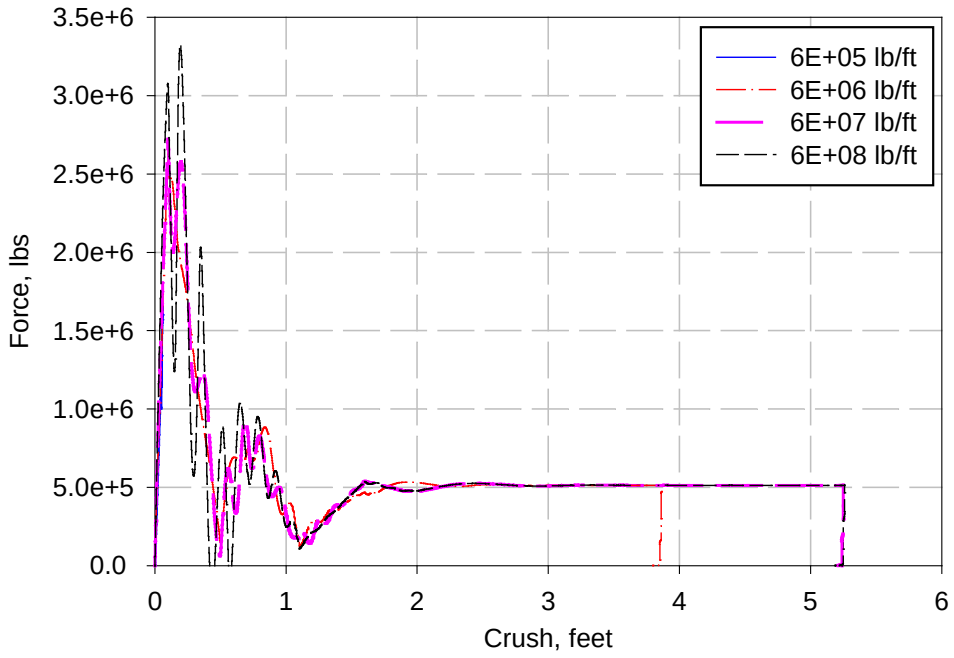

Figure 4-8. Influence of Variation of K on F=M*A vs. Crush

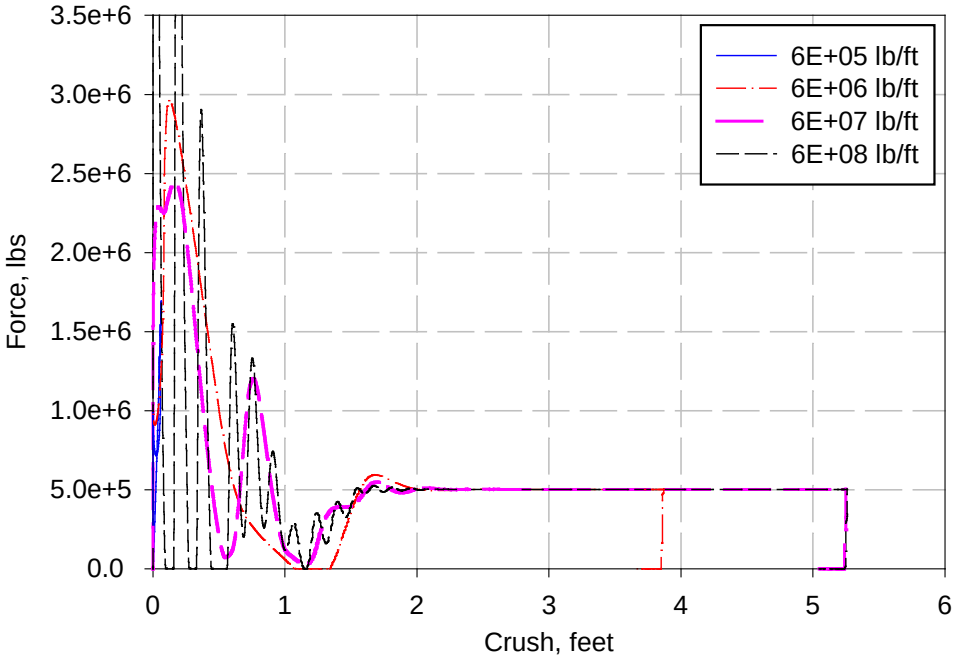

Figure 4-9. Influence of Variation of K Force in Impact Element vs. Crush

4.2. LOCATION OF IMPACT SPHERE

In addition to the IMPACT function parameters, the vertical location of the impact sphere on the front of the car also had an effect on the transfer of collision forces to the vehicle. In both full-scale tests, the tendency of the impacting end of the lead car to dip slightly, then rise about 6 inches was observed. The vertical location of the impact sphere was varied within a reasonable range to observe if that alone was sufficient to cause the vertical motion observed.

If the impact point is below the car's center of gravity, the impact will induce a pitching moment that acts to push down the lead end of the car. If the impact point is above the CG, the car will pitch upwards. In both tests, the cars pitched downward initially, when the contact was between the coupler and the wall. As the coupler was pushed backward and contact occurred between the front face of the car and the wall, the car began to pitch upward, resulting in a vertical displacement of about 6 inches at the end of the car.

To evaluate the sensitivity of the vertical car motion to the height of the impact sphere, two additional computer runs were performed with the single-car model. In the baseline model used to estimate the test results, the height of the sphere was 3.725 feet above the rail. This was approximately the height of the coupler, which was the first part of the car to make contact with the wall. In the two additional runs, the height was raised by 2 and 4 feet, respectively. To illustrate the effect on the rigid body motion, the vertical displacement of the lead end of the car and the CG of the car were plotted in Figure 4-10 and Figure 4-11, respectively.

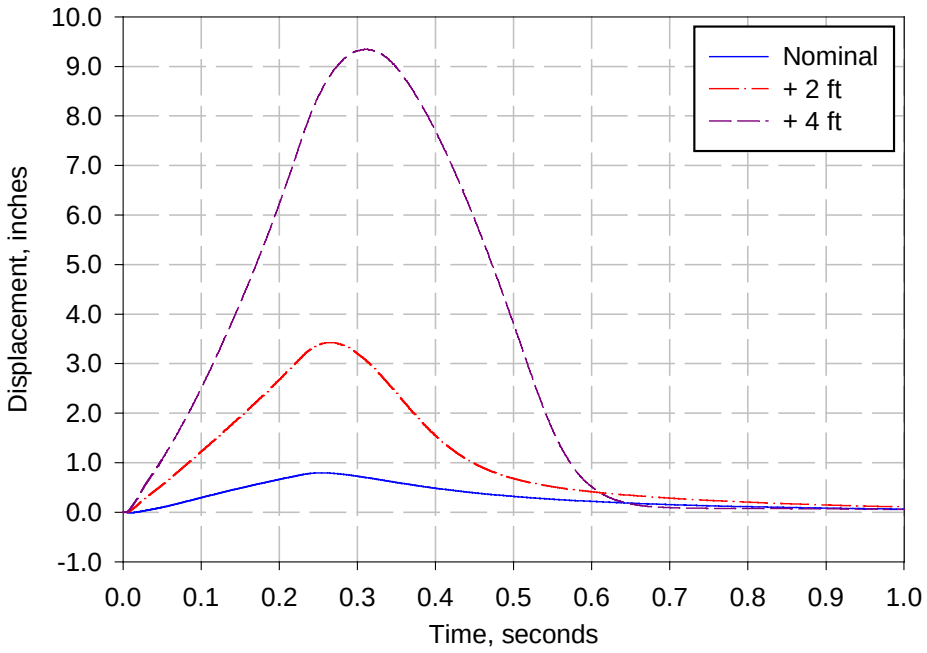

Figure 4-10. Vertical Displacement Time Histories of Front End, Based on Vertical Position of IMPACT Sphere

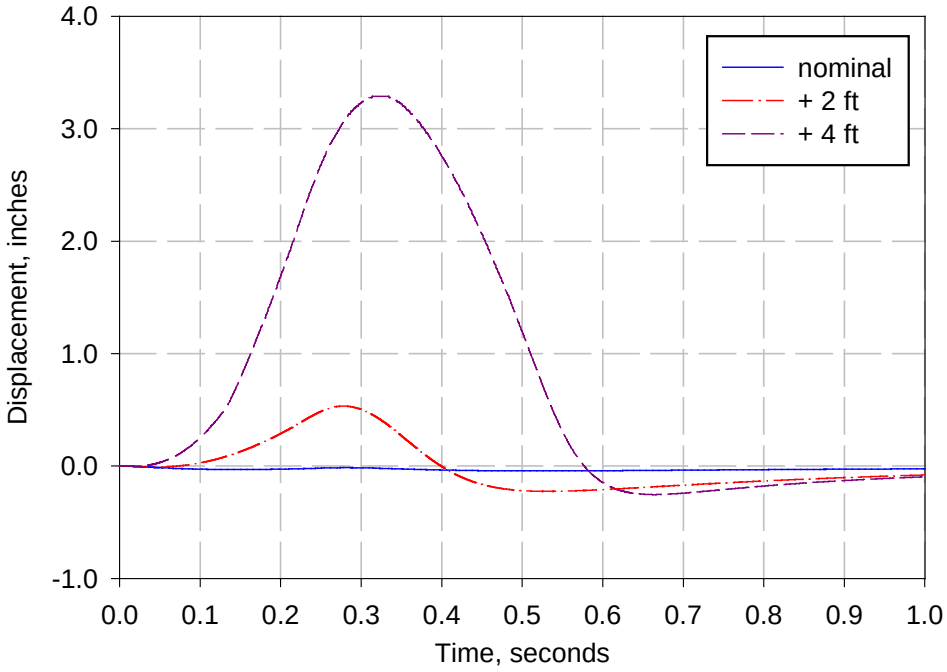

Figure 4-11. Vertical Displacement Time Histories of CG, Based on Vertical Position of IMPACT Sphere

With the impact sphere in the nominal location, i.e., at the coupler, the end of the car was raised by almost an inch. By raising the contact point by 4 feet, which placed the contact approximately in the middle of the front face of the vehicle, the end was raised by nearly 10 inches, which is similar to what happened in the tests. The model could be improved by incorporating two impact spheres, one at the coupler, and one near the middle of the impact surface of the car body, to more accurately position the location of the contact between the car and the wall.

4.3. COLLISION SPRINGS

The force/crush behavior for the collision springs was originally developed based on results from the finite element model of a single passenger rail car [27]. The force/crush behavior of the full car and the draft sill alone were simulated and used to approximate the strength of the draft sill, side sills and roof sills. Dynamic test results of the end beam/side sill assembly [29] were also used initially to estimate the force/crush behavior at the bottom corners of the car.

The force/crush behavior of the collision springs was modified once data were available from the single-car and two-car full-scale tests (see test results in Chapters 5 and 6). It was expected that because the cars tested were not designed to crush in a controlled fashion, identical tests would not have repeatable results. While the models were based on data from two tests, similar subsequent tests might indicate different force/crush results. In order to investigate the effect of different spring behavior, three separate cases were considered in the collision spring parametric evaluation. In each case, the force/crush results were compared with those calculated with the spring characteristics that were validated against the test data. In all plots, the force was represented by the total vehicle mass multiplied by the longitudinal acceleration at the center of gravity of the car body. Both the baseline and

modified forces were plotted as a function of the crush of the collision springs at the lead end of the car.

The results of the parametric study on collision springs was also intended to show that it is possible to get the same maximum crush and energy dissipated for many different input force/crush definitions.

4.3.1. Strengthened Side Sills

The side sill springs contributed a relatively small portion of the total car's crush resistance. The steady force in the baseline side sill spring definition was 50,000 lb. In this study, the steady force was increased to 100,000 lb. The force during the first foot of crush was not changed. In a typical passenger car, there is roughly a 3-foot break in the side sill, designed to accommodate a stair well. This interruption significantly decreases the yield load at the bottom corner of the car. The purpose of this study was to approximate the difference in the force/crush behavior of the entire car body when the side sill is interrupted, compared to a continuous side sill.

Since there are two side sills, the steady force is 100,000 lb greater for the case with strengthened side sills, which results in nearly a foot less crush of the end of the vehicle (see Figure 4-12). This result illustrates the possibility of design changes that could reduce the maximum crush, or intrusion into occupied areas, without adversely affecting the initial peak acceleration of the vehicle.

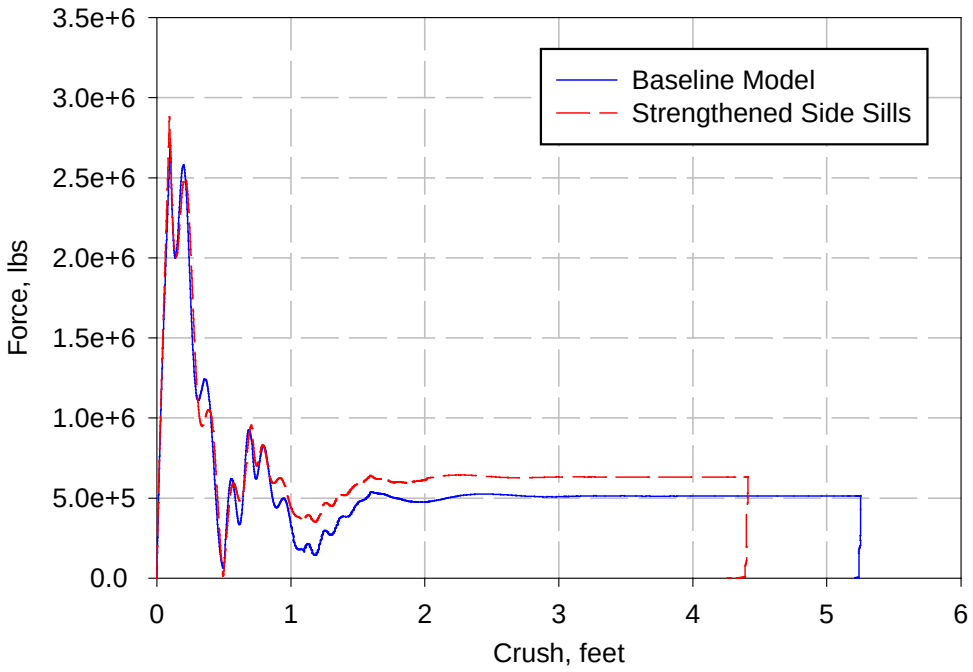

Figure 4-12. Force/Crush Results with and without Strengthened Side Sills

4.3.2. Conventional Car Force/Crush Behavior

Figure 4-13 shows the "conventional" car force/crush behavior used in an earlier analysis of longitudinal train-to-train collisions [23]. The conventional force/crush behavior was developed by Calspan for the Silverliner car [36], modified to allow for a shear-back coupler design and a more gradual crushing of the end structure. This force/crush curve assumed a quasi-static loading condition, and increasing strength until 1.6 million pounds of force was reached, at which point the force remained constant for an indefinite amount of crush. The results of the full-scale tests were not consistent with these assumptions.

To model the conventional force/crush behavior, all the stiffness was attributed to the draft sill spring behavior, and the four corner springs were set to zero. The conventional behavior was compared with the sum of the five collision springs used in the original model validated with test data (see Figure 4-13). The conventional data indicated a much weaker structure initially, but after the first foot of crush, the conventional data indicated a much

stronger structure than observed in the test results. The consequence of the difference was that the conventional car modeled in the 1995 analysis likely underestimated the total crush. If crush developed in excess of 10 feet so that the body bolster was loaded, then the 1.6 million-lb steady force in the conventional model may be reasonable.

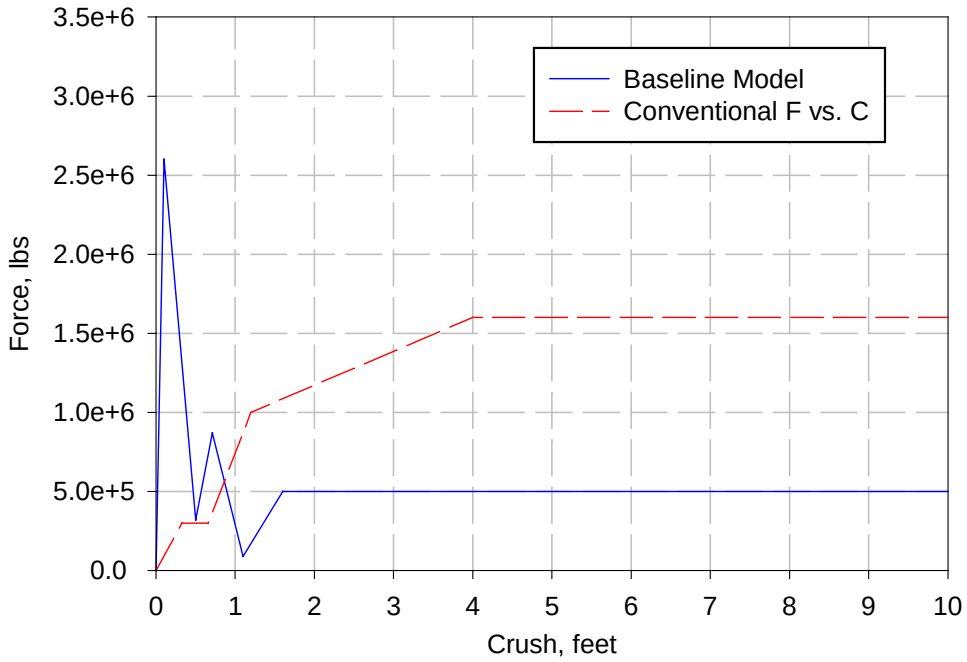

Figure 4-13. Input Force/Crush Characteristics for Baseline and Conventional Models

The force/crush responses in a 35-mph impact using the baseline and modified models are compared in Figure 4-14. The force in the modified model never reaches the peak value because all the kinetic energy from the collision has been dissipated before the 1.6 million-lb force is reached. With the conventional force/crush characteristic, the car crushes just over 3 feet, as compared with over 5 feet of crush in the model/test.

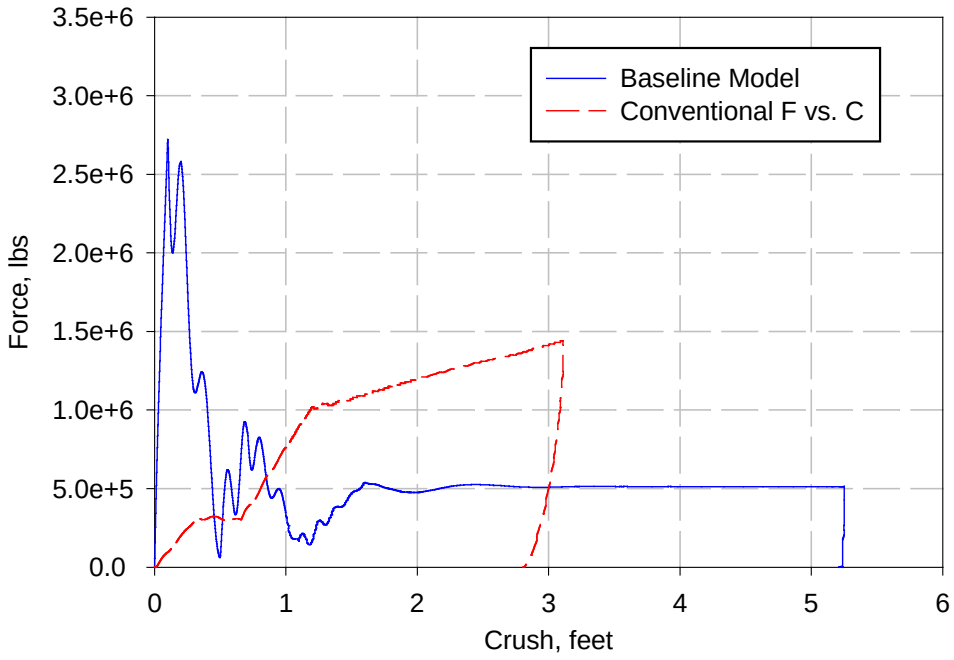

Figure 4-14. Force/Crush Results for Baseline and Conventional Models

4.3.3. 'Quasi-Static' Force/Crush Behavior

In keeping with the piece-wise linear force/crush behavior of increasing strength, a third variation on the spring behavior was analyzed to determine the steady force required to match the amount of crush observed in the single-car test. The steady force required was about 630,000 lb (see Figure 4-15), greater than the 500,000-lb force observed in the test.

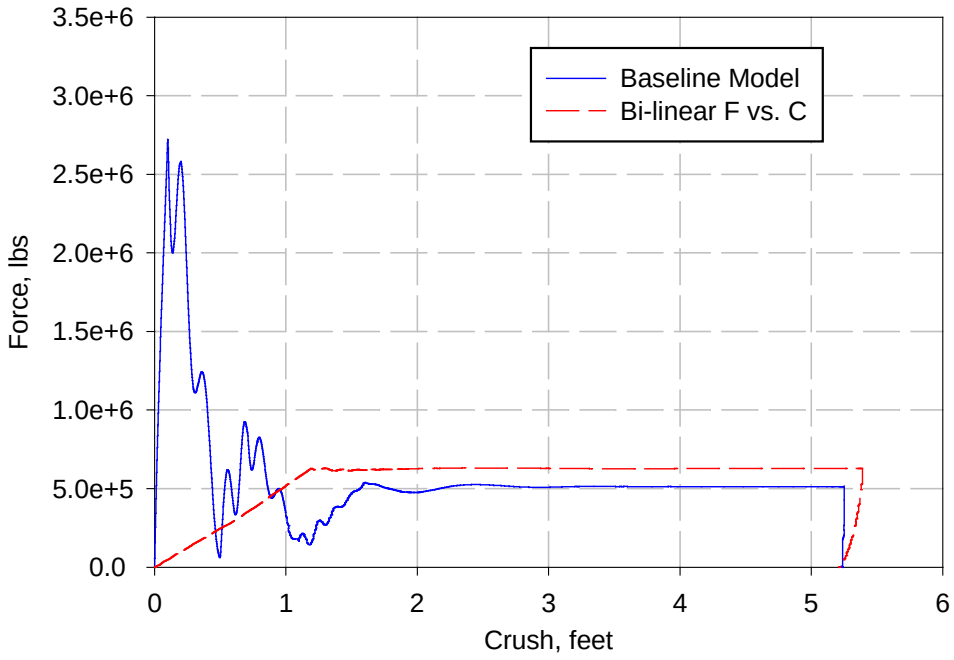

Figure 4-15. Force/Crush Results for Baseline and Bi-linear models

4.4. VELOCITY

The impact velocity was varied to determine over what range of velocities might the model provide valid results. Just because a model estimated results for a particular impact velocity, that does not ensure that the model will necessarily provide accurate results for a large range of impact velocities. The models could be used in the future to determine the impact speed required to crush a car by a given amount. It needs to be determined if the model could be valid at speeds that differ from the tests.

The single-car model was exercised at eight impact speeds, in 10 mph increments, ranging from 5 mph to 65 mph. (35.1 mph is used rather than 35 mph, because that was the exact speed at impact in the single-car test.) In all plots, the force was represented by the total vehicle mass multiplied by the longitudinal acceleration at the center of gravity of the main car body, and plotted against the crush of the collision springs at the lead end of the car. This force was an approximation of the total force acting between the wall and the car.

A comparison of $\frac{1}{2}mv^2$ versus $\int Fdx$ was used to evaluate the results. While agreement of $\frac{1}{2}mv^2$ and $\int Fdx$ does not necessarily mean the model is valid at a given speed, if they do not agree the model is likely not valid. Unfortunately, there is little else to verify the results.

Another objective of this parametric analysis was to determine the impact speed at which the maximum strength of the end structure was reached. In a previous analysis of passenger rail equipment using the conventional force/crush curve from section 4.3.2 [23] it was noted that the maximum force, and consequently the maximum vehicle deceleration, was achieved at approximately 35 mph. At speeds greater than 35 mph, increasing amounts of crush were incurred, particularly by the lead vehicle, which generally led to more fatalities. However, once the maximum strength of the structure was reached, the vehicle was incapable of providing further resistance, i.e. a larger force. The results of the current model were analyzed to determine if there was a particular speed at which the maximum strength of the car structure was reached.

A range of +/- 30 mph from the single-car test velocity was selected. The force/crush results for impact speeds of 5-35.1 mph and 45-65 mph are plotted in Figure 4-16 and Figure 4-17, respectively. Figures a. are plotted over the entire range of crush; figures b. are focused on the first foot of crush only, so the finer detail can be observed. It appears that the maximum force of about 2.7 million pounds is achieved at a speed in between 5 and 15 mph. At higher speeds, there is not a significant increase in the peak force. It is likely that this phenomenon would be observed if a series of actual tests were conducted at a range of impact speeds.

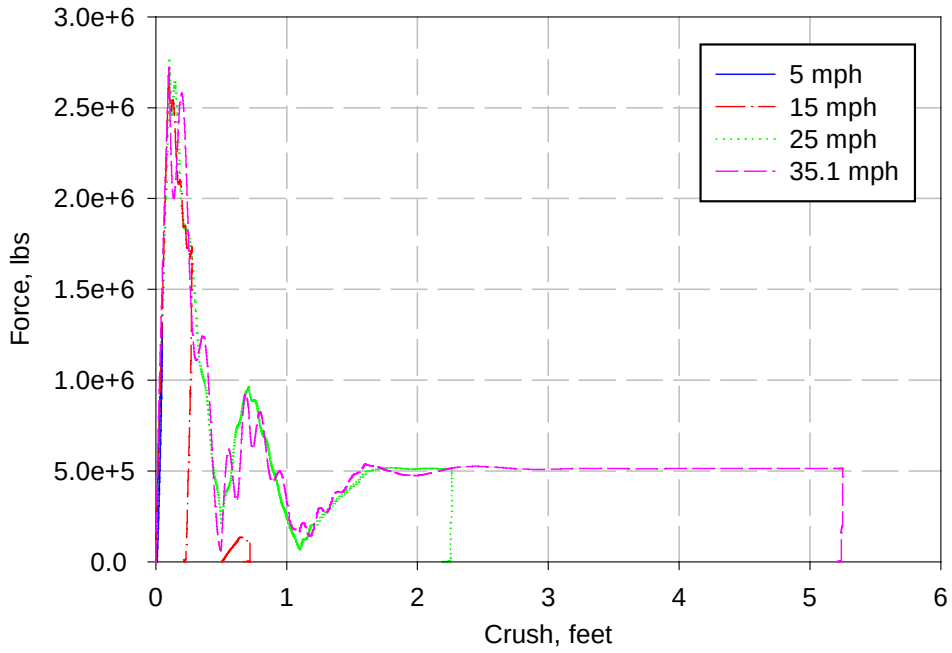

Figure 4-16a. Force/Crush Behavior at Collision Speeds from 5 – 35.1 mph

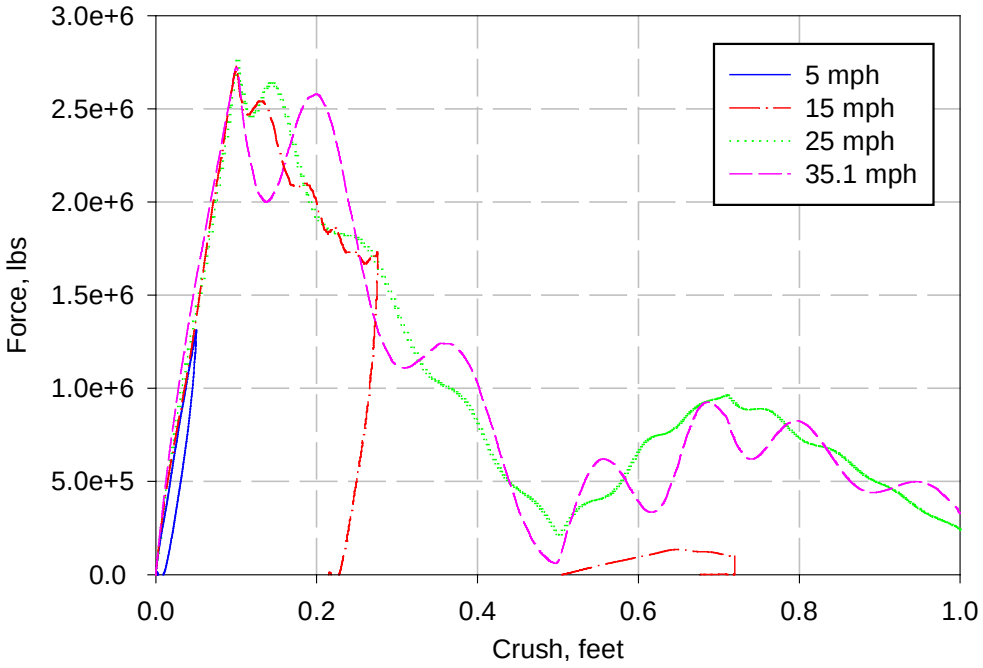

Figure 4-16b. Force/Crush Behavior at Collision Speeds from 5 – 35.1 mph (First Foot of Crush Only)

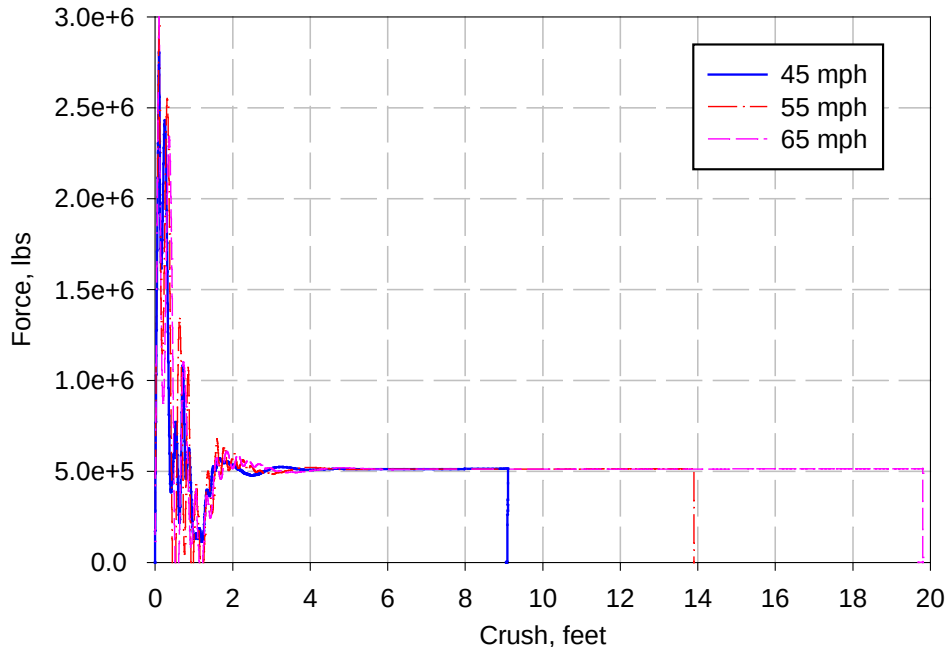

Figure 4-17a. Force/Crush Behavior at Collision Speeds from 45 - 65 mph

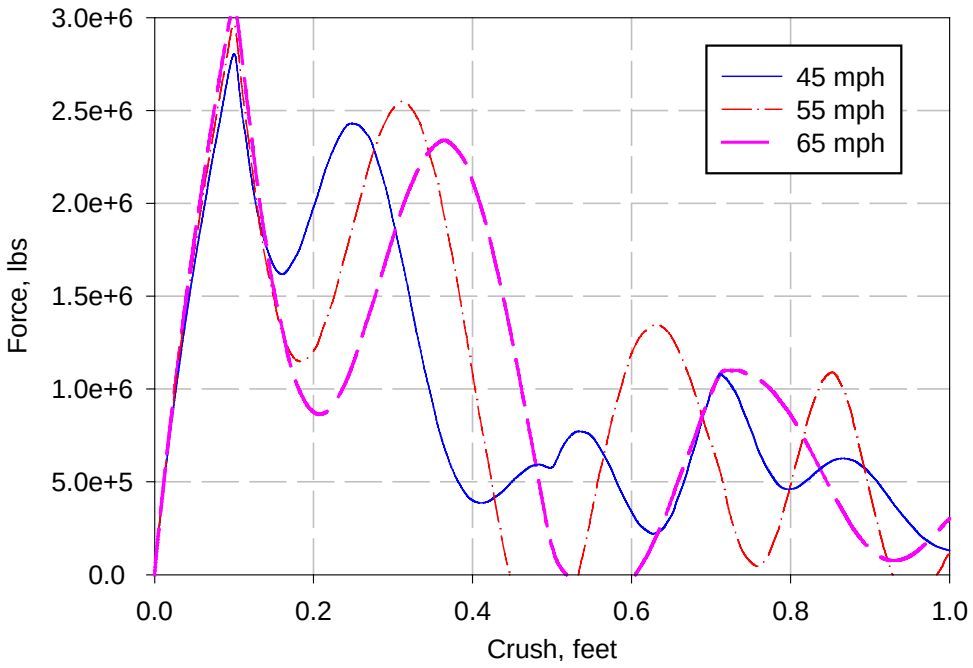

Figure 4-17b. Force/Crush Behavior at Collision Speeds from 45 - 65 mph (First Foot of Crush Only)

Based on these force/crush curves, the energy absorbed ($\int F dx$, where $F = M \cdot A$) was calculated and compared with $\frac{1}{2}mv^2$, where *m* was the total mass of the vehicle, for each of the impact speeds (see Table 4-2). For speeds 25 mph and greater, the difference was less than 2%. For speeds less than 25 mph, the accuracy of $\int F dx$ decreased with impact speed. The cause was likely related to the initial dynamic effects. The dynamic spike in the collision spring representing the draft sill was defined such that the model would estimate the results of the single-car test, which was run at 35.1 mph. This spike was partially rate-sensitive and would likely be less extreme at lower speeds. If this model were to be used to estimate collision results for impact speeds below 25 mph, the initial spike in the draft sill collision spring should be decreased and the stiffness parameter of the IMPACT function may need to be adjusted.

Table 4-2. Energy Comparison by Impact Speed

Impact Speed, mph	$\frac{1}{2}mv^2$	$\int F dx$	% Difference
5	6.204E+04	3.465E+04	44.14%
15	5.583E+05	5.073E+05	9.14%
25	1.551E+06	1.530E+06	1.36%
35.1	3.057E+06	3.064E+06	-0.23%
45	5.025E+06	5.025E+06	-0.33%
55	7.506E+06	7.506E+06	-0.32%
65	1.048E+07	1.048E+07	-0.56%

4.5. SUMMARY

One advantage of using a collision dynamics model was that parametric analyses could be performed very efficiently. Each run took approximately a minute to run. In most cases, the parameters to be modified were set to increment automatically with each run, so ADAMS could perform each run in succession without the user redefining the variables manually. As an example, the velocity analysis took approximately 7 minutes to return all the results for each of the seven cases.

The results of the parametric analysis indicated that the IMPACT parameters used in the baseline model were reasonable; however, care must be taken when selecting the stiffness value. To improve the simulation of vertical motion, a second collision sphere could be added to simulate the movement of the acting point of the impact force from the coupler to a point on the middle of the front of the car body.

Different collision spring definitions were evaluated to investigate the effect on the results. The spring force/crush behavior adapted from the test data was significantly different from the assumptions used in previous models of rail vehicle collisions. Because the steady force levels measured in the tests were considerably lower than the steady values used in Reference 23, considerably more crush would be incurred for a given collision speed. The results indicated that the conventional spring definition would have underestimated the crush in the single-car test by roughly 60%. The results of stiffening the side sill springs indicated that it is possible to increase the strength of the vehicle to reduce the maximum crush, without increasing the initial peak acceleration/force on the vehicle.

The velocity parameter study indicated that the single-car model is likely valid for speeds between approximately 20 and 50 mph. It is probably not valid at speeds below 20 mph because the force/crush definitions for the collision springs were based on a higher speed collision. The rate-sensitive dynamic effects built into the force/crush definitions do not appear to represent the lower speed collisions as well, based on the discrepancy between $\frac{1}{2}mv^2$ and $\int Fdx$. While the energy comparisons were quite good for all speeds 25 mph and above, the model was not designed to handle crush that proceeds beyond the body bolster, or approximately 12 feet. For impact speeds about 50 mph and above, the total car crush would likely exceed 12 feet, engaging additional structure.

5.ANALYSIS AND TEST RESULTS OF SINGLE-CAR TEST

5.1. SINGLE-CAR TEST OBJECTIVES

The objectives of the single-car test were to measure the rigid body motions of the car, to measure the force/crush characteristic, to observe failure modes of the major structural components, and to evaluate selected occupant protection strategies.

In a train collision, large lengths of the cars can crush. Significant parts of the car body structure also can be separated from the car. Very little validated data exist for material failure and structural crush in excess of about 3 feet. The collision speed for this test was chosen to develop enough crush at the impacting end of the car in order to validate collision dynamics models with large crush distances.

The occupant protection strategies tested included lap and shoulder belts, rear-facing seats, and compartmentalization. Compartmentalization requires that seats or restraining barriers be positioned in a manner that provides a compact, cushioned protection zone surrounding each occupant. By reducing the distance the occupant travels prior to the secondary impact, the secondary impact velocity can be reduced, resulting in less severe injuries. The secondary impact refers to the collision between an occupant and some part of the car interior – likely the seat ahead of the occupant. To study this collision between the occupant and the seat, dynamic sled tests were performed with crash test dummies in rail passenger seats. In these seat tests, assumptions were made in an attempt to simulate actual conditions. For instance, the crash pulse, or vehicle acceleration time history, was calculated from a single degree-of-freedom lumped mass model. Also, only the longitudinal motion of the train was considered – the influence of the pitch and yaw motions of the car on occupant response were neglected. Both the single- and two-car tests were designed to demonstrate whether or not these simplifications and assumptions were reasonable.

5.2. SINGLE-CAR TEST DESCRIPTION

On November 16, 1999, a full-scale impact test was conducted with a single commuter rail car impacting a rigid wall at 35.1 mph [7,8,9]. The test was conducted at the Transportation Technology Center (TTC) in Pueblo, Colorado, which is owned by the USDOT. The test was the first in a series of tests sponsored by the FRA. The ultimate goal of the testing program was to learn more about the collision performance of existing vehicles in order to develop appropriate modifications to improve the crashworthiness of future vehicles.

The collision speed for this test was chosen to develop 3 to 5 feet of crush at the impacting end of the car in order to validate finite element and collision dynamics models with large crush distances. The kinetic energy in this test was approximately 3 million ft-lb.

The rail car tested was a Pioneer car, designed and built by the Budd Company [33]. The car was donated by the SouthEastern Pennsylvania Transit Authority (SEPTA). A locomotive was used to push the car down a constant-gradient slope and release it such that it impacted the wall at the desired speed. Calibration runs were made on a parallel track to calculate the appropriate release distance and speed of the locomotive at release. The target impact velocity was 35 mph. The actual impact velocity was 35.1 mph.

The car was stripped of the original passenger seats and some auxiliary equipment to make room for the interior seat/occupant experiments. About 10,000 lb of ballast were added to the car, resulting in a total weight of approximately 75,000 lb. The weight of a fully equipped car used in passenger service is about 100,000 lb. Conducting the test with the lighter vehicle resulted in less damage than would occur in a test with a fully equipped car at the same speed.

The car was instrumented to measure material strain, three-dimensional acceleration of the car body (see Figure 5-1 for accelerometer locations), vertical displacements of the truck suspension, and longitudinal forces and displacements at the coupler. Ninety-three channels of data were collected from the structural car body instrumentation. The car was also equipped with crash test dummies in several different seating configurations.

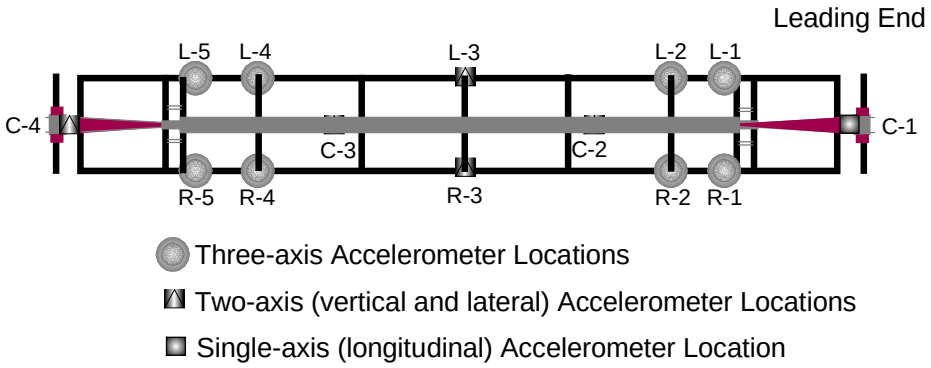

Figure 5-1. Accelerometer Locations

The accelerometer labeled R-4 was used to represent the longitudinal motion of the car body. This accelerometer was located on the right side sill. R-4 was chosen by analyzing the data from all the accelerometers, as well as the integrated displacement data. R-4 appeared to be a reasonable average of all the accelerometers.

The material in this thesis focuses on the structural crashworthiness rather than the interior crashworthiness. However, the secondary impact velocity for unrestrained occupants seated in forward-facing rows, as determined from the test and model results, are presented in this chapter. The secondary impact velocity gives an indication of the severity of the secondary impact. Further details on the occupant protection experiments in the single-car test are covered in Reference 9.

The test was filmed using high-speed and video cameras. A photometric analysis of the high-speed film was performed to calculate the displacement of several target points on the

cars during the impact. These photometric data were used to determine appropriate processing of the accelerometer data (see Appendix B for details on processing of the accelerometer data).

The test data of principle interest for comparison with the model results were the accelerometer data. The data from the accelerometers were used to approximate the total force on the wall, and integrated twice to approximate the displacement of the car body (see Appendices A and B for more detail on the interpretation and processing of the accelerometer data). A single accelerometer near the CG was selected and multiplied by the mass of the entire vehicle to approximate the total force on the wall. In the test, there was no direct measurement of the force on the wall. However, total force between the car and the wall was calculated with the model. The model was used to compare the force acting on the wall with the product of the total vehicle mass and the acceleration at the CG, to determine if the two forces were comparable. The photometric data and the post-test geometry measurements were also used to corroborate the double-integrated accelerometer data.

5.3. TEST AND ANALYSIS RESULTS

Selected test results are presented and discussed in this section. For more test measurements, see Appendix C.

5.3.1. Force/Crush Behavior

The duration of the test was approximately 0.3 seconds. All the visible damage occurred at the impacting end of the car. The amount of permanent crush, calculated by subtracting the post-test car length measurement from the pre-test measurement, was 4.5 feet. The photometric displacement data and the double-integrated accelerometer data show a maximum crush of about 5.4 feet, which includes nearly a foot of elastic deformation of the car body. See Figure 5-2 and Figure 5-3 for pre- and post-test photos of the impacting end of

the car. The elastic recovery as determined from the force/crush plot of the test data in Figure 5-4 is approximately 4 inches. The corresponding elastic recovery in the model was approximately 1 inch.

The first four passenger windows on each side of the car popped out during the impact, indicating that a wave of elastic and possibly plastic deformation propagated through the body panels, extending approximately 25-30 feet from the lead end of the car.

A majority of the collision energy was absorbed during deformation of the draft sill. The draft sill split along the longitudinal seam welds of the box. The top plate folded up in a vertical plane, and the two side plates folded up in a lateral plane.

Figure 5-2. Photo of Impact End of Car Prior to Single-Car Test

Figure 5-3. Photo of Impact End of Car After Single-Car Test

Figure 5-4 shows three force/crush curves based on the test data, the pre-test finite element model and the post-test collision dynamics model. Prior to the test, force/crush behavior had to be estimated. A finite element model provided the best approximation of what could be expected during the single-car test. The force/crush curve calculated in the finite element model (also shown in Figure 5-4) was used as input to the collision dynamics model to estimate the impact speed required to cause 3 to 5 feet of crush. After running the single-car test, the test data was used to modify the assumptions in the collision dynamics model to more accurately reflect the test results. The collision dynamics curve in Figure 5-4 was calculated subsequent to the model improvements.

The peak force ($m \cdot a$) between the car and the impact wall during the test was about 2.8 million pounds, with a steady force of approximately 600,000 pounds. (The accelerometer labeled R-4 in Figure 5-1 was used to represent the longitudinal motion of the car body.) The peak force was a function of the acceleration of the car body, which was significantly influenced by the channel frequency class (CFC) used to filter the acceleration (see Appendix

B for a discussion of filtering techniques). The test and collision dynamics model results compared well, in terms of the timing of the peak force, the average force and the total crush.

.

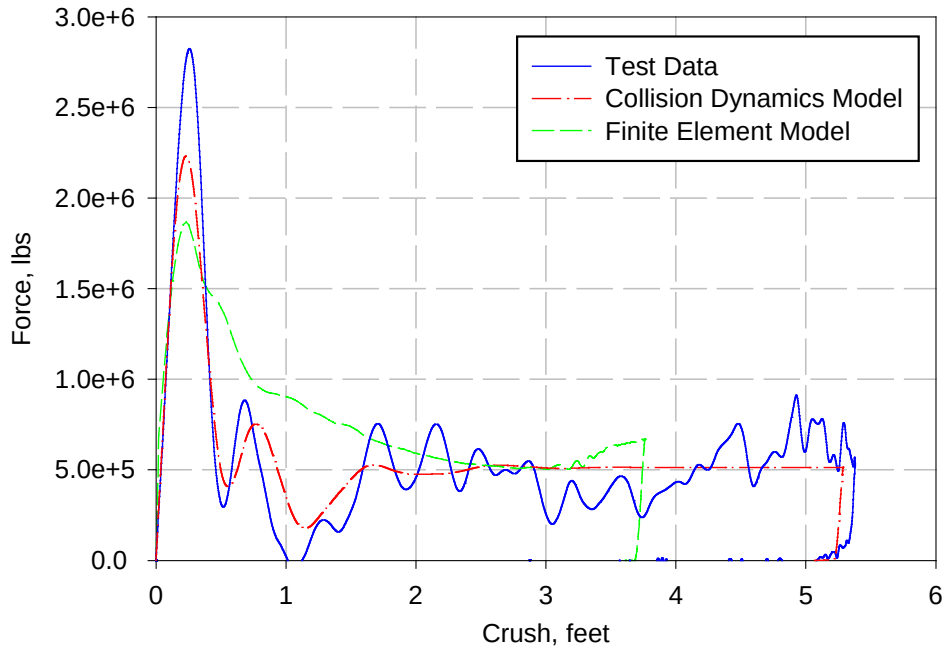

Figure 5-4. Comparison of Force/Crush Behavior from Single-Car Test

As an additional check that the force and displacement data were calculated properly, the energy absorbed during the collision was calculated by integrating the force/crush curves and comparing the result to the total energy available, i.e., $\frac{1}{2}mv^2$. The $\int Fdx$, where $F = m \cdot a$, for both the test and collision dynamics curves differed by 1% when compared to $\frac{1}{2}mv^2$. The $\int Fdx$ for the finite element curve varied by 3.5% when compared to $\frac{1}{2}mv^2$. The force/crush curve developed with the finite element model overestimated the strength during the first 2 feet of crush and underestimated the total crush, but the energies still compared well. This illustrated that comparing energies was not a sufficient check of the validity of the model – the maximum crush also must be compared.

5.3.2. Rigid Body Motion

The collision environment in the single-car test was extremely severe – like one car moving at 70 mph colliding with a stationary car, resulting in a large initial peak deceleration (see the acceleration time history of the car body in Figure 5-5). After the initial peak, the steady acceleration level was between 6-7 Gs. The longitudinal acceleration governed the motion of the dummies, and determined the impact velocity with which the dummies struck the forward seats. The model results captured the timing of the peaks in the test results quite well. The magnitude of the initial peak in the model was somewhat less than that measured in the test, but overall the model results were reasonable.

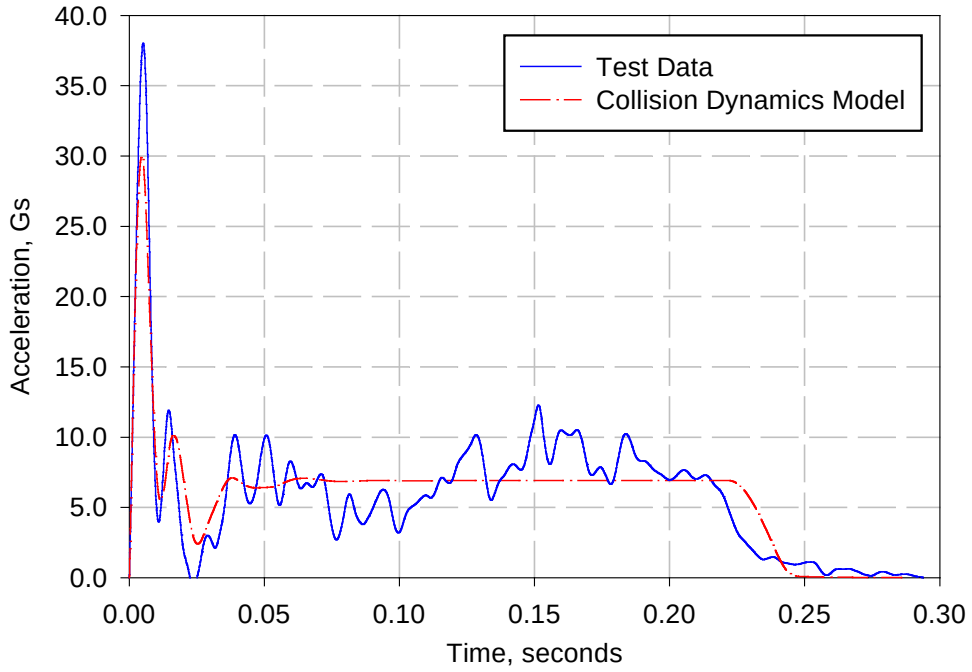

Figure 5-5. Comparison of Longitudinal Car Body Accelerations from Single-Car Test

The impacting end of the leading car rose about 6 inches during the impact, based on the photometric data. The maximum lateral displacement of the lead end of the car was approximately 1 foot. The vertical and lateral accelerations are plotted in Figure 5-6 and Figure 5-7, respectively. The interpretation of the lateral and vertical accelerometer data was difficult, because the accelerometers measured the elastic vibration of the car body, in

addition to the rigid body motion. To date, efforts to isolate the rigid body motion have not been successful, making a comparison of test and analytical data difficult. Also, the accelerometers that measured the data plotted in Figure 5-6 and Figure 5-7 had ranges of 200 G and 100 G, respectively. The magnitude of the vertical and lateral acceleration was too small to be measured accurately with these accelerometers.

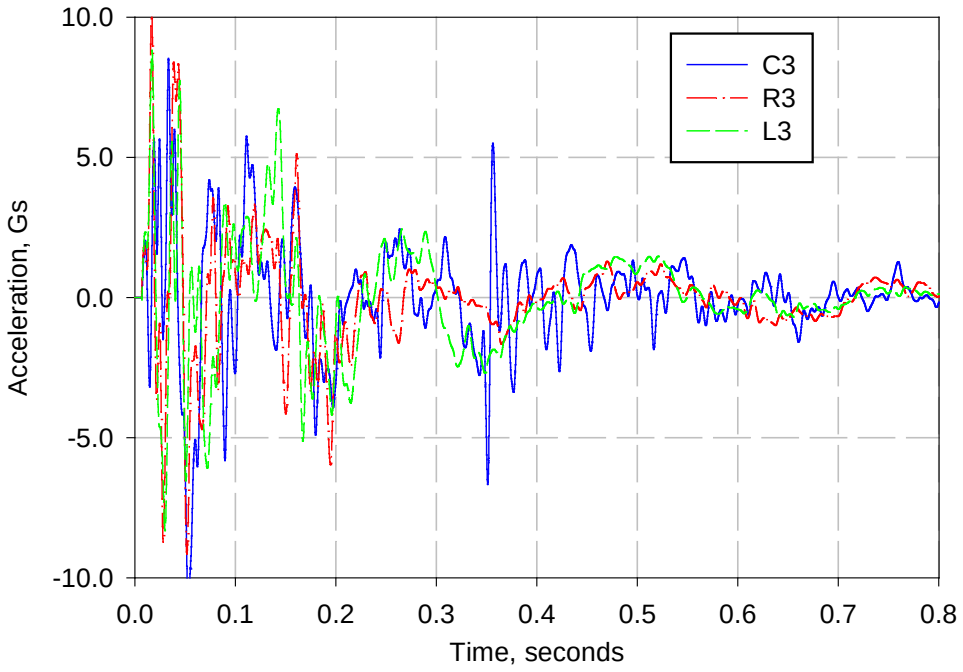

Figure 5-6. Vertical Accelerations Near Longitudinal CG

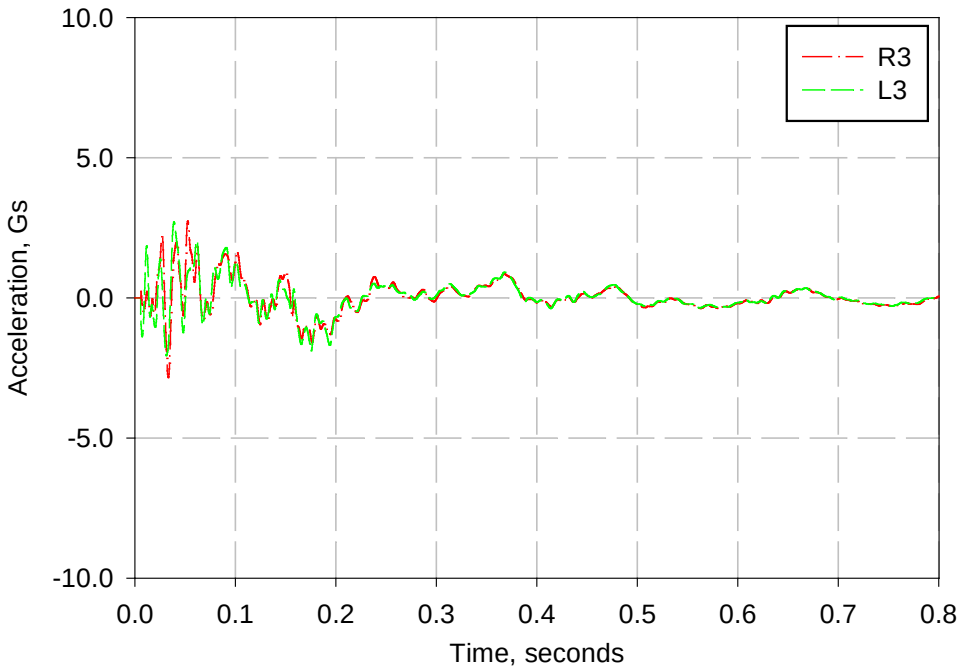

Figure 5-7. Lateral Accelerations Near Longitudinal CG

5.3.3. Secondary Collision Environment

During the test, the dummies struck the forward seats and in some cases, tore the seats away at the car attachments. All the dummies exceeded at least one injury criterion. Compartmentalization was not an effective strategy in this severe collision environment. It did not appear that the vertical motion of the cars resulted in the dummies overriding the forward seats. In the case where a dummy did override the forward seat, it was likely caused by the flexibility of the forward seat back, which could not contain the dummy. Again, more detailed information on the results of the occupant experiments can be found in Reference 9.

Peak acceleration is not particularly significant in terms of the collision environment experienced by an unrestrained, forward-facing occupant. The occupant's velocity relative to the vehicle governs the severity of the secondary impact, which is a function of the car's acceleration time history. The force imparted to the test dummy when it strikes the interior is related to the relative speed at impact. The heads of the unrestrained dummies seated in the forward-facing commuter seats travel approximately 2 feet before striking the back of the

seat ahead, or 2.5 feet if they are seated in the inter-city seats. (In service, inter-city seats are generally positioned with a seat pitch about 6 inches greater than that of commuter seats, thus the 6-inch difference in travel distance).

The accelerometer data measured during the test and calculated with the model were used to calculate the relative velocity vs. relative displacement for forward-facing, unrestrained dummies (see Figure 5-8). The relative impact velocities for dummies in the commuter and inter-city seats in the test were approximately 19 mph and 22 mph. The analysis results compare well with the test data in terms of estimating the relative impact velocity for the test dummies. For comparison, the relative velocity associated with an 8 G triangular crash pulse [30] is also plotted in Figure 5-8. The car body acceleration during the single-car test results in a more severe secondary collision environment than the 8 G crash pulse when the seat pitch is greater than 2 feet.

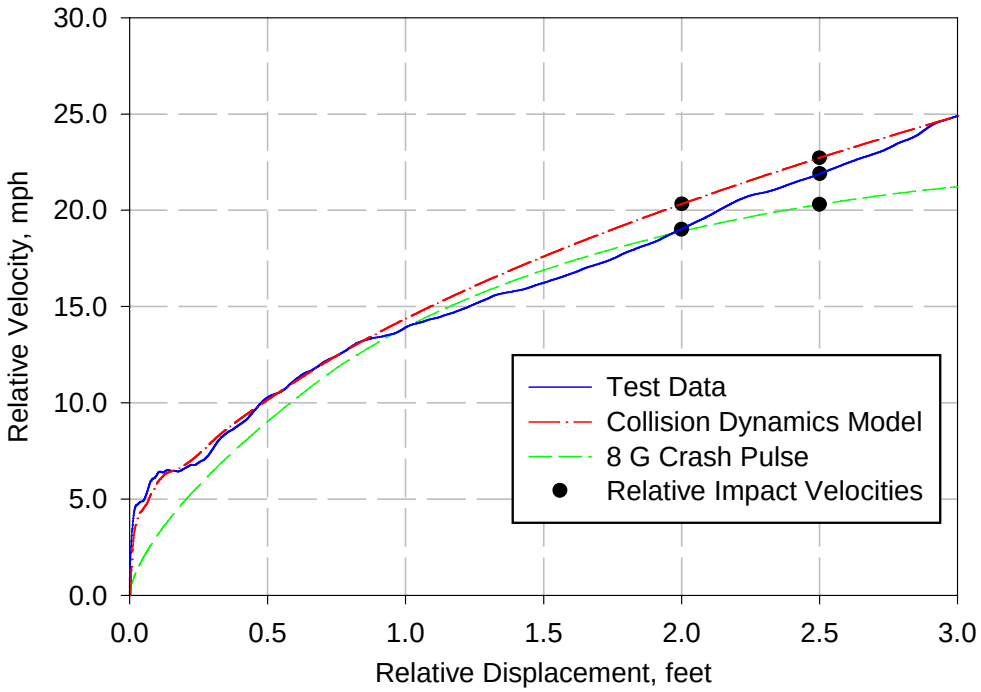

Figure 5-8. Comparison of Secondary Impact Velocity for Dummies in Single-Car Test and an 8 G Sled Test

Relative impact velocity was used as a simple measure to compare the relative severity of different collisions with different crash pulses. It was not meant to be used to predict the likelihood of injury or fatality for occupants exposed to a particular environment. For a more accurate identification of actual forces and accelerations likely to be experienced by occupants in a collision, it would be necessary to review the data collected by the instrumented test dummies [9].

5.4. SUMMARY OF TEST AND ANALYSIS RESULTS

The single-car model was shown to represent the longitudinal car motion measured in the test reasonably well. The acceleration, force/crush and relative impact velocity all agreed well with the test data. It was also shown with the model that multiplying the total vehicle mass and the acceleration at the CG to obtain an estimate of the total force on the wall is a reasonable approximation.

Lacking reliable test data for the vertical and lateral accelerations, not a lot of attention was paid to modeling the vertical and lateral motion. The vibratory modes of the car body made it difficult to decipher the rigid body motion from the test data. Without a reliable target, it was difficult to tune the suspension properly. If future tests provide more reliable data, the suspension springs and dampers and the wheel/rail contact could be modified to better estimate the vertical and lateral motion.

6. ANALYSIS AND TEST RESULTS OF TWO-CAR TEST

6.1. TWO-CAR TEST OBJECTIVES

As in the single-car test, the objectives of the two-car test were to measure the rigid body motions of the car, to measure the force/crush characteristic, to observe failure modes of the major structural components, and to evaluate selected occupant protection strategies. The measurements taken during the test were used to expand and validate the single-car model to analyze two coupled cars in a collision.

This test was also designed to improve the understanding of the coupled car-to-car interaction, and also the conditions that lead to car buckling. During train collisions, one car can override another car, or the trainset can buckle laterally. Override occurs when the relatively strong underframe of one car rides up and over the underframe of an adjacent car, causing extensive crush of the relatively weak superstructure of the adjacent car. Lateral buckling occurs when the cars in the train end up in a zig-zag pattern. Lateral buckling can lead to encroachment of adjacent track, side-to-side impacts between cars, and impacts with wayside structures. Both override and lateral buckling are consequences of the rigid body motions of the cars (e.g., the bouncing and pitching of the car on its suspension), the initial geometry of the coupling system and the cars, and the dynamic collapse of the car structures during the collision.

Prior to the test, the collision dynamics model was used to bound the range of likely test outcomes, in terms of lateral and vertical motion. The vertical motion at the lead end of the impacting car can be affected by the failure mode of the draft sill. The draft sill could potentially act like a linkage, causing the car to pitch upwards.

The two-car model was exercised with small lateral and vertical perturbations in the direction of the impact force to estimate the magnitude of lateral and vertical motion. The lateral motion was induced by laterally moving the impact sphere by up to 3 feet. A lateral displacement of 0.5 feet was required to initiate lateral buckling at the coupled connection between cars. The vertical motion was induced by applying a vertical force to the end of the draft sill that was proportional to the longitudinal impact force. The proportionality constant ranged from 0.05 to 0.075, which resulted in a maximum vertical displacement of 0.5 to 2.5 feet of the lead end of the impacting car.

6.2. TWO-CAR TEST DESCRIPTION

On April 4, 2000, a full-scale impact test was conducted with two coupled commuter rail cars impacting a rigid wall at 26.25 mph [10,11,12]. This test was also conducted at the Transportation Technology Center in Pueblo, Colorado. The test was the second test in a series of tests sponsored by the FRA to learn more about the crashworthiness of existing equipment.

The impact speed was chosen in order to crush the impacting end of the lead car by approximately 5 feet, as in the single-car test. The kinetic energy in the two-car test was roughly the same as in the single-car test (~ 3 million ft-lb).

Both vehicles tested were Pioneer cars, similar to the car tested in the single-car test, and built by the Budd Company. These cars were also donated by SEPTA. A locomotive was used to push the coupled cars down a constant-gradient slope and release them such that they impacted the wall at the desired speed. The target impact velocity was 26 mph. The actual impact velocity was 26.25 mph.

As in the single-car test, the cars were stripped of the original passenger seats and some auxiliary equipment to make room for the interior seat/occupant experiments. About 10,000 lb of ballast were added to each car, resulting in a total weight of approximately 75,000 lb for each car.

The cars were instrumented to measure material strain, three-dimensional acceleration of the car body (see Figure 6-1 and Figure 6-2 for accelerometer locations), vertical displacements of the truck suspension, and longitudinal forces and displacements at the coupler. In this test, the coupled connection was also instrumented with displacement transducers to measure the relative motion of the couplers with respect to the cars. One-hundred-seven channels of data were collected from the structural car body instrumentation.

The accelerometers labeled C-3 in both the leading and trailing cars were used to represent the longitudinal motion of the respective car bodies. These accelerometers were both located on the center sill at the longitudinal center of the car, near the center of gravity. Due to this mounting location, it was expected that the data would be less effected by car body pitch and yaw, than data from accelerometers located further away from the CG.

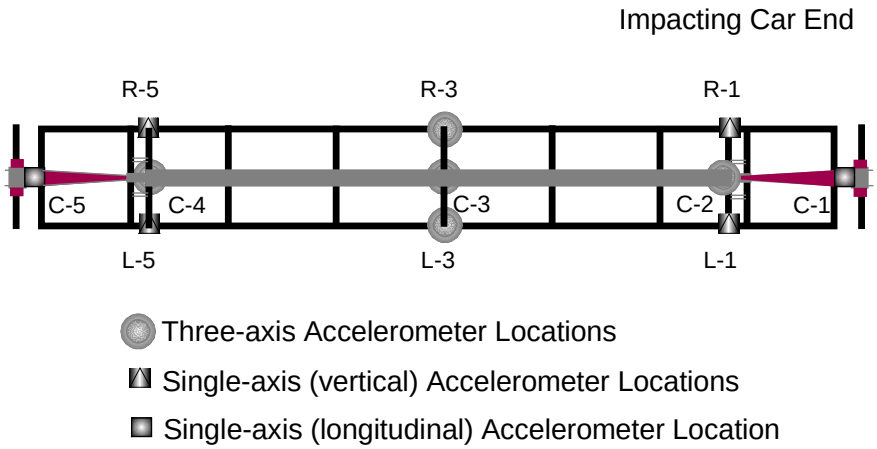

Figure 6-1. Leading Car Accelerometer Locations

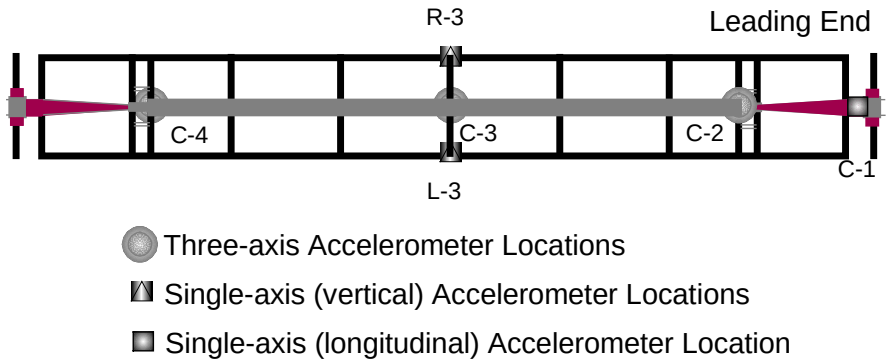

Figure 6-2. Trailing Car Accelerometer Locations

The test was filmed using five high-speed cameras and three video cameras, positioned to focus on the impacting end of the lead car, and the coupled connection between cars. A photometric analysis of the film was performed to calculate the displacement of several target points on the cars during the impact. This photometric data was used in processing the accelerometer data.

To estimate the results of the two-car test, a trailing car was added to the single-car collision dynamics model. The trailing car and coupled connection between the cars was adapted from a collision dynamics model previously developed to investigate lateral buckling [25]. Following the two-car test, the model of the impacting car was modified to better reflect the results of both tests. The impacting car was identical in the single-car and two-car models. This chapter compares the two-car test data with the results of the corresponding collision dynamics model.

6.3. TEST AND ANALYSIS RESULTS

Selected test results are presented and discussed in this section. For more test measurements, see Appendix D.

6.3.1. Force/Crush Behavior

During the two-car impact test, most of the damage occurred at the impacting end of the lead car. The amount of permanent crush, calculated by subtracting the post-test car length measurement from the pre-test measurement, was 5.5 feet. The photometric displacement data and the double-integrated accelerometer data show a maximum crush of about 6 feet, which includes the elastic deformation of the car body. See Figure 6-3 and Figure 6-4 for pre- and post-test photos of the impacting end of the lead car. There was little damage at the coupled connection between the cars. The peak force between the lead car and the impact wall (calculated as the product of the total vehicle mass and the acceleration near the CG) was nearly 2.5 million pounds, with a steady force of approximately 500,000 pounds (see Figure 6-5). The peak force was a function of the acceleration of the two-car bodies, which was significantly influenced by the CFC used to filter the acceleration. See Appendices A and B for more detail.

Figure 6-3. Photo of Impact End of Leading Car Prior to Two-Car Test

Figure 6-4. Photo of Impact End of Leading Car After Two-Car Test

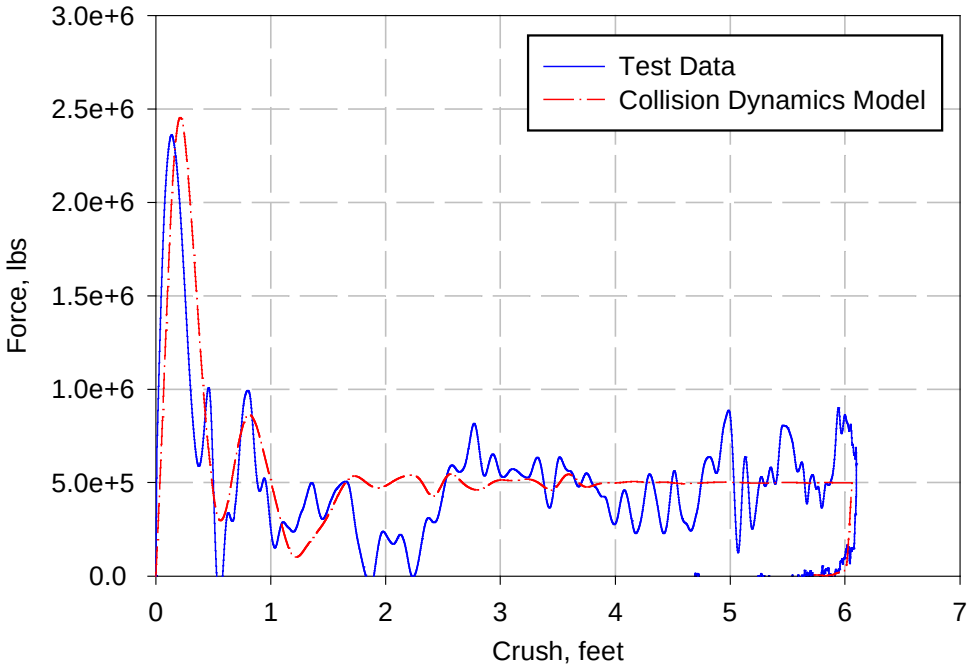

Figure 6-5. Comparison of Force/Crush Behavior from Two-Car Test

Both the single-car and two-car collision dynamics models were modified subsequent to the two-car test to further improve the results of each model. The principal components modified were the force/crush behavior for the collision springs and the IMPACT function parameters. As shown in Chapter 5 and in the following figures, the test and analysis data for both tests compare well, in terms of the timing of the peak force, the average force and the total crush. For comparison, the force/crush behavior from the single-car test is plotted with the two-car test data in Figure 6-6. The curves from both tests were very similar in terms of peak force, average force and total crush. The similarity in the two force/crush curves indicated that even under different collision conditions, the manner in which the overall structure collapsed was similar.

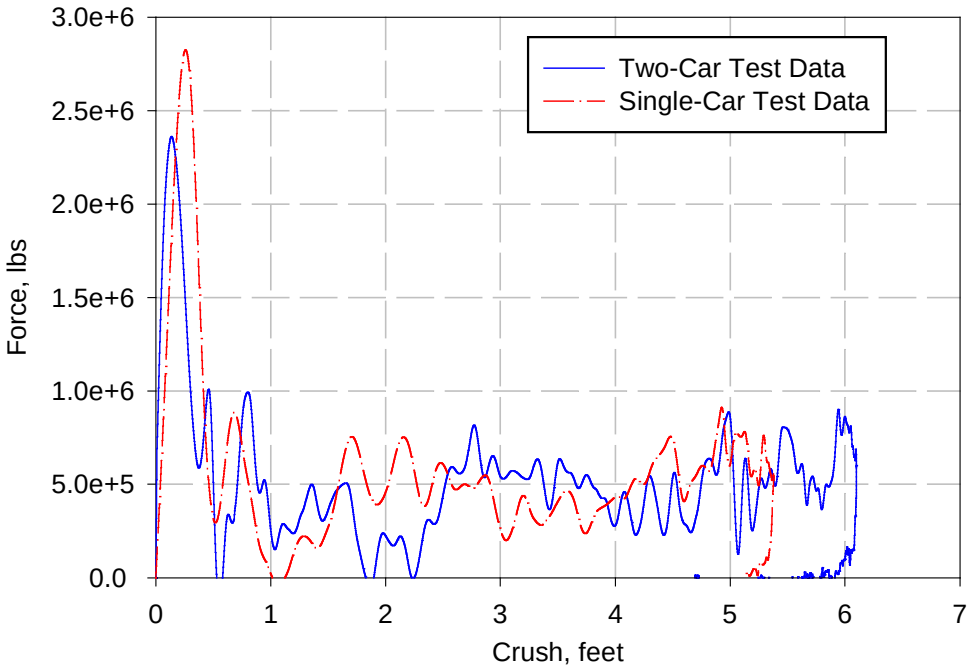

Figure 6-6. Comparison of Force/Crush Behavior from Single-Car and Two-Car Tests

As an additional check that the force and displacement data were calculated properly, the energy absorbed during the collision was calculated by integrating the force/crush curve

and comparing the result to the total energy available, i.e., $\frac{1}{2}mv^2$. While the respective test and analysis curves were not identical, the total energy absorbed, i.e. the area under the each of the curves, varied by less than 1% when compared to $\frac{1}{2}mv^2$.

The mode of crush of the draft sill was quite different between the two tests. In the single-car test, the draft sill split along the longitudinal seam welds of the box. The top plate folded up in a vertical plane, and the two side plates folded up a lateral plane. In the two-car test, the widest part of the draft sill at the end of the car stayed relatively intact, pushing back on the buckled neck of the draft sill. Although the mode of crush of the draft sills was different in each test, it did not have a significant influence on the force/crush behavior of the car.

6.3.2. Rigid Body Motion

The two cars remained coupled during the test, but buckled in a saw-tooth mode. Saw-tooth buckling is a term used to describe cars that translate laterally with respect to one another, until the ends of the cars come into contact. The maximum lateral displacement between the cars during the collision was approximately 30 inches, with a final lateral displacement of 15 inches following the test (see Figure 6-7). The maximum lateral motion was estimated from the high-speed film, and the final lateral motion was measured after the test. The left track buckled under the lateral load from the front truck of the trailing car, allowing the right wheels of the front truck of the trailing car to drop. The impacting end of the leading car rose about 6 inches during the impact.

Figure 6-7. Photo of Coupled Connection After Two-Car Test

The deceleration time histories from the leading and trailing cars are shown in Figure 6-8 and Figure 6-9, respectively, along with the corresponding analytical data. The trailing car in the two-car test acted to minimize the acceleration of the lead car during the first 100 milliseconds. While the lead car was decelerating due to the impact with the wall, the trailing car was simultaneously trying to accelerate the lead car. The peak acceleration of the trailing car was much less than that of the leading car because it was effectively buffered by the crushing of leading car.

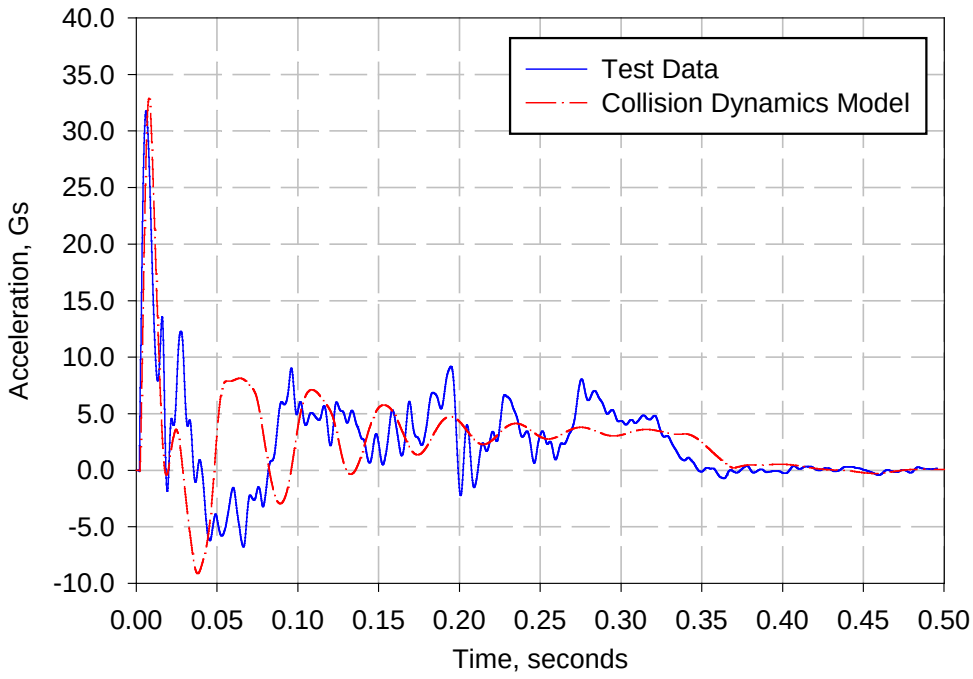

Figure 6-8. Comparison of Longitudinal Car Body Accelerations of Leading Car from Two-Car Test

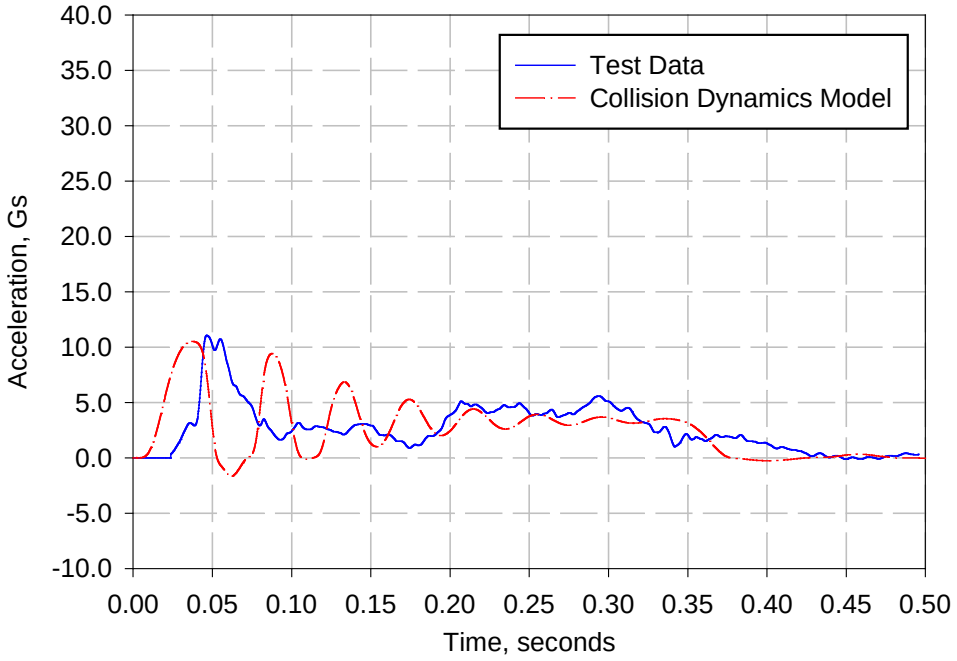

Figure 6-9. Comparison of Longitudinal Car Body Accelerations of Trailing Car from Two-Car Test

Although the test and analysis curves were not identical, the peak and steady values were reasonably accurate. The timing of the peaks after the initial peak was affected by the modeling of the coupler. Apparently the actual coupler had a larger travel distance before any significant longitudinal force developed, resulting in a phase shift between the test and analysis results.

The vertical car body accelerations for the leading and trailing cars were plotted in Figure 6-10 and Figure 6-11, respectively. After the elastic vibration died out, the acceleration in the lead car had a sinusoidal pattern at about 6 Hertz with an amplitude of 2-3 Gs, that damped out after about 3 cycles. The lateral car body accelerations in the two-car test were smaller (see Figure 6-12 and Figure 6-13). The lateral and vertical displacements integrated from the accelerometer data did not agree well with the observations and post-test measurements.

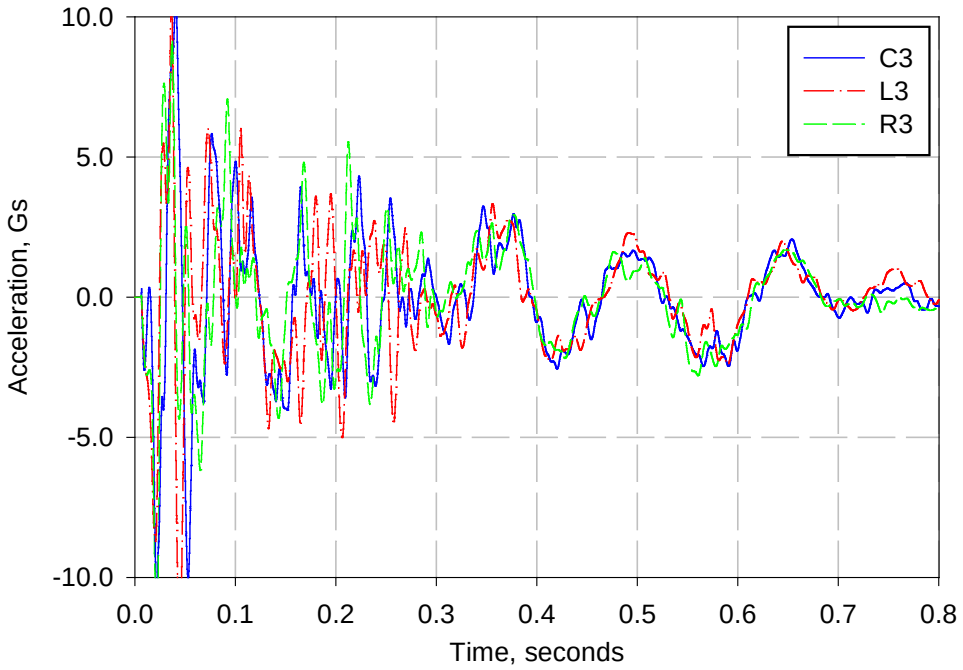

Figure 6-10. Vertical Accelerations at Longitudinal CG of Leading Car

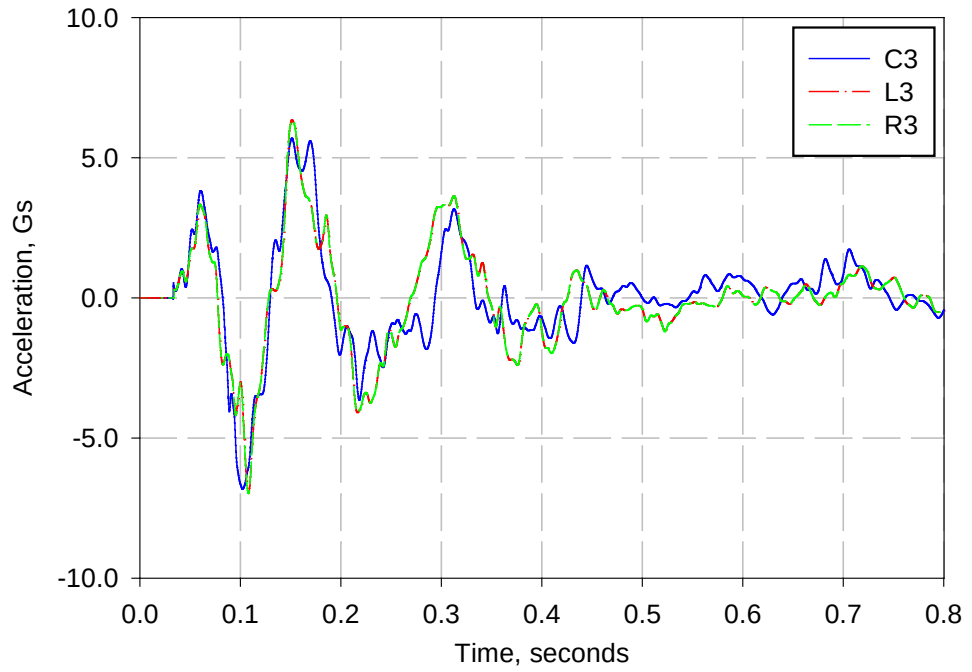

Figure 6-11. Vertical Accelerations at Longitudinal CG of Trailing Car

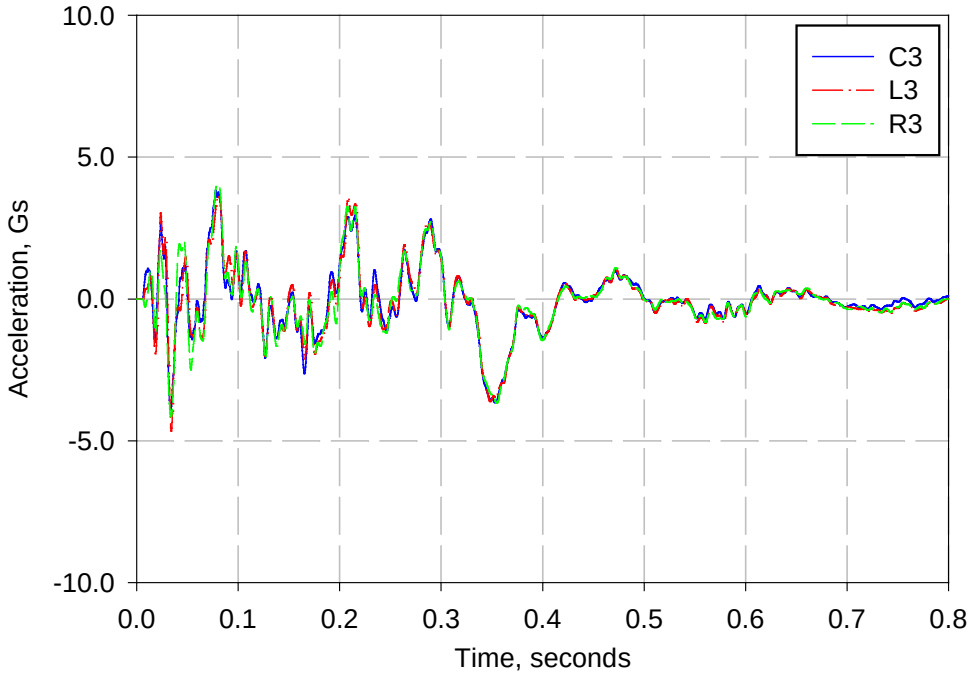

Figure 6-12. Lateral Accelerations at Longitudinal CG of Leading Car

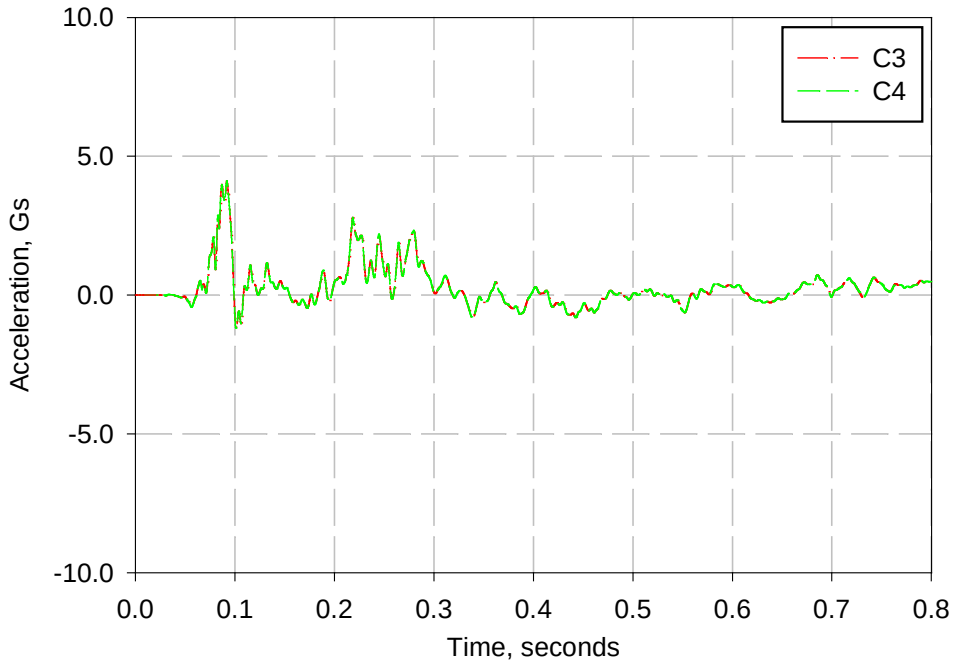

Figure 6-13. Lateral Accelerations at Longitudinal CG and Rear Body Bolster of Trailing Car

6.3.3. Secondary Collision Environment

The secondary impact velocities for the forward-facing test dummies in the leading and trailing cars were plotted in Figure 6-14 and Figure 6-15, respectively. The single-car test data was also plotted in Figure 6-14 for a comparison of the collision severity between the two tests. The two-car analysis results compared well with the test data in terms of estimating the relative impact velocity for the test dummies. There was a phase shift between the two-car test and analysis results that was due to the modeling of the force/crush behavior of the coupler. The secondary impact velocities for unrestrained dummies in the commuter and inter-city seats in both cars of the two-car test were approximately 13 mph and 16 mph, respectively. The impact velocities in the two-car test were significantly lower than in the single-car test, reducing the likelihood of severe injuries. The lower secondary impact velocities in the two-car test were due to the influence of the trailing car, which acted to minimize the $\int a \cdot dt$.

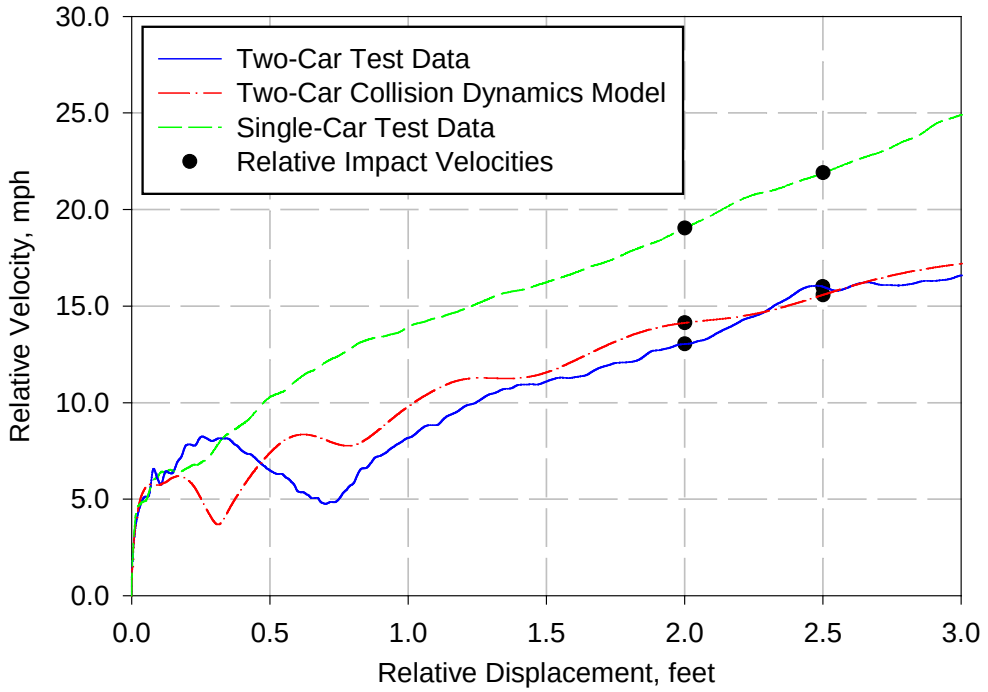

Figure 6-14. Comparison of Secondary Impact Velocity for Dummies in Leading Car of Two-Car Test

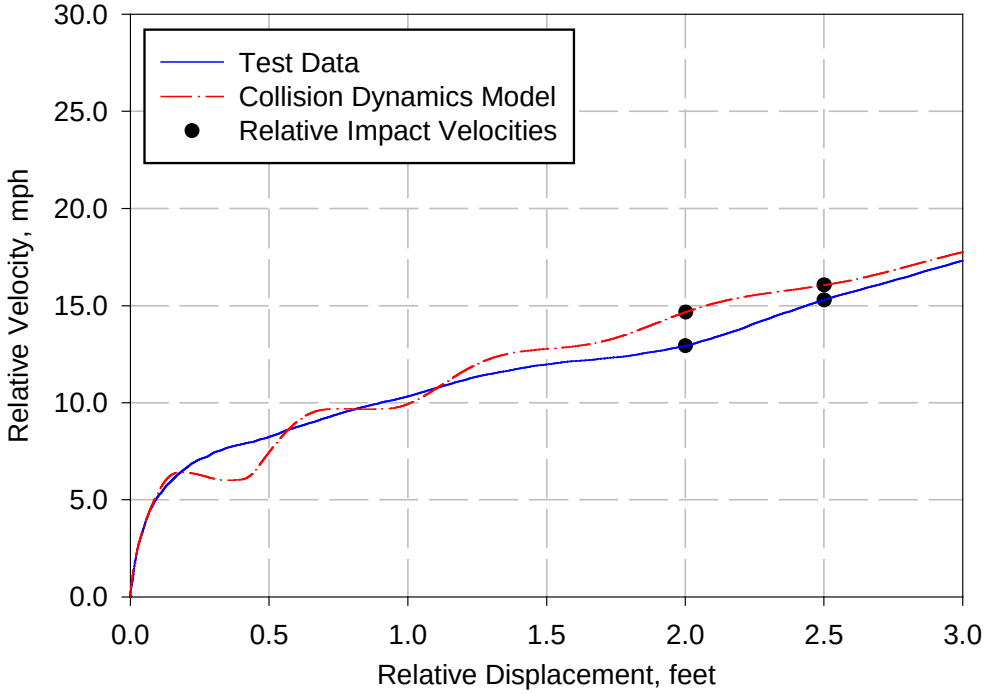

Figure 6-15. Comparison of Secondary Impact Velocity for Dummies in Trailing Car of Two-Car Test

6.4. SUMMARY OF TEST AND ANALYSIS RESULTS

The two-car model was shown to represent the longitudinal car motion measured in the test reasonably well. The acceleration, force/crush and relative impact velocity all agreed well with the test data. There was a slight phase shift in the acceleration time history data that was due to the modeling of the coupler. The coupler was initially estimated to be too stiff, resulting in the first acceleration peak of the second car occurring too early. It was also shown with the two-car model that multiplying the mass of each vehicle with the respective acceleration at the CG and summing the two products to obtain an estimate of the total force on the wall was a reasonable approximation.

The model was used to bound the range of lateral motion likely to occur during the test. The saw-tooth buckling that occurred was predicted in the model if a slight lateral perturbation in the direction of the impact force was incorporated. As in the single-car test, the vibratory modes of the car body made it difficult to decipher the rigid body motion from the test data. Consequently, not a lot of attention was paid to modeling the vertical and lateral motion time histories. If future tests provide more reliable data, the suspension springs and dampers and the wheel/rail contact could be modified to better estimate the vertical and lateral motion.

7. CONCLUSIONS

Two collision dynamics models were developed and exercised to simulate single-car and two-car in-line collisions with a rigid wall. The models simulate the car-to-wall interaction, the force/crush behavior of the end structure, the 3-dimensional rigid body motion and the car-to-car interaction (two-car model only). The models incorporate a user-defined FORTRAN subroutine to handle the path-dependent loading and unloading of the crushable springs that represent the lead end of the impacting car.

A parametric study was conducted with the single-car model to determine the sensitivity to particular parameters. The parameters studied were the k, c, and m for the sphere-to-sphere IMPACT function, the vertical location of the impact sphere, the force/crush behavior of the collision springs, and the impact velocity. The results appeared to be the most sensitive to the stiffness parameter, k. The vertical height of the application of the impact force appeared to be the cause of the vertical motion during the tests. By adding a second impact sphere above the coupler, the model would likely estimate the vertical motion time history with better accuracy.

The collision springs were modified to represent a quasi-static crush behavior, which resulted in significantly less crush than was observed during the single-car test. It was also shown that a modest increase in the side sill strength minimized the total crush without affecting the initial peak acceleration. The combined effect was to reduce the likelihood of occupant injury due to loss of occupant volume, without increasing the secondary impact velocity.

The model was exercised under a range of impact velocities from 5 to 65 mph. The results indicated that the model is likely valid at moderate speeds between 20 and 50 mph.

At speeds below 20 mph, the rate-sensitive force/crush definition of the springs did not appear to represent the collision as well, based on the discrepancy between $\frac{1}{2}mv^2$ and $\int Fdx$. At speeds above 50 mph, the model indicates that the car will likely incur crush beyond the forward body bolster. Crush beyond the body bolster was not accounted for in the model. Most likely the force would increase as the body bolster was challenged, but the details of its force/crush behavior are not known. Therefore, the model should not be used to estimate collision results in which the body bolster is challenged, which is expected to occur at or above a 50 mph impact.

The two models were calibrated against the test data, and used to estimate the test results with reasonable accuracy. The models are capable of estimating the force-time history and the longitudinal motion quite well. The models are capable of estimating the range of likely rigid body vertical and lateral motions of the rail cars, using vertical and lateral perturbations in the direction of the impact force. They are not capable of accurately estimating the vertical motion time histories, which consist of both rigid body motion and flexible body vibrations.

The models were used to determine the test requirements, including the size and placement of accelerometers, the impact speed, and the placement of video cameras. It was also shown that the models can be extrapolated to estimate the collision behavior during collision conditions beyond those of the test scenarios.

The results of the parametric study and the comparison of the test and analysis data indicate that the total force on the wall can be approximated by $m \cdot a(t)$, where *m* is the total mass of the vehicle and $a(t)$ is the acceleration-time history at or near the CG.

7.1. DISCUSSION

One advantage of using a lumped-parameter model was the speed with which runs were completed. Both models developed here executed in 1 to 2 minutes for a collision duration of 0.5 seconds. Prior to the single-car test, the test car was assumed to be approximately 105,000 pounds. This was the weight of a fully equipped, loaded car in passenger service. The collision speed was chosen to be 30 mph, which was expected to develop enough energy to achieve at least 3 to 5 feet of crush at the end of the car, as desired.

Less than a week before the impact test was to be conducted, it was learned that the car had been stripped of a significant amount of equipment, reducing total car weight by about 35,000 lb. About 10,000 lb of cement was added to offset the loss of weight; however, the vehicle still weighed in at not quite 75,000 lb. The mass and inertias of the main car body were adjusted accordingly, and the model was exercised at a range of speeds to determine the necessary impact velocity to produce the required 3- to 5- foot minimum crush. The appropriate velocity was determined to be 35 mph. After conducting the single-car test, the maximum crush achieved was just over 5 feet.

The models developed here were also very useful for evaluating the relative impact velocity for a variety of collision conditions, which can be used to compare the relative collision severity associated with different crash pulses. Previous sled tests were conducted using a triangular crash pulse, or acceleration time history, with a peak of 8 Gs and a duration of 0.25 seconds. This acceleration time history was developed from earlier single degree-of-freedom collision dynamics models, in lieu of actual test data. The 8 G acceleration curve may appear much less benign than the acceleration curves measured in the single-car and two-car tests because the peak of 8 Gs is much less than the 32-38 G peak measured in the impacting car during the two tests. However, the corresponding secondary impact velocities for test dummies subjected to the 8 G crash pulse were 19 mph and 20 mph for

unrestrained, forward-facing dummies seated in commuter seats and inter-city seats, respectively. The corresponding secondary impact velocities for the two-car test were significantly lower at 13 mph and 15 mph, respectively. The peak acceleration cannot be taken alone as a measure of collision severity. However, the acceleration time-history calculated with these models can be used to compare the severity of different collisions.

Another important result of the work in this thesis was the method developed to interpret the test data. The most important test result was the force/crush behavior of the car, but neither the force-time history nor the crush-time history could be directly measured. The accelerometer data were relied upon to estimate the force-time history. The double-integrated accelerometer data, in combination with the photometric data were used to estimate the crush-time history. Proper filtering techniques were established, based on SAE-J211/1 [37], to minimize error.

While car body accelerations were measured during the test, there was no measurement of the total force on the wall. The models, however, were able to calculate the force on the wall, as well as the car body accelerations, which allowed the comparison of the force on the wall and $F = ma$. The technique of multiplying the data from an appropriate accelerometer with the total vehicle mass to represent the force-time history on the wall was shown to be reasonably accurate. The model was used to determine that there is not a significant difference in the force-time history calculated at the sphere-to-sphere impact and the force-time history calculated by multiplying the vehicle mass and acceleration-time history (when the IMPACT sphere parameters are chosen properly). As a further check, the kinetic energy, $\frac{1}{2}mv^2$, was compared with $\int Fdx$, the energy dissipated during the collision, where $F = ma$, for both the test and analysis data. In the velocity analysis (at speeds above

25 mph) and in the comparison of the test and analysis data, $\frac{1}{2}mv^2$ and $\int F dx$ differed by less than 1.5%. This check did not confirm that the model results were correct, but it did confirm that the model results were not wrong.

The use of user-defined subroutines (see Appendix E) was shown to be a reliable method of incorporating the force-crush behavior for the collision springs. Alternatively, one could define a series of force/deflection data pairs. ADAMS then could curve-fit a spline to the data pairs. However, the spline developed with this method would not necessarily represent the piece-wise linear force/crush behavior as well as would be desired, nor would it handle the spring unloading properly. The sub-routine allowed easy adaptation of the force/crush definition for the purposes of test validation.

7.2. RECOMMENDED MODIFICATIONS TO MODELS

The two-car collision dynamics model predicted the lateral buckling of the cars when there was a small perturbation in the direction of the impact force. However, the model could be improved to better capture the timing of the longitudinal forces transferred through the coupler. From the test data, it appears that the coupler compresses several inches before any significant force develops. Tuning this "gap" in the model will result in a better estimation of the timing of the acceleration peaks of both cars. Also, the model requires more damping at the coupler to minimize the longitudinal oscillation of both cars, as observed in the plots of longitudinal car body accelerations.

The model's ability to estimate the vertical motion could be improved with two separate modifications. First, the suspension springs and dampers need to be tuned, based on shake-and-bake tests conducted on the car prior to the impact test [7], as well as the displacement-time histories measured during the dynamic tests. Second, another impact sphere could be added to account for contact between the front face of the vehicle (above the coupler) and the

wall. Both of these modifications should result in better estimates of the bounce and pitch motion of the car.

Eventually the models should be modified to represent an oblique collision, which could be used to better understand and thus improve the ability of the structure to preserve occupied areas when the draft sill/center sill are not directly challenged.

7.3. APPLICATIONS FOR COLLISION DYNAMICS MODELS

The models can be exercised at different impact velocities. The two-car consist can be extended to include more vehicles. Rather than impacting a wall, the model could be modified such that a multiple-car consist collided with another consist. The models could be modified to analyze the consequences of oblique impacts. Also, the models could be used to evaluate different collision spring behavior, specifically spring behavior associated with a crash energy management system. The Force/crush behavior of a potential CEM design could be developed with a detailed finite element model. By making small changes to the collision dynamics models to incorporate the FEM results, the benefits of CEM in a range of collision conditions could be evaluated in a timely manner.

REFERENCES

[1] Federal Rail Safety Authorization Act of 1994, Pub. L. No. 103–440, 108 Stat. 4619, 4623–4624 (November 2, 1994).

[2] Passenger Equipment Safety Standards; Final Rule, 49 CFR, Part 216, et al., May 12, 1999, Federal Railroad Administration, U.S. Department of Transportation.

[3] Tyrell, D.C., Severson, K.J., Marquis, B.P., "Train Crashworthiness Design for Occupant Survivability," 1995 *ASME International Mechanical Engineering Congress and Exposition*, AMD-Vol. 210, BED-Vol. 30, pp. 59-74.

[4] Tyrell, D.C., Severson, K.J., Marquis, B.P., "Analysis of Occupant Protection Strategies in Train Collisions," 1995 *ASME International Mechanical Engineering Congress and Exposition*, AMD-Vol. 210, BED-Vol. 30, pp. 539-557.

[5] Tyrell, D.C., Severson, K.J., Mayville, R.A., Stringfellow, R.G., Berry, S., Perlman, A.B., "Evaluation of Cab Car Crashworthiness Design Modifications," 1997 ASME/IEEE Joint Railroad Conference, Boston, Massachusetts.

[6] Tyrell, D.C., Severson, K.J., Marquis, B.P., Perlman, A.B., "Simulation of an Oblique Collision of a Locomotive and an Intermodal Container," 1999 *ASME International Mechanical Engineering Congress and Exposition*, AMD-Vol. 237, BED-Vol. 45.

[7] Brickle, B., "Single Passenger Rail Car Impact Test Volume III: Test Procedures, Instrumentation and Data," May 2000, DOT/FRA/ORD-00/02.3.

[8] Tyrell, D., Severson, K., Perlman, A.B., "Single Passenger Rail Car Impact Test Volume I: Overview and Selected Results," 2000, US Department of Transportation, DOT/FRA/ORD-00/02.1.

[9] VanIngen-Dunn, C., "Single Passenger Rail Car Impact Test Volume II: Summary of Occupant Protection Program," 2000, U.S. Department of Transportation, DOT/FRA/ORD-00/02.2.

[10] Severson, K.J., Tyrell, D.C., Perlman, A.B., "Rail Passenger Equipment Collision Tests: Analysis of Structural Measurements," published in proceedings of the 2000 *ASME International Mechanical Engineering Congress and Exposition*.

[11] Tyrell, D., Zolock, J., VanIngen Dunn, C., "Rail Passenger Collision Tests: Analysis of Occupant Protection Measurements," published in proceedings of the 2000 *ASME International Mechanical Engineering Congress and Exposition*.

[12] Tyrell, D., Brickle, B., Severson, K., Perlman, A.B., VanIngen Dunn, C., "Rail Passenger Equipment Crashworthiness Testing: Requirements and Implementation," published in proceedings of the 2000 *ASME International Mechanical Engineering Congress and Exposition*.

[13] Smith, R.A., "Crush Zone Development," Rail Vehicle Crashworthiness Symposium, June 24-26, 1996, Cambridge, Massachusetts, DOT/FRA/ORD-97-08, pp. IIA-4-16 to IIA-4-30.

[14] Tong, P., “Mechanics of Train Collision,” 1976,Final Report FRA-OR&D-76-246, Cambridge, Massachusetts.

[15] Cassidy, R.J. and Romeo, D.J., “Assessment of Crashworthiness of Existing Urban Rail Vehicles,” 1975,Final Report DOT-TSC-681, Washington, D.C.

[16] Raidt, J. B. and Manos, W.P., “A Preliminary Study of Vertical Motions During Impact,” 1972, Pullman-Standard Research, Final Report, Project No. 3901853.

[17] Widmayer, E., “Application of KRASH to the SOAC Accident,” 1975, Presented at the Symposium on Aircraft Crashworthiness, Cincinnati, Ohio.

[18] Hahn, E.E., Walgrave, S.C., Liber, T., “Increased rail transit vehicle crashworthiness in head-on collision – Volume II – Primary Collision”, 1980, Final Report UMTA-MA-06-0025-80-2, Chicago, Illinois.

[19] Scholes, A., “Railway Passenger Vehicle Design Loads and Structural Crashworthiness,” 1987, Proc. Instn. Mech. Engrs. Vol. 201, No. D3, pp. 201-207.

[20] Lewis, J.H., “Development of a Structural Specification for Crashworthy Rail Vehicles,” 1995 *ASME International Mechanical Engineering Congress and Exposition*, AMD-Vol. 210, BED-Vol. 30, pp. 1-16.

[21] Lewis, J.H., “Validation of Measures to Improve Vehicle Safety in Railway Collisions,” 1995 *ASME International Mechanical Engineering Congress and Exposition*, AMD-Vol. 210, BED-Vol. 30, pp. 17-34.

[22] “SNCF Structural Crashworthiness Design Strategy Design Examples of Duplex TGV and XTER Diesel Multiple Unit,” Rail Vehicle Crashworthiness Symposium, June 24-26, 1996, Cambridge, MA, DOT/FRA/ORD-97-08, pp. IIB-2-23 to IIB-2-56.

[23] Tyrell, D.C., Severson, K.J., Marquis, B.P., “Crashworthiness of Passenger Trains,” 1998, DOT/FRA/ORD-97-10, FRA, U.S. Department of Transportation.

[24] Mayville, R.A., Stringfellow, R.G., Rancatore, R.J., Hosmer, T.P., “Locomotive Crashworthiness Research,” July 1995, DOT/FRA/ORD-95-08.

[25] Mayville, R., Rancatore, R., Tegeler, L., “Investigation and Simulation of Lateral Buckling in Trains,” Published in Proceedings of the 1999 IEEE/ASME Joint Railroad Conference, April 13-15, 1999, IEEE Catalog Number 99CH36340, ASME RTD Volume 16.

[26] Mayville, R.A., Stringfellow, R.G., Rancatore, R.J., Johnson, K., “Development of a Rail Passenger Vehicle Crush Zone,” Published in Proceedings of the 1999 IEEE/ASME Joint Railroad Conference, April 13-15, 1999, IEEE Catalog Number 99CH36340, ASME RTD Volume 16.

[27] Kirkpatrick, S.W., and Simons, J.W., “High-Speed Rail Collision Safety,” Rail Vehicle Crashworthiness Symposium, June 24-26, 1996, Cambridge, Massachusetts, DOT/FRA/ORD-97-08, pp. IIA-3-13 to IIA-3-27.

[28] Kokkins, S.J., Snyder, M., Allen, D., Kirkpatrick, S., Simons, J., Peacock, W., Spezzafero, K., “Case Studies in Collision Safety,” DOT/FRA/ORD-96/01.

[29] Mayville, R.A., Hammond, R.P., Johnson, K.N., 1999, “Static and Dynamic Crush Testing and Analysis of a Rail Vehicle Corner Structural Element,” Proceedings of the 8th ASME Symposium on Crashworthiness, Occupant Protection and Biomechanics in Transportation November 14-19, 1999; Nashville, Tennessee.

[30] Tyrell, D., and K.J. Severson, “Crashworthiness Testing of Amtrak's Traditional Coach Seat,” October 1996, DOT/FRA/ORD-96/08.

[31] VanIngen-Dunn, C., Manning, J., “Commuter Rail Seat Testing and Analysis,” Draft Final Report, U.S. Department of Transportation, Cambridge, Massachusetts.

[32] Wierzbicki, T., “Body Shell and Beam Interaction,” Draft Final Report, U.S. Department of Transportation, Cambridge, Massachusetts, 1999.

[33] White, J.H., Jr., “The American Railroad Passenger Car,” 1978, The Johns Hopkins University Press.

[34] ADAMS Version 9.0.1, 1997, Mechanical Dynamics, Inc., Ann Arbor, Michigan.

[35] Bing, Alan J., Berry, Shaun R. and Henderson, Hal B., “Engineering Data on Selected North American Railroad Passenger Cars and Trucks,” November 1995, DOT-VNTSC-FRA-95-5.

[36] Romeo, D., Cassidy, R., “Interim Report on Assessment of Crashworthiness of Existing Urban Rail Vehicles,” 1974, DOT-TSC-681, RSPA, U.S. Department of Transportation.

[37] SAE J211/1, Surface Vehicle Recommended Practice – Instrumentation for Impact Tests – March 1995.

APPENDIX A - INTERPRETATION OF ACCELEROMETER DATA

The most significant result to be determined from the tests was the force/crush behavior of the car, but neither the force-time history nor the crush-time history could be directly measured. The accelerometer data were relied upon to estimate the force-time history. The double-integrated accelerometer data, in combination with the photometric data, were used to estimate the crush-time history.

While car body accelerations were measured during the test, there was no measurement of the total force on the wall. The models, however, were able to calculate the force on the wall, as well as the car body accelerations, which allowed the comparison of the force-time history on the wall and $F(t) = m \cdot a(t)$ to determine if *ma* is a reasonable approximation. The model was used to determine that there is not a significant difference in the force-time history calculated at the sphere-to-sphere impact and the force-time history calculated by multiplying the total vehicle mass and acceleration-time history (when the IMPACT sphere parameters are chosen properly).

As a further check, the kinetic energy, $\frac{1}{2}mv^2$, was compared with $\int F dx$, the energy dissipated during the collision, where $F = ma$, for both the test and analysis data. Though the two calculations were close (within 1.5%), this check can not confirm that the model results were correct, but it did confirm that the model results were not wrong.

In calculating $F = ma$, *m* equals the total vehicle mass and *a* equals the acceleration measured at one particular accelerometer. Other possible methods to calculate *F* were investigated:

1) Multiplying the total mass by the average of all accelerometers (except those that saturated during the test),

2) Multiplying each accelerometer (except those that saturated during the test) by a fraction of the total vehicle mass and summing the parts.

The first method was rejected because averaging the data-time histories for all of the accelerometers resulted in the loss of significant data. For example, there was a slight phase shift in the data as the impact wave proceeded down the length of the car. When the data was averaged, the acceleration peaks were lost, and the character of the acceleration was lost. Also, when integrated, the force/crush curve calculated in this manner did not produce an energy dissipation value consistent with $\frac{1}{2}mv^2$. The second method was rejected because it was also subject to the phase shift in the accelerometer data, in which the peaks were lost when averaged together.

To estimate the crush-time history, longitudinal data from an individual accelerometer were chosen and integrated twice. Other possible methods to estimate the crush included:

1) Averaging the double-integrated data from all of the accelerometers,

2) Using the photometric displacement data.

The first method was rejected because there was a significant discrepancy in the displacement-time histories of the integrated accelerometer data, and some of the data were clearly inaccurate based on the photometric data. The second method was used to help determine which accelerometer was the most appropriate.

To select the most appropriate accelerometer, all of the double-integrated longitudinal accelerometer data were compared. Data from accelerometers that had saturated were

discarded. Data that were markedly different in terms of rebound characteristics were also discarded. Data from accelerometers in the crushed end structure were also discarded. Data that were significantly different from the photometric data were discarded. The acceleration-time histories for the remaining accelerometers were then compared. A single curve that appeared to be most representative of the car body acceleration was selected to represent the acceleration and displacement of the car.

In the single-car test, the total force on the wall as a function of time was estimated by multiplying the total mass of the car and the acceleration of the car measured with accelerometer R4:

$$F_w(t) = m * a(t)$$

In the two-car test, the total force on the wall was estimated by multiplying the mass of each car with the acceleration measured with accelerometer C3. The sum of the two products is the estimated force time history at the wall (see Figure A-1):

$$F_w(t) = m_1 * a_1(t) + m_2 * a_2(t)$$

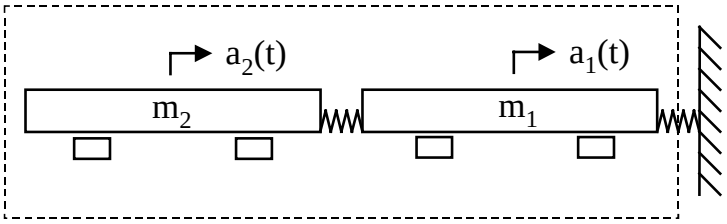

Figure A-1. Free Body Diagram

The resulting $F_w(t)$ was cross-plotted against the double-integrated displacement-time history of the leading vehicle to represent the total force on the wall as a function of crush of the impacting vehicle.

APPENDIX B - DESCRIPTION OF ACCELEROMETER DATA PROCESSING

The raw accelerometer data contained components attributable to car body flexibility. The data were filtered in order to remove the high-frequency content while retaining the essential rigid body motion of the car body. The filtered accelerometer data were then integrated to calculate the corresponding velocity and displacement data.

The choice of cut-off frequency has a significant effect on the double-integrated displacement data. Comparison of the integrated displacement data and the photometric displacement data from the two-car test was used to define the appropriate cut-off value. Accelerometer data from FC4X from the two-car test were filtered at several frequencies and integrated twice. The results are plotted in Figure B-1, along with the photometric displacement data for comparison.

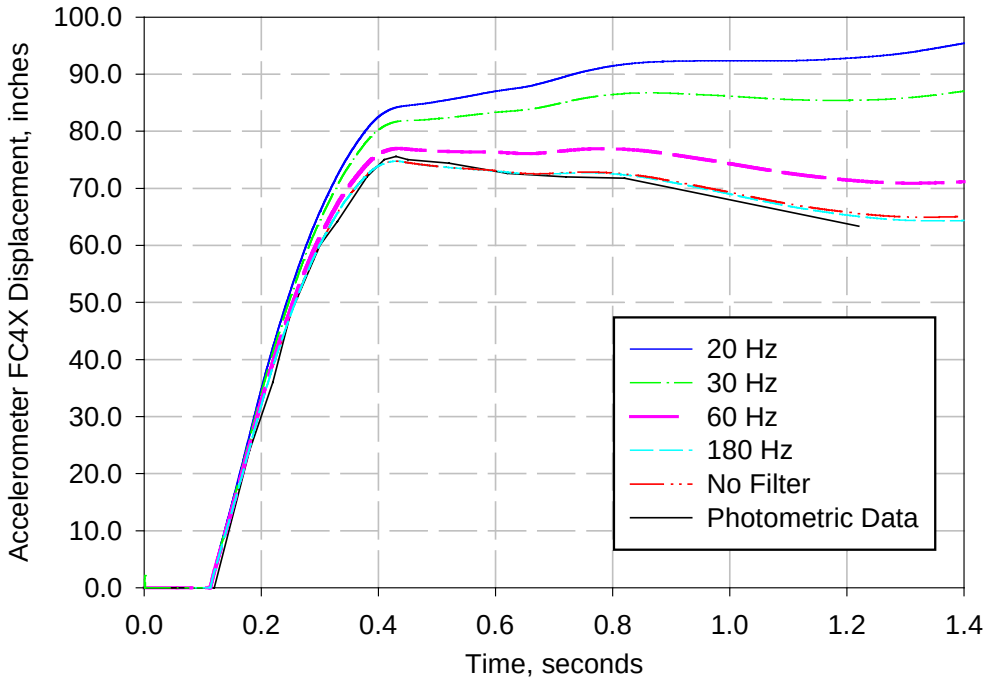

Figure B-1. Comparison of Effect of Filtering Frequency on Displacement Time History

To minimize the error in integrated displacement, the accelerometer signal was processed in accordance with SAE J211.1 (Surface Vehicle Recommended Practice – Instrumentation for Impact Tests). To compute the acceleration, a CFC 60 Butterworth 4-pole phaseless digital filter was used. To compute the displacement, a CFC 180 Butterworth 4-pole phaseless digital filter was used. The difference in the displacement time histories for the 180 Hertz and the unfiltered accelerometer data is negligible.

Accelerometer data from the single-car test that were reported in [8] had originally been filtered using a 30 Hertz low-pass filter. It was apparent that a significant error in the integrated displacement data had been introduced by over-filtering the acceleration. The single-car test data were reprocessed in accordance with J211.1. The peak acceleration is approximately 14 Gs when a CFC 30 is used in filtering the accelerations, versus a peak of about 38 Gs that results from using a CFC 60 filter. However, the peak acceleration is not particularly significant in terms of the collision environment experienced by an unrestrained, forward-facing occupant.

Filtering Algorithm

By John Zolock

Flow Diagram of Post-Processing Algorithm

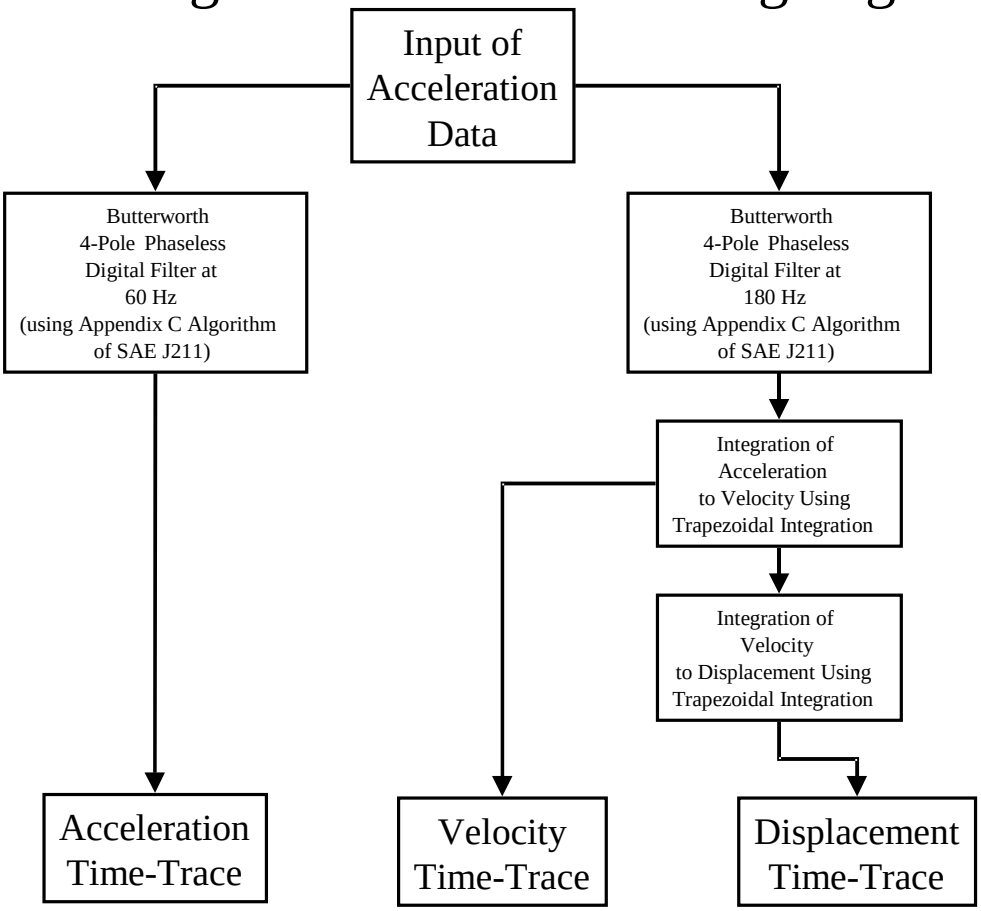

1. Accelerometer data is read from the data bricks using the program Brick.exe. Each channel of data is read out into it's own ASCII file containing a header of general information followed by a column of data.

2. The data is read into the post-processing software program after stripping off all header information.

3. The custom algorithm written to post-process the accelerometer data is described in the steps below.

4. Using Appendix C of SAE J211, the coefficients for a Butterworth 2-pole 60 and 180 Hz Low Pass filters are calculated. The 60 Hz filter is used to determine the resulting acceleration trace. The 180 Hz filter is used for integration of acceleration to approximate velocity and displacement.

5. The time of the initial impact point is determined. The point is determined using a graphical input pick from a plot of the unfiltered acceleration versus time. The point

picked is subjectively and systematically picked as the point where the acceleration is first above the noise floor. The time of this point changed for each accelerometer location and each direction of multi-axial accelerometers. The process was repeated several times to ensure as accurate a point as possible.

6. A second point was picked to determine the length of the transition region. The transition region is reversed and reflected about the initial point (throwing out all prior data to the initial point) so that the effects of filtering are minimized (see description in SAE J211 specification for more information).

7. The acceleration is filtered at 60 Hz and the mean is calculated from the data before the initial point and subtracted. This trace is output as the acceleration.

8. The original signal with the transition region is now filtered again using the 180 Hz filter. The data is integrated using a 2-point trapezoid algorithm. The results of the integration are cumulatively summed and subtracted from the initial velocity in each respective direction. This trace is the resulting velocity.

9. The cumulatively summed velocity trace is integrated using a 2-point trapezoid algorithm and cumulatively summed. The resulting trace is the displacement.

10. Traces are converted to pre-determined output units.

Summary:

The accelerometer data from the single and two-car crash tests, and finite element analyses were post processed using a fundamentally similar algorithm. Since the data collection process was designed to comply with the SAE J211-1 (Surface Vehicle Recommended Practice – Instrumentation for Impact Tests – Revised March 1995), corresponding recommended practices were used in post-processing to report the test results. Although the SAE J211-1 standard is applied in particular to impact tests for road vehicles, it was adopted here because currently no standard exists for railway vehicle impact testing. From the J211-1 specification, the Channel Frequency Classes (CFC) of vehicle structural accelerations for use in total vehicle comparison, and integration for velocity or displacement were adopted as well as the filter algorithm in Appendix C of J211-1.

From the original data bricks, the stored binary accelerometer data is converted and output into individual ASCII files with appropriate header information. The post-processing program reads in the acceleration data, and the user picks two points to define the “zero”, and transition point (minimum difference of 10 ms). The region between the points is transposed about the “zero” point to eliminate filter start-up effects (see J211-1 for more information). The acceleration data is filtered with a CFC 60 Butterworth 4-pole phaseless digital filter to obtain the output acceleration. The original acceleration data is now filtered using a CFC 180 Butterworth 4-pole phaseless digital filter, integrated using 2-point trapezoidal integration, and cumulatively summed to obtain the output velocity. The cumulative velocity integrated using 2-point trapezoidal integration and cumulatively summed to obtain the output displacement.

APPENDIX C - ADDITIONAL SINGLE-CAR TEST DATA

See Figure 5-1 for accelerometer locations.

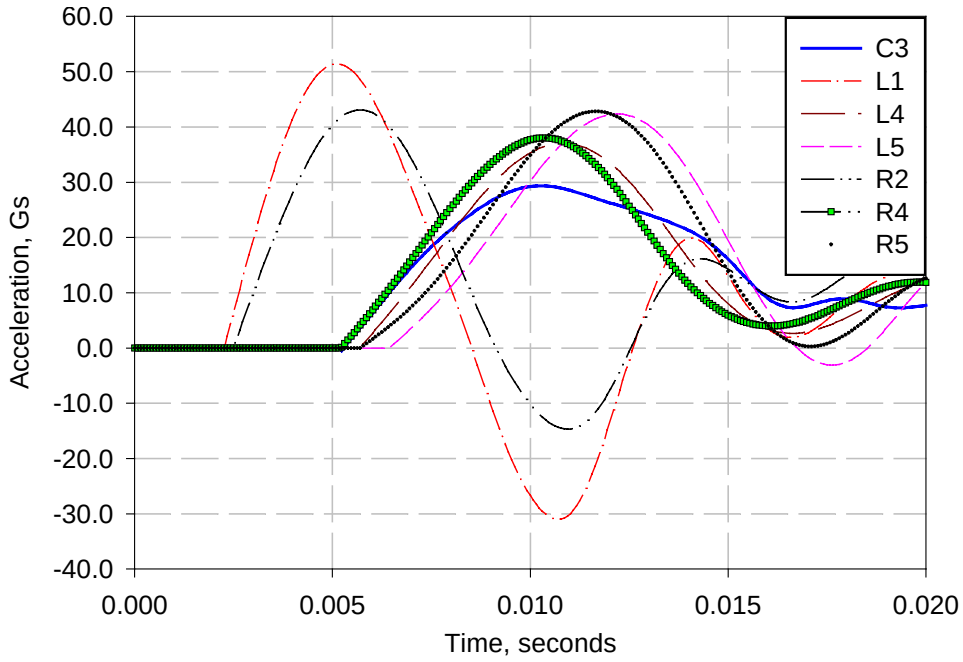

Figure C-1. Single-Car Accelerometer Measurements, Filtered at 180 Hz, to 0.02 Seconds

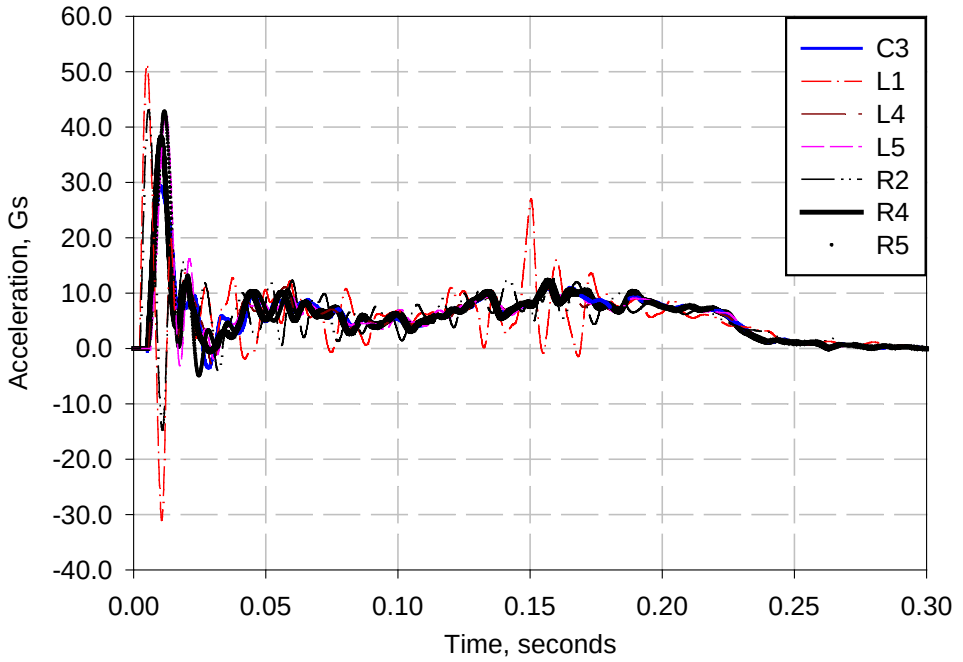

Figure C-2. Single-Car Accelerometer Measurements, Filtered at 180 Hz, to 0.3 seconds

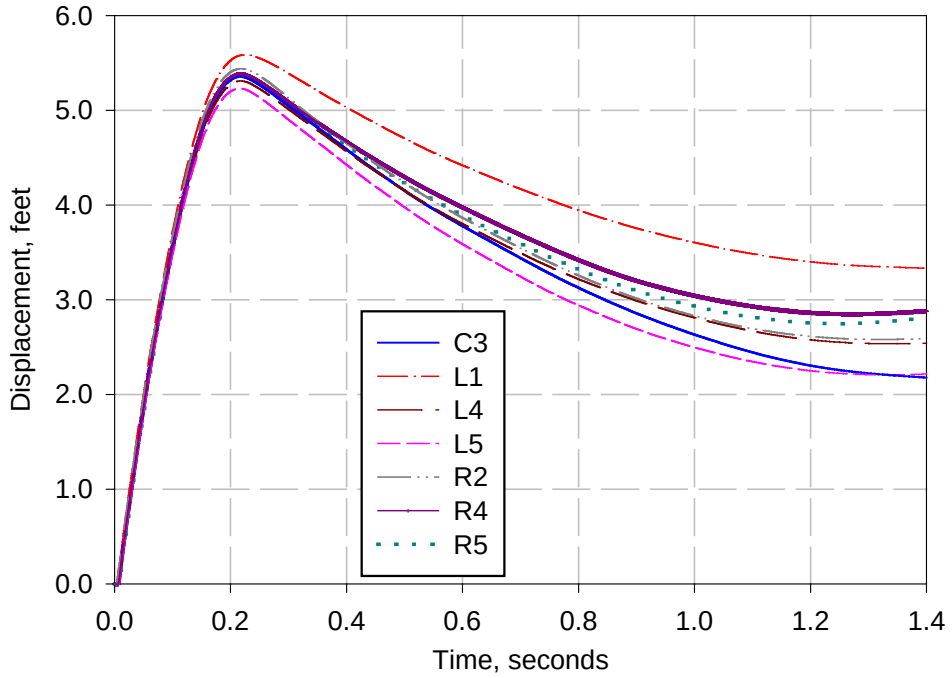

Figure C-3. Single-Car Displacements, Integrated from Accelerometer Measurements

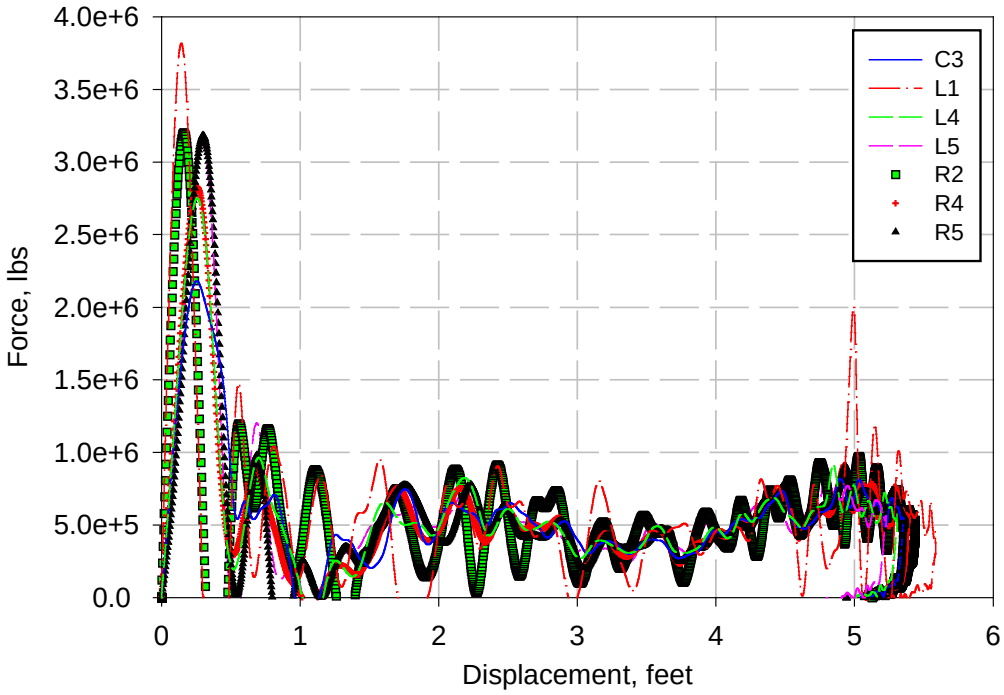

Figure C-4. Single-Car Force vs. Crush Curves Associated with Accelerometer Data

APPENDIX D - ADDITIONAL TWO-CAR TEST DATA

See Figure 6-1 and Figure 6-2 for accelerometer locations.

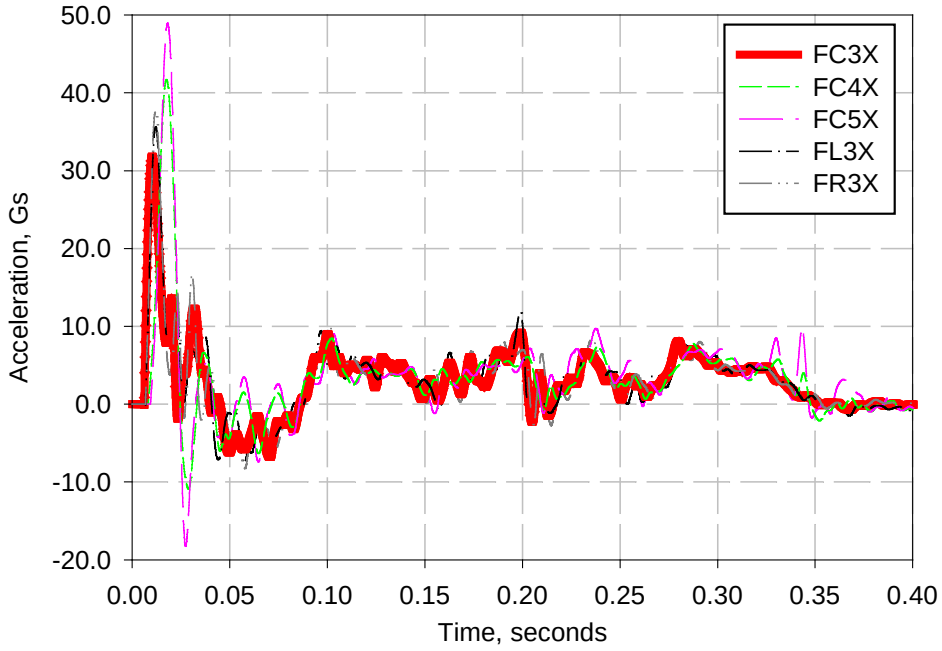

Figure D-1. Front Car Accelerometer Measurements, Filtered at 180 Hz, to 0.4 seconds

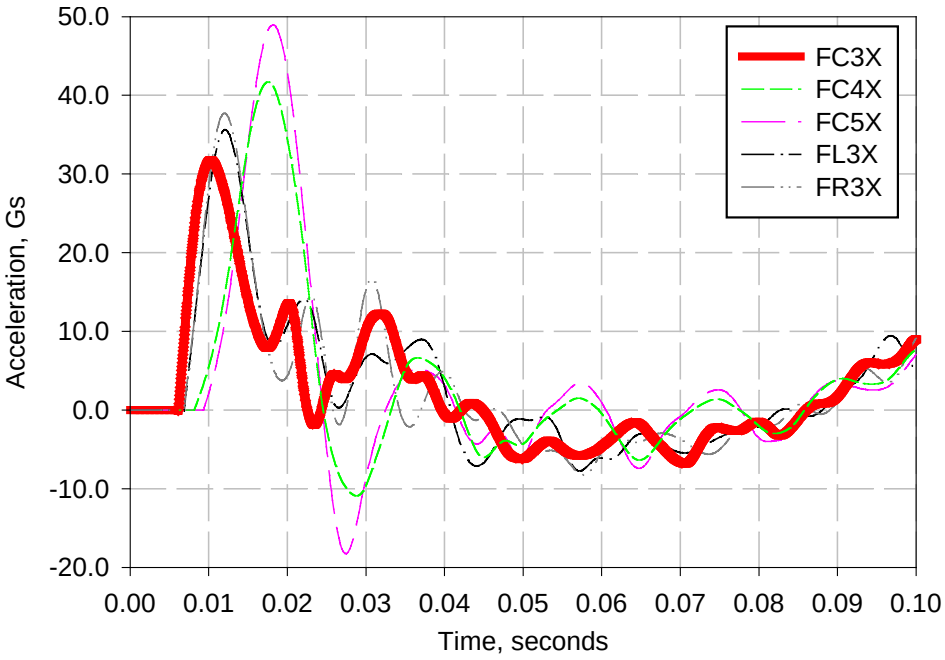

Figure D-2. Front Car Accelerometer Measurements, Filtered at 180 Hz, to 0.1 seconds

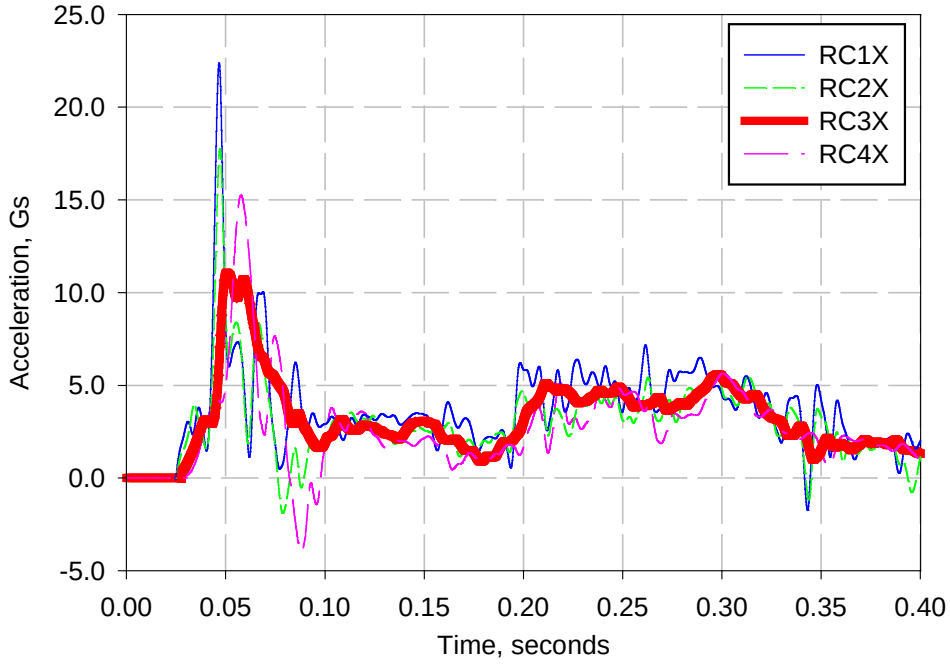

Figure D-3. Rear Car Accelerometer Measurements, Filtered at 180 Hz, to 0.4 seconds

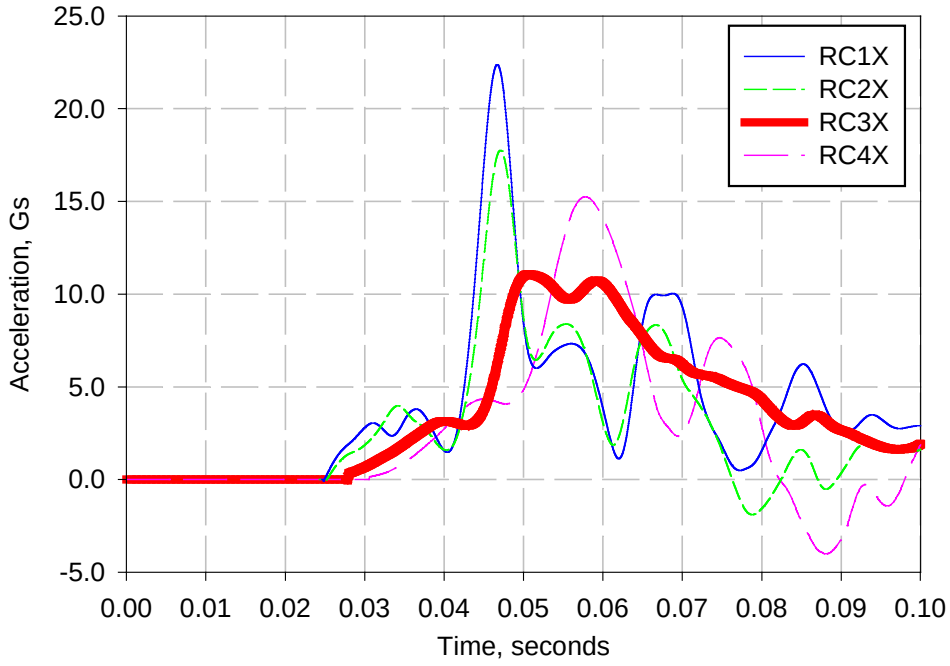

Figure D-4. Rear Car Accelerometer Measurements, Filtered at 180 Hz, to 0.1 seconds

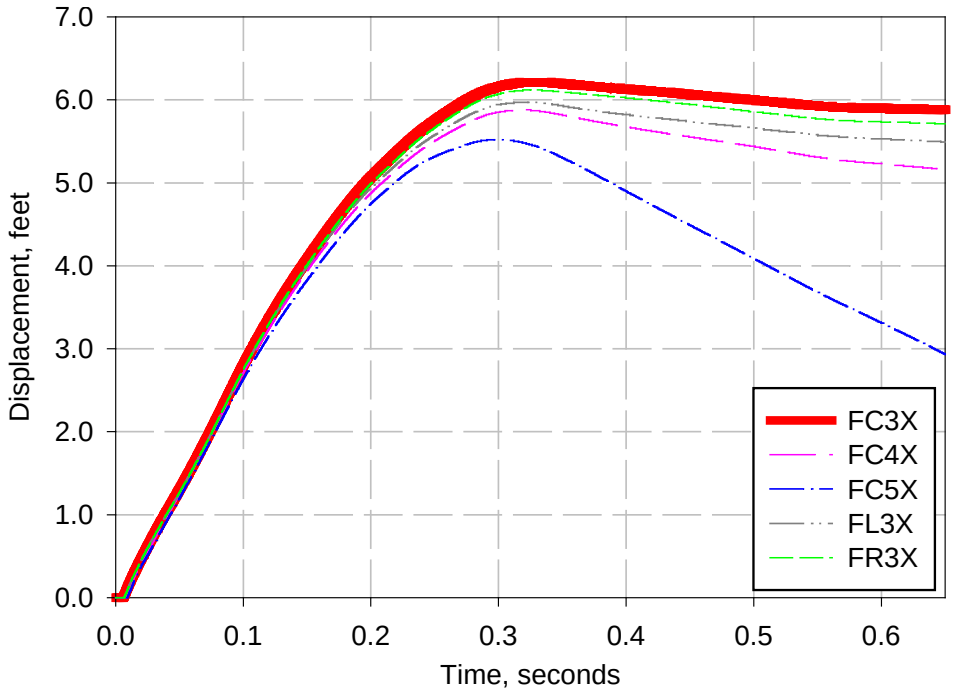

Figure D-5. Front Car Displacements, Integrated from Accelerometer Data

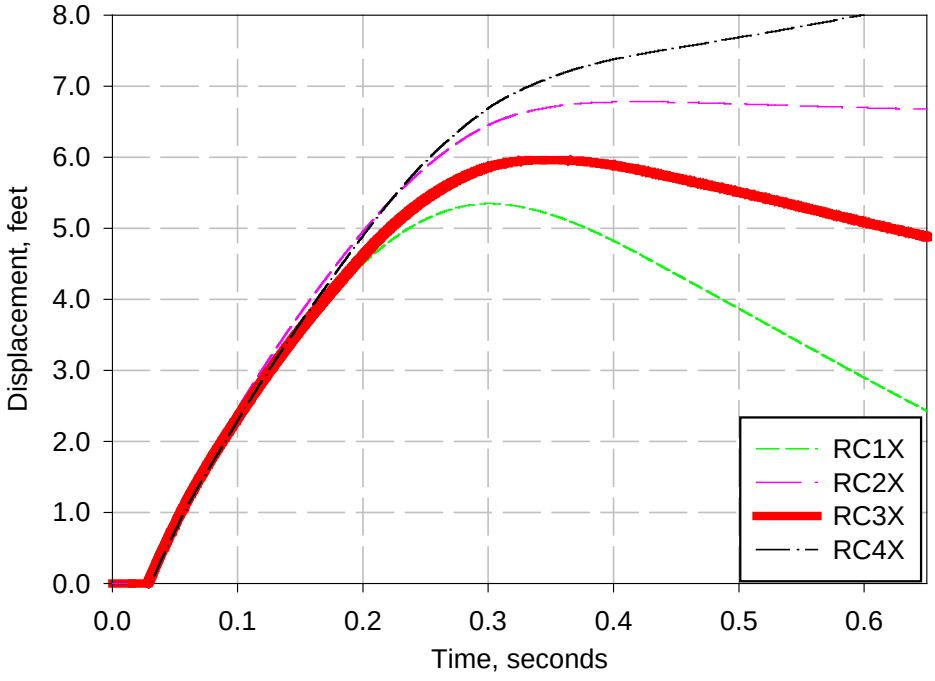

Figure D-6. Rear Car Displacements, Integrated from Accelerometer Data

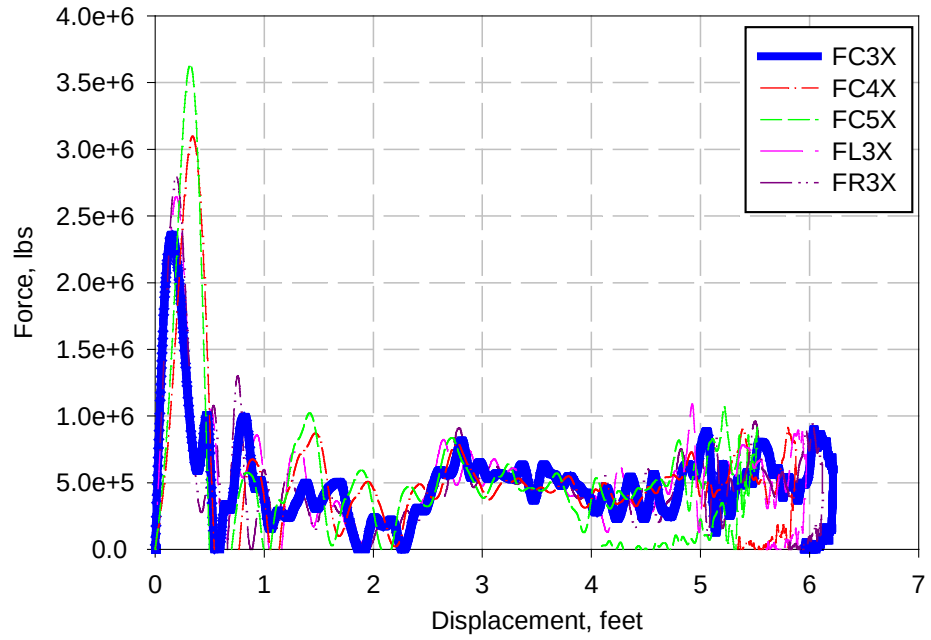

Figure D-7. Front Car Force vs. Crush Curves Associated with Accelerometer Data

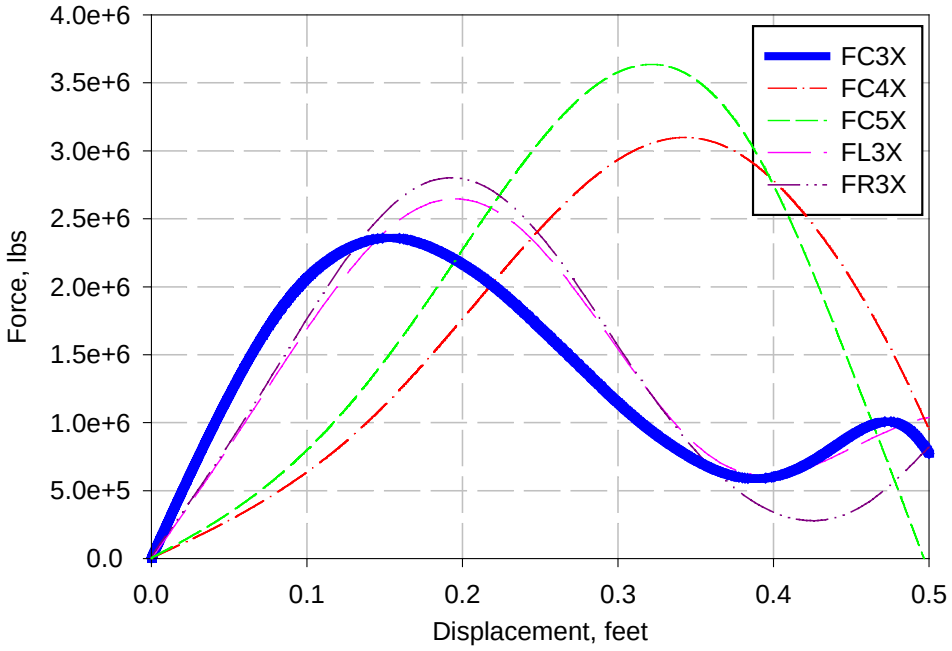

Figure D-8. Front Car Force vs. Crush Curves Associated with Accelerometer Data, First 0.5 Feet of Displacement

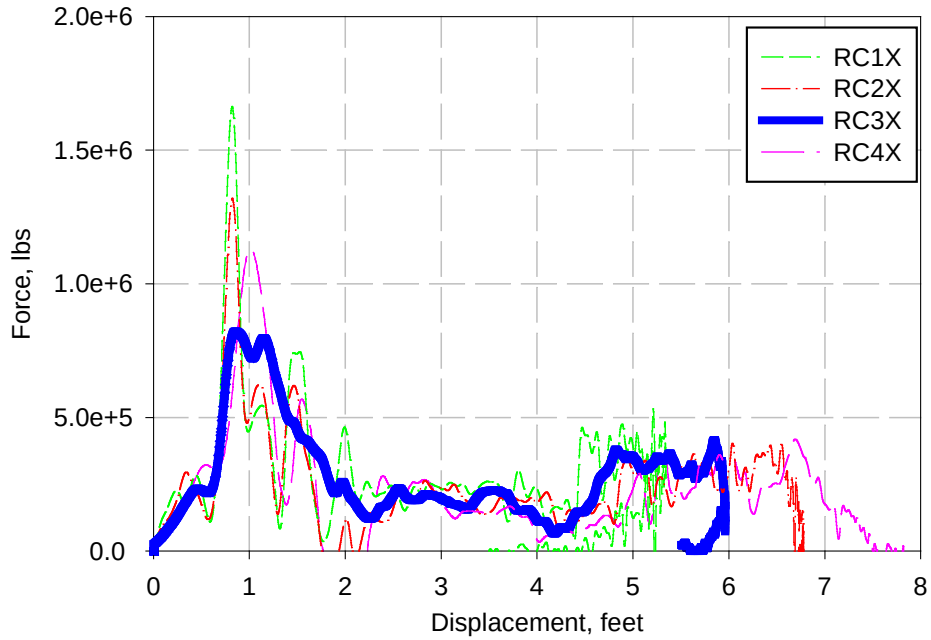

Figure D-9. Rear Car Force vs. Crush Curves Associated with Accelerometer Data

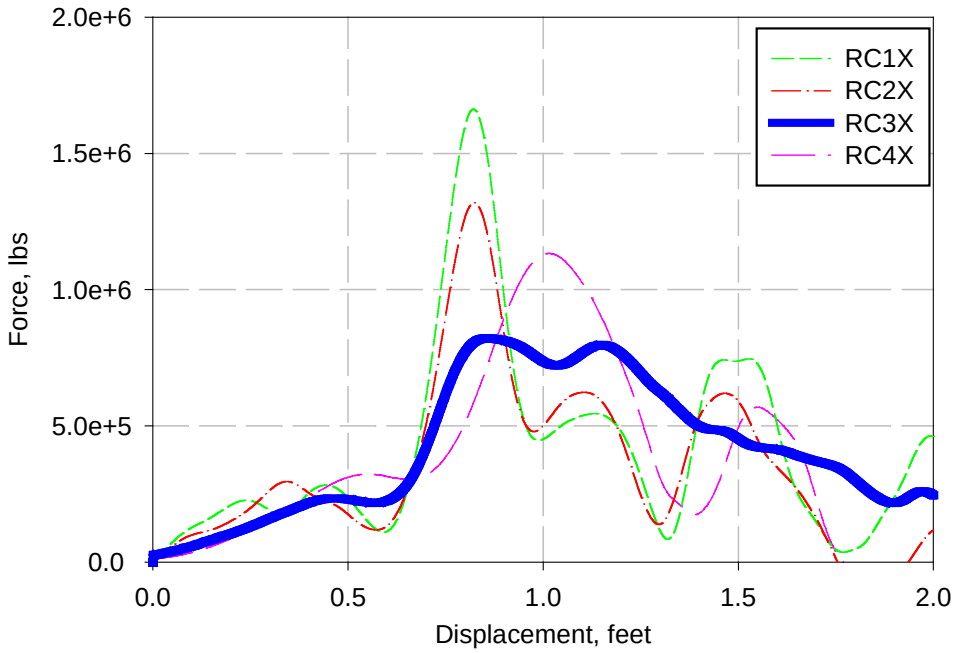

Figure D-10. Rear Car Force vs. Crush Curves Associated with Accelerometer Data, First 0.5 Feet of Displacement

APPENDIX E - USER-DEFINED SUBROUTINE, SFOSUB

Following is the user-defined subroutine, SFOSUB.f, that calculates the force in the collision springs and returns the values to the ADAMS program at each time step. This subroutine was developed at the Volpe Center and modified for this application. ADAMS passes the spring ID, the current crush value and the maximum crush value to the subroutine and it updates the current crush accordingly.

The basic algorithm behind the subroutine, which computes the forces in the springs, was developed in the Mathcad program (shown below the subroutine). The program calculates the slope, K, of each segment of the piecewise linear force/crush curve. The piecewise linear spring characteristic can be represented by segments as shown in Figure E-1, where the values to the right of the dotted line are activated by a step function. The composite path-dependent force is calculated by multiplying $k \cdot x$ by a step function that determines where the crush is on the force/crush path. A tensile force is not allowed.

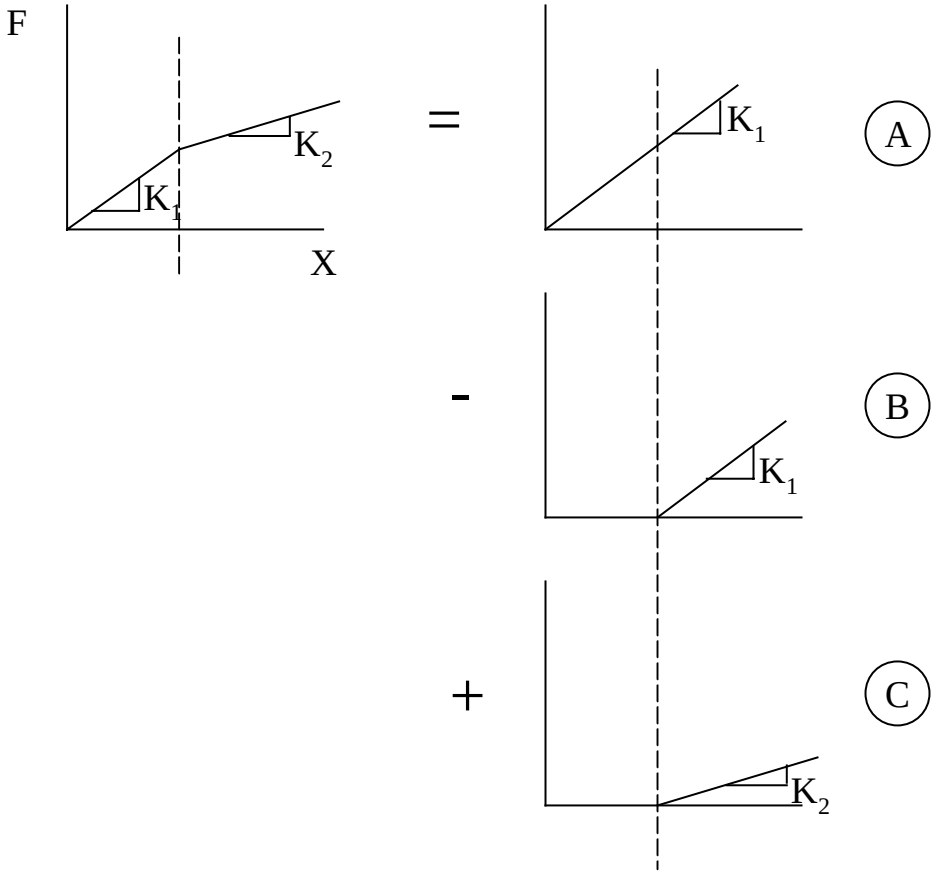

Figure E-1. Sum of Force Segments

Input arguments for the subroutine include 1) an identification number, indicating the force statement that is requesting the information, 2) the simulation time, and 3) the current and maximum crush in the spring (PAR values). The output argument is the force (VALUE).

```
SUBROUTINE SFOSUB(ID, TIME, PAR, NPAR, DFLAG, IFLAG, VALUE)
C
C   Piecewise linear segment force-displacement
C     current displ. = DX
C     max displ (for step fns) = MAXD
C     unloading down initial slope
C     + force is compression
C     no tensile force
C
C****&***1*********2*********3*********4*********5*********6*********7*
*
C   Arguments
      INTEGER ID, NPAR
      DOUBLE PRECISION TIME, PAR(*), VALUE
      LOGICAL DFLAG, IFLAG
C   Local
      INTEGER NSEG, NFORCE, I, J, L, IPAR, IDIF,JT
      PARAMETER (NSEG = 6, NFORCE = 5)
      INTEGER IDF(NFORCE), JD
      DOUBLE PRECISION P(NSEG,NFORCE), D(NSEG,NFORCE),
     &     KS(NSEG,NFORCE), K(NSEG,NFORCE), VARVAL, Dx, MAXD, FORCE
      LOGICAL ERRFLG, FIRST
C
      SAVE K, FIRST
C
C   Data pairs P,D are for Force,Displacement characteristic.
C   There must be 6 data pairs (NSEG=6) for each NFORCE.
C   List all P1,P2,P3,etc.D1,D2,D3,etc.
C   Draft SIll=10
C   Side Sill L = 7
C   Roof Sill L = 6
C   Side Sill R = 9
C   Roof Sill R = 8
      DATA P,D/2.6E06,3.2E05,6.7E05,5.80E04,3.5E05,3.5E05,
     &         0.0E00,0.0E00,6.67E04,1.0E04,5.0E04,5.0E04,
     &         0.0E00,0.00E00,3.33E04,5.0E03,2.5E04,2.5E04,
     &         0.0E00,0.0E00,6.67E04,1.0E04,5.0E04,5.0E04,
     &         0.0E00,0.00E00,3.33E04,5.0E03,2.5E04,2.5E04,
     &         0.10,0.50,0.71,1.1,1.6,10.0,
     &         0.10,0.50,0.71,1.1,1.6,10.0,
     &         0.10,0.50,0.71,1.1,1.6,10.0,
     &         0.10,0.50,0.71,1.1,1.6,10.0,
     &         0.10,0.50,0.71,1.1,1.6,10.0/
C  SFORCE ID's in Adams
      DATA IDF/10,7,6,9,8/
      DATA FIRST/.FALSE./
C****&***1*********2*********3*********4*********5*********6*********7*
*
C   Initialization: step fn slopes for all springs are "SAVED"
      IF(.NOT.FIRST) THEN
        DO 400 I = 1, NFORCE
          KS(1, I) = P(1, I)/ D(1, I)
          DO 100 J = 2, NSEG
            KS(J, I) = ( P(J, I) - P(J - 1, I) )/(D(J, I) - D(J - 1,
I))
  100     CONTINUE
          DO 300 J = 1, NSEG
```

```
            K(J, I) = KS(J, I)
            IF(J .GT. 1) THEN
              DO 200 L = 1, J - 1
                K(J, I) = K(J, I) - K(L, I)
  200         CONTINUE
            ENDIF
  300     CONTINUE
          DO 500 J = 1, NSEG
             WRITE(95,*) I, D(J,I), P(J,I)
C            WRITE(95,*) J , KS(J, I), K(J, I), D(J,I)
  500     CONTINUE
  400   CONTINUE
      FIRST = .TRUE.
      ENDIF
C   Renumber ADAMS SFORCE IDs 1,2,3,etc.
      JT=1
      DO 600 I=1,NFORCE
        IF (IDF(I).EQ.ID) THEN
          JD=I
          JT=I
          ELSE
            JD=JT
          ENDIF
C          WRITE(95,*) IDF(I),JD
  600 CONTINUE
C   COMPUTE FORCE
C
C  get current crush, PAR(1) is VARVAL ID passed through USER in PAR
array
C
      IPAR = PAR(1)
C
      CALL SYSFNC('VARVAL', IPAR, 1, VARVAL, ERRFLG)
      DX = VARVAL
C
      CALL ERRMES(ERRFLG,
     &           'Error getting current crush in SFOSUB', ID, 'STOP' )
C
C  get max displ,  PAR(2) is VARVAL ID passed through USER in PAR array
C
      IPAR = PAR(2)
C
      CALL SYSFNC('VARVAL', IPAR, 1, VARVAL, ERRFLG)
      MAXD = VARVAL
C
      CALL ERRMES(ERRFLG,
     &            'Error getting max displ. in SFOSUB', ID, 'STOP' )
C
C  compute force here
      FORCE = K(1, JD)*DX
      DO 1000 I = 2, NSEG
C  IF statement equivalent to unit step function
        IF(MAXD .GT. D(I-1,JD) ) THEN
          FORCE = FORCE + K(I,JD)*(MAXD - D(I-1,JD))
        ENDIF
 1000 CONTINUE
C
```

```
      VALUE = MAX(FORCE,-70000)
C
      RETURN
      END
```

Mathcad file

Step function, function definition:

$U(x, x0) := \Phi(x - x0)$

Construction of stiffnesses for step function segments:

Charateristic for Draft Sill:

$nseg := 6$ $\quad jseg := 1..nseg$

$P_{jseg} :=$

$2.6 \cdot 10^6$
$3.2 \cdot 10^5$
$8.7 \cdot 10^5$
$8.8 \cdot 10^4$
$5 \cdot 10^5$
$5 \cdot 10^5$

$\delta_{jseg} :=$

0.1
0.5
0.71
1.1
1.6
10

segment slopes:

$jseg := 2..6$

$K_1 := \frac{P_1}{\delta_1}$ $\quad K_{jseg} := \frac{P_{jseg} - P_{jseg-1}}{\delta_{jseg} - \delta_{jseg-1}}$

$K =$

$2.6 \cdot 10^7$
$-5.7 \cdot 10^6$
$2.619 \cdot 10^6$
$-2.005 \cdot 10^6$
$8.24 \cdot 10^5$
0

step function slopes:

$k_1 := K_1$ $\quad k_{jseg} := K_{jseg} - \sum_{i=1}^{jseg-1} k_i$

$k =$

$2.6 \cdot 10^7$
$-3.17 \cdot 10^7$
$8.319 \cdot 10^6$
$-4.624 \cdot 10^6$
$2.829 \cdot 10^6$
$-8.24 \cdot 10^5$

Initial/unloading force:

$f1(z) := k_1 \cdot z$ $\quad f(jseg, z) := k_{jseg} \cdot (z - \delta_{jseg-1}) \cdot U(z, \delta_{jseg-1})$

Composite crush characteristic:

$$A(\delta t, \delta 1) := \begin{bmatrix} f1(\delta t) + \sum_{i=2}^{nseg} f(i, \delta 1) \\ 0 \end{bmatrix}$$

$F(\delta t, \delta 1) := \max(A(\delta t, \delta 1))$ $\quad x := 0, 0.1..55$

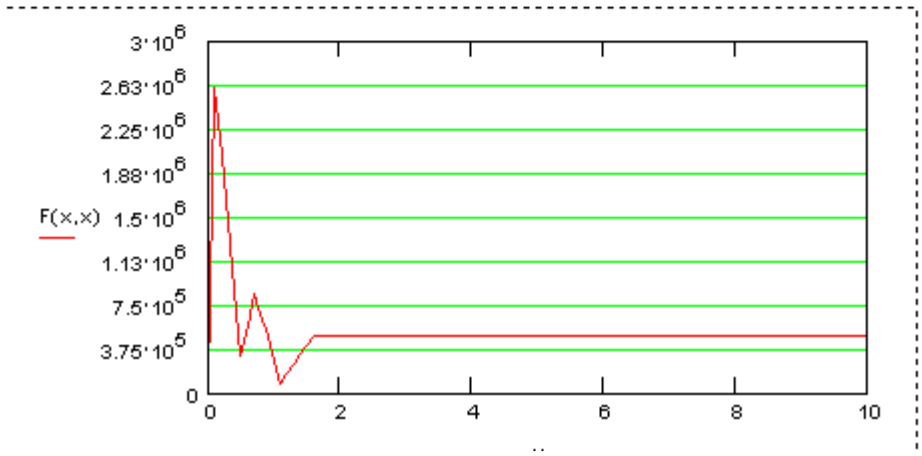

APPENDIX F - SECTIONS OF ADAMS COMMAND FILE FOR SINGLE-CAR MODEL

Following are selected details from the ADAMS Command file on the mass, inertia and geometry properties for the car body, truck, and front plate (i.e., Cab_End). Also included are the VARs and DIFFs associated with the user-defined force subroutine. The analysis settings are described. Examples of the vertical car body/truck suspension forces and the wheel/rail contact forces derived from R. Rancatore's model are also shown here.

```
!----------------- Default Units for Model --------------------------!
defaults units  &
   length = foot  &
   angle = deg  &
   force = pound_force  &
   mass = pound_mass  &
   time = sec
!----------------------- CAR_BODY ---------------------------------!
part create rigid_body initial_velocity  &
   part_name = .c31.CAR_BODY  &
   vx = 51.48  &
   vy = 0.0  &
   vz = 0.0  &
   wx = 0.0  &
   wy = 0.0  &
   wz = 0.0
!
part create rigid_body mass_properties  &
   part_name = .c31.CAR_BODY  &
   mass = 3.5579E+04  &
   center_of_mass_marker = .c31.CAR_BODY.cm  &
   ixx = 9.67E+05  &
   iyy = 2.22E+07  &
   izz = 2.245E+07  &
   ixy = 0.0  &
   izx = 0.0  &
   iyz = 0.0
!
geometry create shape extrusion  &
   extrusion_name = .c31.CAR_BODY.EXT2  &
   reference_marker = .c31.CAR_BODY.MAR1  &
   points_for_profile = 34.95, 3.725, 0.0  &
      , 34.95, 12.7, 0.0  &
      , -41.95, 12.7, 0.0  &
      , -41.95, 3.725, 0.0  &
      , 34.95, 3.725, 0.0  &
   length_along_z_axis = 10.0
!------------------------ R_TRUCK ---------------------------------!
part create rigid_body initial_velocity  &
   part_name = .c31.R_TRUCK  &
   vx = 51.48  &
   vy = 0.0  &
   vz = 0.0  &
   wx = 0.0  &
   wy = 0.0  &
   wz = 0.0
!
part create rigid_body mass_properties  &
```

```
   part_name = .c31.R_TRUCK  &
   mass = 1.37E+04  &
   center_of_mass_marker = .c31.R_TRUCK.cm  &
   ixx = 3.55E+04  &
   iyy = 1.08E+05  &
   izz = 9.28E+04  &
   ixy = 0.0  &
   izx = 0.0  &
   iyz = 0.0
!
geometry create shape block  &
   block_name = .c31.R_TRUCK.BOX3  &
   adams_id = 814  &
   corner_marker = .c31.R_TRUCK.MAR5  &
   diag_corner_coords = 10.0, 3.5, 10.0
!------------------------- Cab_End ----------------------------------!
part create rigid_body initial_velocity  &
   part_name = .c31.Cab_End  &
   vx = 51.48
!
part create rigid_body mass_properties  &
   part_name = .c31.Cab_End  &
   mass = 2252.1833989491  &
   center_of_mass_marker = .c31.Cab_End.cm  &
   ixx = 9.6168231135E+04  &
   iyy = 4.7456721621E+04  &
   izz = 4.8936727854E+04  &
   ixy = 0.0  &
   izx = 0.0  &
   iyz = 0.0
!
geometry create shape block  &
   block_name = .c31.Cab_End.BLOCK_1  &
   adams_id = 9  &
   corner_marker = .c31.Cab_End.MAR_1  &
   diag_corner_coords = 0.5, 8.975, 10.0
!
geometry attributes  &
   geometry_name = .c31.Cab_End.BLOCK_1  &
   color = RED
!
geometry create shape ellipsoid  &
   ellipsoid_name = .c31.Cab_End.SPHERE_1  &
   center_marker = .c31.Cab_End.MAR_5  &
   x_scale_factor = 1.0  &
   y_scale_factor = 1.0  &
   z_scale_factor = 1.0
!---------------------- Data storage -------------------------------!
data_element create variable  &
   variable_name = .c31.VAR1  &
   adams_id = 24  &
   function = ""
!
data_element create variable  &
   variable_name = .c31.VAR2  &
   adams_id = 29  &
   function = ""
```

```
!
data_element create variable  &
   variable_name = .c31.VAR3  &
   adams_id = 30  &
   function = ""
!
data_element create variable  &
   variable_name = .c31.VAR4  &
   adams_id = 31  &
   function = ""
!
data_element create variable  &
   variable_name = .c31.VAR5  &
   adams_id = 33  &
   function = ""
!
data_element create variable  &
   variable_name = .c31.VAR6  &
   adams_id = 35  &
   function = ""
!
data_element create variable  &
   variable_name = .c31.VAR10  &
   adams_id = 100  &
   function = ""
!
data_element create variable  &
   variable_name = .c31.VAR11  &
   adams_id = 101  &
   function = ""
!
data_element create variable  &
   variable_name = .c31.VAR12  &
   adams_id = 102  &
   function = ""
!
data_element create variable  &
   variable_name = .c31.VAR13  &
   adams_id = 103  &
   function = ""
!
data_element create spline  &
   spline_name = .c31.Coupler_spline  &
   adams_id = 10  &
   x = -1.0, 0.0, 0.15, 0.25, 0.291667, 0.308333, 0.320833, 0.333333,
0.35,  &
       0.366667, 0.383333, 0.4, 0.425, 0.5, 0.583333, 0.666667,
0.708333,  &
       0.75, 0.833333, 0.916667, 1.166667, 1.333333, 1.458333,
1.583333,  &
       1.833333, 2.25, 2.833333, 3.166667, 3.666667, 4.166667,
4.583333, 5.0,  &
       5.333333, 5.75, 6.0, 6.666667, 8.333333, 8.5, 9.0, 9.5, 10.0,
11.0,  &
       12.0, 13.0, 14.0, 15.0, 20.0, 25.0, 30.0  &
   y = -1.0E+07, 0.0, 1.13E+06, 1.8E+06, 2.05E+06, 2.14E+06, 2.195E+06,
&
```

```
       2.23E+06, 2.255E+06, 2.265E+06, 2.255E+06, 2.23E+06, 2.18E+06,
&
       2.0E+06, 1.8E+06, 1.608E+06, 1.52E+06, 1.45E+06, 1.39E+06,
1.35E+06,  &
       1.25E+06, 1.1875E+06, 1.155E+06, 1.125E+06, 1.078E+06, 1.03E+06,
&
       9.7E+05, 9.2E+05, 8.3E+05, 7.0E+05, 6.3E+05, 5.8E+05, 5.5E+05,
&
       5.1E+05, 5.0E+05, 5.0E+05, 5.0E+05, 5.0E+05, 5.5E+05, 6.0E+05,
&
       6.5E+05, 7.5E+05, 8.5E+05, 9.5E+05, 1.05E+06, 1.15E+06,
1.65E+06,  &
       2.15E+06, 2.65E+06  &
   linear_extrapolate = no  &
   units = force
!------------------------ Accgrav ----------------------------------!
force create body gravitational  &
   gravity_field_name = gravity  &
   x_component_gravity = 0.0  &
   y_component_gravity = -32.1740485564  &
   z_component_gravity = 0.0
!------------------ Analysis settings -----------------------------!
executive_control set numerical_integration_parameters  &
   model_name = c31  &
   integrator_type = wstiff  &
   error_tolerance = 1.0E-02  &
   maxit_corrector_iterations = 25  &
   adaptivity = 5.0E-07  &
   scale = 1.0, 1.0, 1.0E-03  &
   kmax_integrator_order = 6
!
executive_control set equilibrium_parameters  &
   model_name = c31  &
   alimit = 0.1d  &
   error = 1.0E-03  &
   imbalance = 10.0  &
   maxit = 100  &
   stability = 10.0  &
   tlimit = 0.1  &
   pattern_for_jacobian = yes, no, yes, no, yes, no, yes, no, yes, no
!-------------------- Simulation Scripts ---------------------------!
simulation script create  &
   sim_script_name = .c31.SIM_SCRIPT_2  &
   solver_commands = "! Insert ACF commands here:", "SIMULATE/STATIC",
&
                     "SIMULATE/DYNAMIC, END=5.0E-02, STEPS=500",  &
                     "SIMULATE/DYNAMIC, END=5.0E-01, STEPS=450"
!------------------- Function definitions ---------------------------!
data_element modify variable  &
   variable_name = v_trkstiff  &
   function = "46440"
!
data_element modify variable  &
   variable_name = l_trkstiff  &
   function = "350000."
!
data_element modify variable  &
```

```
   variable_name = VAR1  &
   function = "7-DX(.c31.Cab_End.MAR_9,.c31.CAR_BODY.MAR_7)"
!
data_element modify variable  &
   variable_name = VAR2  &
   function = "7-DX(.c31.Cab_End.MAR_10,.c31.CAR_BODY.MAR_8)"
!
data_element modify variable  &
   variable_name = VAR3  &
   function = "7-DX(.c31.Cab_End.MAR_11,.c31.CAR_BODY.MAR_9)"
!
data_element modify variable  &
   variable_name = VAR4  &
   function = "7-DX(.c31.Cab_End.MAR_12,.c31.CAR_BODY.MAR_10)"
!
data_element modify variable  &
   variable_name = VAR5  &
   function = "7-DX(.c31.Cab_End.MAR_13,.c31.CAR_BODY.MAR_11)"
!
data_element modify variable  &
   variable_name = VAR6  &
   function = "DIF(.c31.DIFF_5)"
!
data_element modify variable  &
   variable_name = VAR10  &
   function = "DIF(.c31.DIFF_1)"
!
data_element modify variable  &
   variable_name = VAR11  &
   function = "DIF(.c31.DIFF_2)"
!
data_element modify variable  &
   variable_name = VAR12  &
   function = "DIF(.c31.DIFF_3)"
!
data_element modify variable  &
   variable_name = VAR13  &
   function = "DIF(.c31.DIFF_4)"
!
part modify equation differential_equation  &
   differential_equation_name = DIFF_1  &
   function = "IF(VR(.c31.CAR_BODY.MAR_7,.c31.Cab_End.MAR_9):1,0,0)",
&
              "*-VR(.c31.CAR_BODY.MAR_7,.c31.Cab_End.MAR_9)"
!
part modify equation differential_equation  &
   differential_equation_name = DIFF_2  &
   function = "IF(VR(.c31.CAR_BODY.MAR_8,.c31.Cab_End.MAR_10):1,0,0)",
&
              "*-VR(.c31.CAR_BODY.MAR_8,.c31.Cab_End.MAR_10)"
!
part modify equation differential_equation  &
   differential_equation_name = DIFF_3  &
   function = "IF(VR(.c31.CAR_BODY.MAR_9,.c31.Cab_End.MAR_11):1,0,0)",
&
              "*-VR(.c31.CAR_BODY.MAR_9,.c31.Cab_End.MAR_11)"
!
```

```
part modify equation differential_equation  &
   differential_equation_name = DIFF_4  &
   function = "IF(VR(.c31.CAR_BODY.MAR_10,.c31.Cab_End.MAR_12):1,0,0)",
&
              "*-VR(.c31.CAR_BODY.MAR_10,.c31.Cab_End.MAR_12)"
!
part modify equation differential_equation  &
   differential_equation_name = DIFF_5  &
   function = "IF(VR(.c31.Cab_End.MAR_13,
.c31.CAR_BODY.MAR_11):1,0,0)",  &
              "*-VR(.c31.Cab_End.MAR_13, .c31.CAR_BODY.MAR_11)"
!
force modify direct single_component_force  &
   single_component_force_name = F_impact  &
   function = "impact(dm(.c31.Cab_End.MAR_5, .c31.ground.MAR_2),",  &
              "vr(.c31.Cab_End.MAR_5, .c31.ground.MAR_2),",  &
              "100.5,",  &
              "6.0E+07,",  &
              "1.2,",  &
              "2.0E+04,",  &
              "9.842519685E-03)"
!
force modify direct single_component_force  &
   single_component_force_name = F_roof_sillL  &
   function = "USER(24,100)"
!
force modify direct single_component_force  &
   single_component_force_name = F_side_sillL  &
   function = "USER(29,101)"
!
force modify direct single_component_force  &
   single_component_force_name = F_roof_sillR  &
   function = "USER(30,102)"
!
force modify direct single_component_force  &
   single_component_force_name = F_side_sillR  &
   function = "USER(31,103)"
!
force modify direct single_component_force  &
   single_component_force_name = F_draft_sill  &
   function = "USER(33,35)"
!
force modify direct single_component_force  &
   single_component_force_name = VFORCE  &
   function = "0.0*impact(dm(.c31.Cab_End.MAR_5, .c31.ground.MAR_2),",
&
              "vr(.c31.Cab_End.MAR_5, .c31.ground.MAR_2),",  &
              "100.5,",  &
              "4.0E+06,",  &
              "1.2,",  &
              "7.0E+04,",  &
              "9.842519685E-03)"
!
force modify direct force_vector  &
   force_vector_name = R_TRUCK_IF  &
   x_force_function = "0.0"  &
```

```
   y_force_function =
"IMPACT(DY(.c31.CAR_BODY.mar29,.c31.R_TRUCK.mar30,.c31.R_TRUCK.mar30),
",  &

"VY(.c31.CAR_BODY.mar29,.c31.R_TRUCK.mar30,.c31.R_TRUCK.mar30), ",  &
              "0.833, STEP(0.833-DY(.c31.CAR_BODY.mar29,
.c31.R_TRUCK.mar30, .c31.R_TRUCK.mar30), 0.395, ",  &
              "VARVAL(.c31.v_trkstiff), 0.4, 1.8e+7), 1.0, 1.56e+04,
0.395)"  &
   z_force_function = "0.0"
!
force modify direct force_vector  &
   force_vector_name = F_TRUCK_DI  &
   x_force_function = "if(mode-4:",  &
              "0.0,",  &
              "VFORCE(.c31.F_TRUCK_DI, 0, 3,",  &
              "
.c31.F_TRUCK.MAR337)*VARVAL(.c31.fground)*",  &
              "step(VX(.c31.F_TRUCK.MAR337, ",  &
              "             .c31.AMF1_DUFI.MAR94, ",  &
              "             .c31.AMF1_DUFI.MAR94), -0.01, 1., 0.01, -
1.)*",  &
              "step(abs(DZ(.c31.F_TRUCK.MAR337, ",  &
              "                    .c31.AMF1_DUFI.MAR94,",  &
              "                    .c31.AMF1_DUFI.MAR94)), 0.1667, 1.0,
0.17, 0.0),",  &
              "0.0)"  &
   y_force_function = "impact(DY(.c31.F_TRUCK.MAR337,
.c31.AMF1_DUFI.MAR94, .c31.AMF1_DUFI.MAR94),",  &
              "VY(.c31.F_TRUCK.MAR337, .c31.AMF1_DUFI.MAR94,
.c31.AMF1_DUFI.MAR94),",  &
              "0.501,1.0e6, 1.0, 1.0e5, 0.0001)"  &
   z_force_function = "if(mode-4:",  &
              "0.0,",  &
              "step(abs(DZ(.c31.F_TRUCK.MAR337, ",  &
              "                    .c31.AMF1_DUFI.MAR94,",  &
              "                    .c31.AMF1_DUFI.MAR94)), ",  &
              "  0.1667,",  &
              "  VFORCE(.c31.F_TRUCK_DI, 0, 3, .c31.F_TRUCK.MAR337)*",
&
              "                         VARVAL(.c31.fground)*",  &
              "  step(VZ(.c31.F_TRUCK.MAR337, ",  &
              "              .c31.AMF1_DUFI.MAR94,",  &
              "              .c31.AMF1_DUFI.MAR94), -0.01, 1., 0.01, -
1.),",  &
              "  0.17,0.),  ",  &
              "-400000*DZ(.c31.F_TRUCK.MAR337, ",  &
              "                     .c31.AMF1_DUFI.MAR94,",  &
              "                     .c31.AMF1_DUFI.MAR94))"
```